UNIVERSITY OF THESSALY

SCHOOL OF ENGINEERING

DEPARTMENT OF MECHANICAL ENGINEERING

LABORATORY OF MECHANICS AND STRENGTH OF MATERIALS

Post-Graduate Diploma

Finite Element Simulation of Pipe Cold-Bend Manufacturing and Structural Performance

Dimitra Testa

Diploma in Mechanical and Aeronautical Engineering,

University of Patras, 2009

Advisor: Dr. S.A Karamanos

Submitted to the Department of Mechanical Engineering in Partial Fulfillment of the Requirements for the Degree of Post-Graduate Diploma

University of Thessaly, March 2014

ΠΑΝΕΠΙΣΤΗΜΙΟ ΘΕΣΣΑΛΙΑΣ

ΠΟΛΥΤΕΧΝΙΚΗ ΣΧΟΛΗ

ΤΜΗΜΑ ΜΗΧΑΝΟΛΟΓΩΝ ΜΗΧΑΝΙΚΩΝ

ΕΡΓΑΣΤΗΡΙΟ ΜΗΧΑΝΙΚΗΣ ΚΑΙ ΑΝΤΟΧΗΣ ΤΩΝ ΥΛΙΚΩΝ

Μεταπτυχιακή Εργασία

Προσομοίωση της Ψυχρής Διαμόρφωσης Καμπύλων Σωλήνων και της Δομικής τους Συμπεριφοράς με τη Μέθοδο των Πεπερασμένων Στοιχείων

Δήμητρα Τέστα

Διπλ. Μηχανολόγος και Αεροναυπηγός Μηχανικός Π. Πατρών, 2009

Επιβλέπων: Σ.Α. Καραμάνος

Υπεβλήθη για την εκπλήρωση μέρους των απαιτήσεων για την απόκτηση του Μεταπτυχιακού Διπλώματος Ειδίκευσης

Πανεπιστήμιο Θεσσαλίας, Μάρτιος 2014

Η έγκριση της μεταπτυχιακής εργασίας από το Τμήμα Μηχανολόγων Μηχανικών της Πολυτεχνικής Σχολής του Πανεπιστημίου Θεσσαλίας δεν υποδηλώνει αποδοχή των απόψεων του συγγραφέα (Ν. 5343/32 αρ. 202 παρ. 2).

Εγκρίθηκε από τα Μέλη της Τριμελούς Εξεταστικής Επιτροπής:

Πρώτος Εξεταστής (Επιβλέπων)	Δρ. Σπυρίδων Καραμάνος Αναπληρωτής Καθηγητής, Τμήμα Μηχανολόγων Μηχανικών, Πανεπιστήμιο Θεσσαλίας
Δεύτερος Εξεταστής	Δρ. Αλέξιος Κερμανίδης Επίκουρος Καθηγητής, Τμήμα Μηχανολόγων Μηχανικών, Πανεπιστήμιο Θεσσαλίας
Τρίτος Εξεταστής	Δρ. Άννα Ζερβάκη Μεταλλουργός Μηχανικός ΕΜΠ, Μηχανικός Υλικών και Μηχανικών Δοκιμών, Τμήμα Μηχανολόγων Μηχανικών Βιομηχανίας, Πανεπιστήμιο Θεσσαλίας

Ευχαριστίες

Ολοκληρώνοντας την προσπάθεια συγγραφής της παρούσας διπλωματικής εργασίας θα ήθελα να ευχαριστήσω τους ανθρώπους που με βοήθησαν και με στήριξαν στην πορεία μου αυτά τα χρόνια.

Πρώτα απ’ όλα, θα ήθελα να ευχαριστήσω τον επιβλέποντα της μεταπτυχιακής μου εργασίας, Αναπληρωτή Καθηγητή κ.Σπύρο Καραμάνο για την πολύτιμη βοήθεια, καθοδήγηση αλλά και κατανόηση κατά τη διάρκεια της δουλειάς μου. Επίσης, είμαι ευγνώμων στα υπόλοιπα μέλη της εξεταστικής επιτροπής της μεταπτυχιακής μου εργασίας, Καθηγητή κ. Αλέξιο Κερμανίδη και Δρ. Ζερβάκη Άννα, για την προσεκτική ανάγνωση της εργασίας μου, τις πολύτιμες υποδείξεις τους καθώς και όλα όσα μου δίδαξαν στα μεταπτυχιακά μαθήματα.

Ευχαριστώ τα μέλη του εργαστηρίου Βάθη Μαρία, Παππά Πατρίτσια και Αγλαία Πουρνάρα για την όμορφη συνεργασία αυτά τα χρόνια. Ένα πολύ μεγάλο ευχαριστώ αξίζει στους συναδέλφους μου Γεώργιο Βαρέλη, Δανιήλ Βασιλική και Γιαννούλα Χατζοπούλου για τον πολύτιμο χρόνο που μου αφιέρωσαν κάθε φορά χρειαζόμουνα τη βοήθειά τους. Οι υποδείξεις τους σε πολλά στάδια της παρούσας εργασίας ήταν καταλυτική.

Ευχαριστώ πολύ τους Βαγγέλη, Σπυριδούλα, Παναγιώτα και Αλίκη για την αμέριστη συμπαράσταση, κατανόηση και ενθάρρυνση ιδιαίτερα την τελευταία περίοδο.

Θα ήθελα επίσης να ευχαριστήσω τις συμφοιτήτριές μου Κορίτσα Λίλα, Λύτρα Αλκμήνη και Παντούσα Δάφνη για την πολύ καλή συνεργασία αλλά και παρέα.

Το μεγαλύτερο ευχαριστώ δικαιωματικά αξίζει στην οικογένεια μου. Χωρίς την υποστήριξη, την αγάπη και την ενθάρρυνσή τους δε θα είχα καταφέρει να φτάσω μέχρι εδώ σήμερα.

Δήμητρα Τέστα

Table of Contents

List of figures

List of tables

Chapter 1

Introduction

Tubes or pipe bends, sometimes referred to as "elbows" are key components of mechanical systems with applications in many high technological industries such as aviation, aerospace, shipbuilding, automobile, industrial facilities, energy pipeline, nuclear facilities and health care. Their properties satisfy the current needs for lightweight, high strength and high performance from both material and structure point of view. The present study primarily focuses on cold pipe bend manufacturing process and subsequently on structural performance of bent tubes.

1.1 Forming characteristics of tube bending process with small bending radius

Tube bending manufacturing process has been a vital manufacturing technology, in order to bend the tubular member at certain bending radius, bending angle and shape, for lightweight products urgently needed in the above industries [1-2]. Many tube bending approaches have been developed in response to the diverse demands of tube specification, shapes, materials and forming tolerance [3-4]. According to the forming conditions, there are cold bending techniques at room temperature and hot (heat) bending methods at elevated temperature. From the viewpoint of loading conditions, there are several methodologies namely pure bending, compression bending, stretch bending, roll bending, rotary draw bending and laser bending. Those methodologies can be used for carbon steel, stainless steel, aluminum alloy, copper alloy, magnesium alloy and titanium alloy tubes. From aspect of tubular shapes, there are round, rectangular and other irregular section tube bending. Moreover, tubes can be seamless or welded depending on the tube fabrication respect. Finally, from the viewpoint of bending radius, there are small radius bending and large radius bending.

For any bending process, upon bending deformation, uneven tension and compression stress distributions are induced at the extrados and intrados of bending tube respectively, which may cause multiple defects or instabilities such as wrinkling, over-thinning (cracking), cross-section distortion and spring-back as shown in Figure 1. The accurate prediction and efficient control of these physical phenomena are necessary for optimizing tube bend forming process [5]. In the present work, cold bending process of tube bends is analyzed using the rotary draw bending technique.

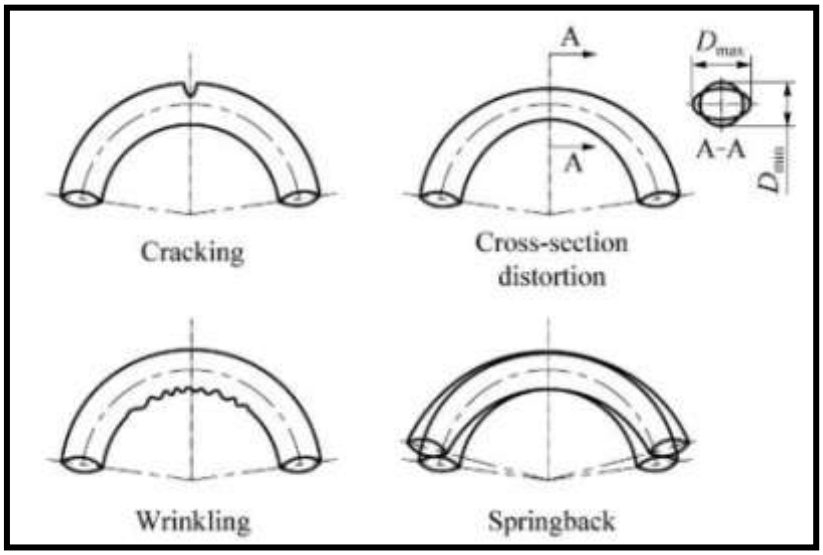

Figure 1: Defects and instabilities during bending process

1.2 Previous publications on cold bending manufacturing of tube bends

Hasanpour et al. [6] simulated the plastic deforming behavior and wrinkling mechanism for a "thin-walled" tube and the results were compared with the available experimental ones. Then, the effect of anisotropy on ovalization, thickness and wrinkling of tube were investigated by using FEM. Extensive numerical results were presented showing the effects of the various kinds of materials and geometric parameters on wrinkling using anisotropic yield function. Zhao et al. [7] investigated the significant and complicated influence of clearances between tube and various dies on the onset of wrinkling during the rotary draw bending process. To study the effect of clearance on wrinkling, a 3D finite element (FE) model of the process for thin-walled

rectangular aluminum alloy tube has been built using the explicit code ABAQUS/Explicit and validated by comparing the experiment. Li et al. [8] developed an energy-based wrinkling prediction model for thin-walled tube bending by using the energy principle, combined with analytical and finite element (FE) numerical methods. Zhao et al. [9] reported a wrinkling prediction model of the rotary-draw bending process for "thin-walled" rectangular 3A21 aluminum alloy tube based on the deformation theory of plasticity. Heng and He [10] reported a study on multi-defect constrained bendability of "thin-walled" tube NC bending under different clearance. A three-dimensional-finite element (3D-FE) model was established to describe the realistic dynamic boundary conditions of multiple dies under ABAQUS/Explicit platform, in terms of wrinkling, wall thinning and cross section deformation. The numerical results were combined with the experimental ones.

Heng et al. [11] investigated the plastic deformation characteristics with small bending radius of "thin-walled" tube. Based on the analysis of the forming characteristics by analytical and experimental methods, a complete 3D elastic-plastic FEM model of the process was developed using ABAQUS/Explicit code, including bending process, balls retracting and unloading process. Li et al. [12], based on an analytical description of the push assistant loading (PAL) functions, reported the deformation behaviors of "thin-walled" tube in RDB under three different PAL conditions with respect to wall thinning, cross-section deformation and wrinkling numerically combined with experiment considering PAL functions. Jing et al. [13] reported a search algorithm of the forming limits of aluminum alloy "thin-walled" tubes based on a 3D elastic-plastic finite element (FE) model and a wrinkling energy prediction model for the bending processes under axial compression loading (ACL) or not. This algorithm enables to be considered the effects of process parameter combinations including die, friction parameters on the multi-indices. Based on this algorithm, the forming limits of the different size tubes are obtained, and the roles of the process parameter combinations in enabling the limit bending processes are also revealed.

1.3 Description of Rotary Draw Bending

The rotary draw bending (RDB) of tubes with ratio D/t≈20 (D-tube diameter, t-wall thickness) is used in numerous applications in aviation, aerospace and automobile industries because of satisfying high strength/weight ratio requirement. Figure 2 shows that, during RDB process, the tube is subjected to multi-die constrains in order to avoid local buckling (wrinkling) of the tube wall due to excessive compression. Clamped against the bend die and drawn by the bend die and the clamp die, the tube goes past the tangent point and rotates along the groove of the bend die for the desired bending radius Rd. When the bending angle is satisfied, the mandrel (including flexible balls) is withdrawn from its working position and the tube is then unloaded by removing the other dies.

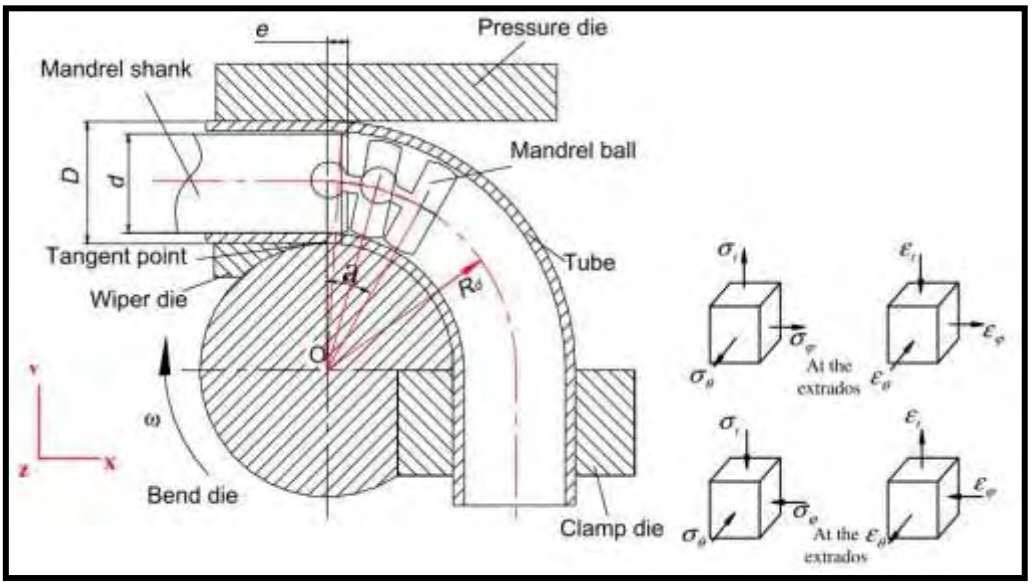

Figure 2: Geometry model for thin-walled tube rotary draw bending process

Compared with other bending processes, for example pure bending, compression bending, stretch bending, roll bending and laser bending, the RDB is the most versatile method to produce precise bent tube parts with high bending limit (small bending radius Rd with respect to tube diameter). However, the process is a nonlinear physical process with large rotation/deformation and multi-factors coupling effects [14]. Therefore, the process needs precise coordination of various dies and strict control of forming parameters [15] in order to improve the inhomogeneous flow states

of tube materials and avoid defects in bending such as wrinkling, over thinning and section distortion. It is well known that the problem resolution relies heavily on experience and involves repeated trial-and-errors in practice, which spends excessive manpower, raw material, and time in designing and adjusting the process and dies, and moreover makes the production efficiency abate drastically. In practice, with lack of understanding of the roles of the contact conditions in bendability of TWTB, the "error and trial" method is still the primary way to assign the suitable contact conditions. For heavy-walled tube with small diameter, the tooling setup may be done within couple of minutes. However, even though the operator's experience is rich, it may take a significant amount of time to carry out the tool setup for thin-walled tube bending with small bending radii ($Rd/D \leq 2.0$). Thus, to optimize the manufacturing process it is necessary to study the effect of contact conditions on the tube bending. To the author's best knowledge, the influence of the contact conditions on plastic bending from respects of the overall bending defects in TWTB has not yet been fully addressed. It is noted that the clearance between tube and dies is the major variable to indicate the boundary conditions if the materials of tube and dies are unchanged as well as the lubricants [10].

1.4 Structural behavior of pipe elbows

Curved pipe segments are widely used in industrial piping and pipelines. Because of the importance for safeguarding their structural integrity, much research has been devoted to the study of their mechanical behavior. It is well-known that the behavior of a tubular member under bending loads is characterized by a significant distortion of the cross-section associated with strains well beyond the elastic limit. This distortion, often referred to as "ovalization" or "Brazier" effect, makes the bent tube more flexible than the corresponding straight parts and produces additional stresses, which need to be considered in analysis and design [16].

1.5 Previous publications

Sobel and Newman [17-18], and Dhalla [19] reported experimental data on the elastic-plastic bending response of elbows through a series of tests on 16-inch 90 deg elbows (D/t=39 and R/r=3) under in-plane closing moments. The test data were compared with numerical results from shell elements and simplified elbow elements. Gresnigt et al. [20] reported test data on five 30 deg, five 60 deg and one 90 deg steel elbows (R/r=6) under bending and pressure. The 30 deg and 60 deg specimens were tested under inelastic in-plane bending, whereas the 90 deg specimen was subjected to out-of-plane bending. An analytical model for the elastic-plastic cross-sectional deformation of elbows was also developed by Gresnigt et al. [21-22], introducing a correction factor to account for the influence of the adjacent straight pipe segments. Greenstreet [23] investigated experimentally the response of carbon steel and stainless steel pipe elbows, under in-plane and out-of-plane bending loading conditions, in the presence of internal pressure. Hilsenkopf et al. [24] reported test data on thin-walled (D/t=89.5) stainless steel elbows and thick-walled (D/t=13.4) ferritic elbows under both in-plane and out-of-plane bending, in connection with their functional capability. Suzuki and Nasu [25] conducted two in-plane closing moment tests on a 12-inch 90 deg elbow (D/t=46.3) and on a 24-inch 90 deg elbow (D/t=64.9) and compared the test data with numerical predictions from four-node shell elements. More recently, Tan et al. [26] reported one closing in-plane moment test and one opening in-plane moment test on 90 deg thick stainless steel elbows (D/t=10.5) and compared their measurements with finite element analysis results.

The development of computational methods (e.g. finite elements) has enabled the numerical investigation of elbow response and the prediction of ultimate capacity. To model elbow deformation at the ultimate limit state, a nonlinear analysis accounting for both material and geometric nonlinearities is necessary. Using the special-purpose "elbow" element ELBOW31B of ABAQUS, Shaleby and Younan [27-28] analyzed standalone 90 deg steel elbows (R/r=3) for a wide range of diameter-to-thickness ratios ($15.5 \leq D/t \leq 97$), under in-plane bending (opening and closing moments) and internal pressure. In subsequent papers, Mourad and Younan [29-30]

analyzed pressurized standalone 90 deg steel elbow segments (R/r=3) under out-of-plane bending for a wide range of diameter-to-thickness ratios (15.5≤D/t≤97), using "elbow" element ELBOW32 of ABAQUS. In those investigations [26-29], only the curved part of the pipe was analysed, neglecting the effects of the adjacent straight parts. Chattopadhyay et al. [31] employed general-purpose program NISA to analyze thick 90 deg elbows (D/t≤25) under in-plane bending, through twenty-node fully-integrated solid elements, accounting for the effects of the adjacent straight parts. Using a curve-fitting procedure, simplified formulae were proposed for the collapse (limit) moment capacity in terms of pressure and the bend factor (h=tR/r2). In a recent publication, Karamanos et al. [32] have presented a numerical study of steel elbow response under in-plane bending. Emphasis was given on the buckling failure of non-pressurized thin-walled elbows, and a good comparison was found between numerical results and test measurements reported in [20].

1.6 Scope of present study

The first objective of this study is to examine the effect of cold bending on an initially straight tube via the rotary draw bending method. A parametric study on the manufacturing process aimed at investigating the effects of different bending angles such as 30, 60 and 90 degrees will be presented, focusing primarily on the geometrical deviations in relation to a perfect tube. In addition, stress distribution, thickness variation and cross-section distortion created on the tubes during the process will be examined. Following, the non-linear elastic-plastic response of the bent tubes under in-plane bending loading will be examined to determine their structural capacity and performance. More precisely, in chapter 2, a detailed description of the finite element model developed for the simulation of the rotary draw bending method will be presented. In chapter 3, numerical results concerning out-of straightness of the upper, middle and lower tube generators and out-of roundness of several deformed tube rings will be depicted. In addition, pipe wall thickness variation and stress distribution on the three generators will be presented with respect to angle θ. In chapter 4, the bending moment M as

well as the ovalization of the elbows will be compared with the perfect elbows. Finally, in chapter 5, the conclusions of this study will be presented.

Chapter 2

Finite element simulation of rotary-draw forming

2.1 Finite element simulation tools

In the present study, the Rotary Draw Bending (RDB) method is simulated using finite elements. An improved three-dimensional-finite element (3D-FE) model of the process for round steel tube has been developed within the explicit code ABAQUS/Explicit. Then, simulation and analysis of the process have been carried out based on the finite elements model. For computational reasons and due to the symmetry of the problem half of model has been considered in the finite element analysis.

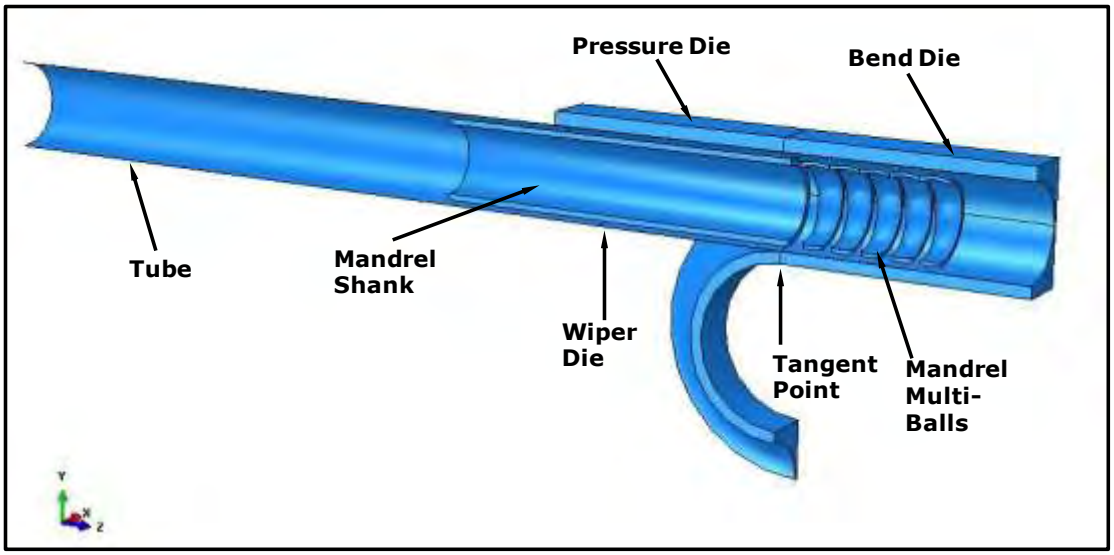

Figure 3: Schematic of tube bending with external and internal tool

As shown in Figure 3, pulled by bend die, the tube goes past the tangent point and rotates along the groove of bend die up to the desired bending degree and bending radius. Then the mandrel retracts and the tube is unloaded.

Each die has a different role, in terms of its effect on the stress and strain distribution and material flow state. More precisely,

1. The bend die is the primary tool which determines the bend radius of the tube.
2. The pressure die is used to maintain constant pressure on the tube, at tangent where the bending is occurring, and pushes it against the wiper die tightly ensuring the free-wrinkling bending tube. Meanwhile, the moving pressure die helps push the material into bending regions reducing the thinning degree.
3. The wiper die is used to prevent the tube from wrinkling and over cross-section distorting. The wiper die nests in the bend die groove with its very thin tip extending to the bend tangent point (the point where the tube will begin to bend). Therefore, it fills up the gap normally left by the bend die, so that, the tube is completely confined and does not have space in which to wrinkle.
4. The mandrel shank with flexible balls is used inside the tube to prevent from wrinkling and over cross-section distorting.

In the present work a initially straight tube with diameter to thickness ratio D/t=19 (D=38 mm and t=2 mm) and R_d/D=1.5 is considered. The tube is rotated to 30°, 60° and 90° with a bending radius R_d=57 mm. The dimensions chosen, taking into account the relevant literature [19, 23, 24], for the tube and the tooling are shown in Table 1.

Tube	Dimensions / mm	
Outer Diameter	38	
Wall Thickness	2	
Length	480	
Tooling Parameter	Dimensions / mm	
	Length	Groove diameter
Pressure Die	100	38.04
Bend die	-	38.12
Wiper die	80	38.12
Mandrel Parameter		
Mandrel Shank	Length = 153 mm, Groove dia. = 33.72 mm	
Balls diameter	33.72 mm	
Balls Thickness	9.9 mm	
Balls Number	5	

Pitch	12 mm

Table 1: Geometry dimensions of tools

Regarding the material properties of the tube and in order to simulate the real mechanical behavior of steel under bending, both the elasto-plastic and the mechanical properties of Steel, API 5L, Grade X52 were used for the tube. Property values are shown in Table 2,Table **3** and Figure 4.

Modulus of Elasticity (E) [MPa]	**Poisson Ratio** (v)
210000	0.3

Table 2: Elastic Properties of Steel X52

Yield Strength [MPa]	**Tensile Strength** [MPa]	**Elongation** (%)
400	440	21

Table 3: Mechanical Properties of Steel X52

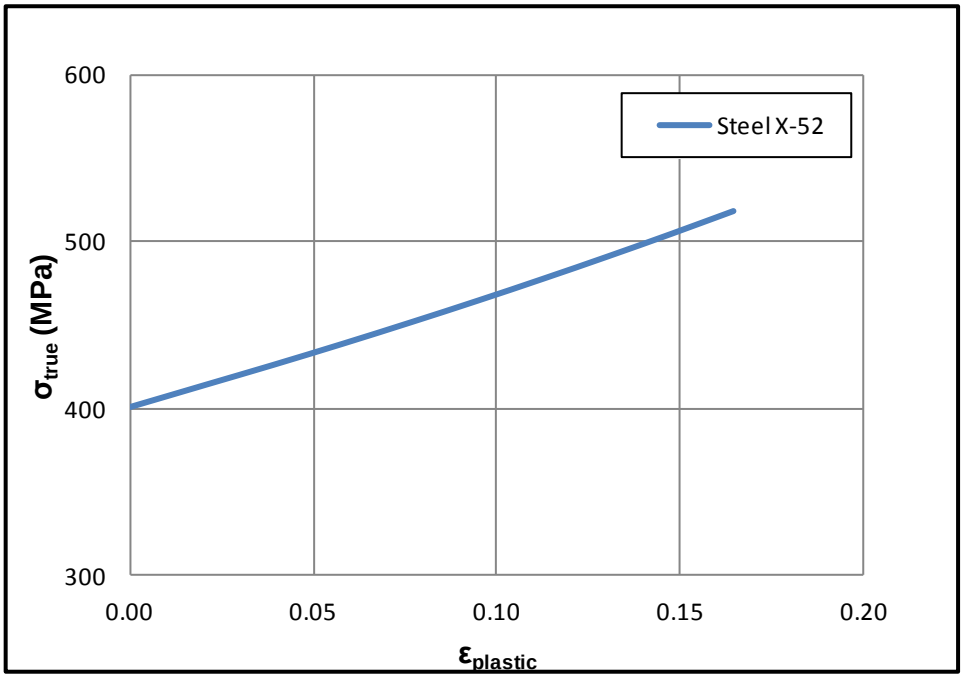

Figure 4: Stress-Strain curve for plastic properties of Steel X-52

From finite element point of view, the steel tube is modeled as a continuous, homogeneous shell having reference surface the inner surface.

The element type used to describe the tube is a 4-node doubly curved thin shell (t=2 mm) S4R. This is a robust, general-purpose reduced integration four-node shell element suitable for a wide range of applications in tubular members subjected to loading that induces significant geometric and material non-linearities.

In this element, to avoid shear and membrane locking, uniform reduced integration (5 integration points), as well as classical shear theory for thin shells is applied.

Concerning the tube mesh, the approximate element size used was 2 mm while the number of the elements was only allowed to increase (Figure 5).

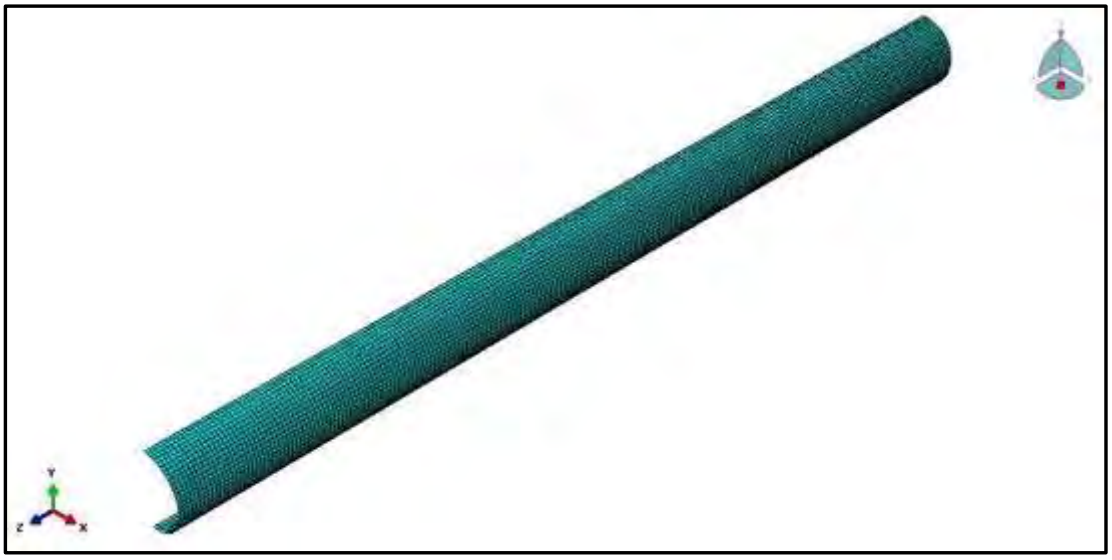

Figure 5: Tube Meshing

In addition, the dies are modeled as discrete, rigid bodies. In Abaqus/Explicit a rigid body is a collection of nodes and elements whose motion is governed by the motion of a single node, known as the rigid body reference node. The shape of the rigid body is defined as a discrete rigid body obtained by meshing the body with nodes and elements. Regarding the modeling of the tube, the size method was used for meshing the dies with element size approximately 2 mm (Figure 6). The element type used for meshing the dies is the R3D4, a 4-node 3-D bilinear rigid element that makes it possible to model complex surfaces with arbitrary geometries. The shape of the rigid body remains unchanged during the simulation but can undergo large rigid body motions.

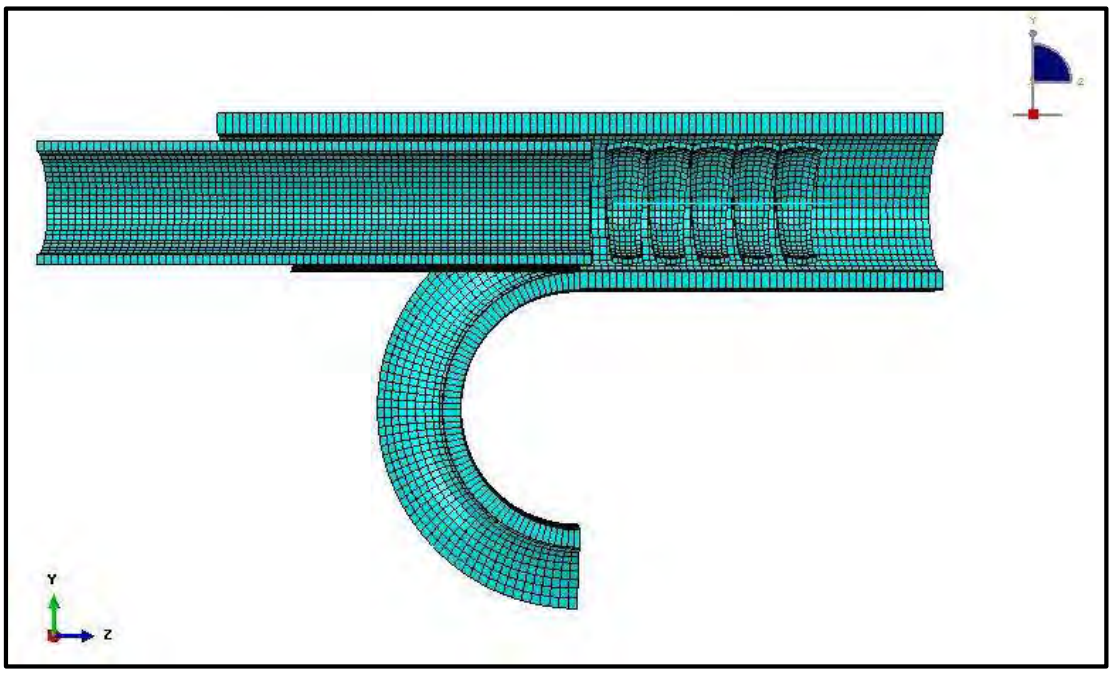

Figure 6: Tooling Mesh

The motion of a rigid body can be prescribed by applying boundary conditions at the rigid body reference node. Loads on a rigid body are generated from concentrated loads applied to nodes and distributed loads applied to elements that are part of the rigid body or from loads applied to the rigid body reference node. Rigid bodies interact with the rest of the model through nodal connections to deformable elements and through contact with deformable elements.

The interaction between tube and tooling is needed to accomplish the thin-walled tube bending process in order to ensure the prevention of wrinkling despite the presence of pipe wall thinning and cross-section distortion.

In this model, the following contact interfaces appear:

1. Tube-Wiper die
2. Tube-Mandrel
3. Tube-Pressure Die
4. Tube-Bend die
5. Tube-Multi Balls

In all these interfaces "surface to surface" contact and "penalty contact method" for mechanical constraint formulation is used.

In addition, mechanical contact properties between the tube and the dies had to be determined for the simulation. Towards this purpose, frictionless contact is applied for the tangential behavior, while "hard" contact is used for the normal direction.

As mentioned above, every rigid body is characterized by a reference point (RP). As shown in Figure 7, RP1 refers to the mandrel shank, while RP2 to RP5 refer to the mandrel balls respectively.
In order to simulate mandrel balls movement mechanism during the bending process, two-node beam elements are used. The beams are constrained using Multi-Point Constraints (MPC) of two different types, namely "pin" and "tie", and are applied to each reference point.

The "Tie" constraint makes all active degrees of freedom equal at each slave node and the control point, while the "Pin" constraint defines a pinned joint between each slave node and the control point.

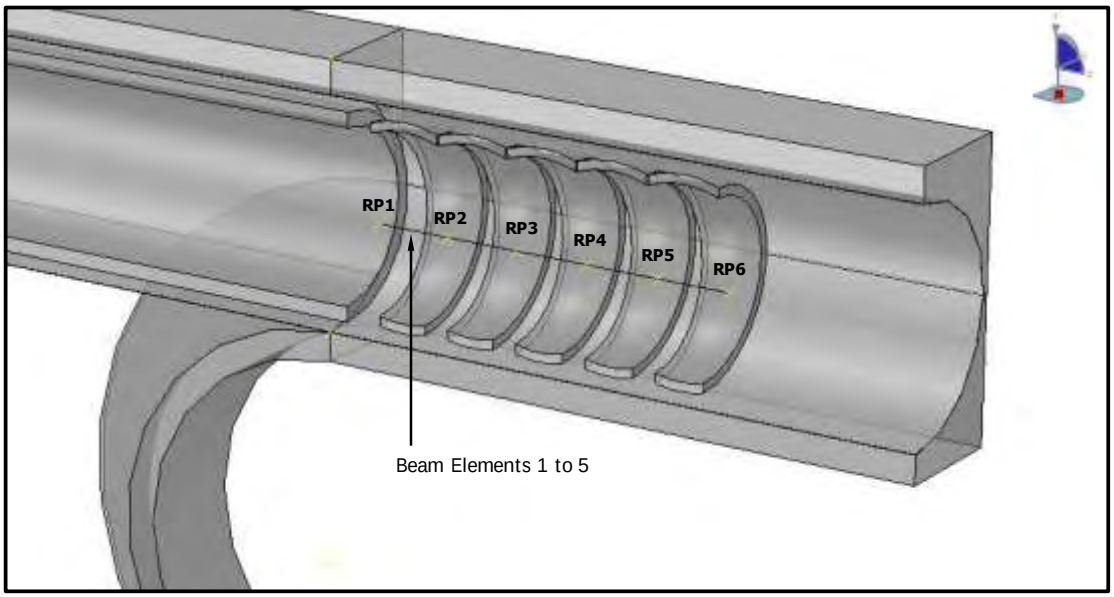

Figure 7: Beam elements

More precisely, at each reference point the following constraints are applied:

- RP1: A pin constraint is created between the mandrel shank and the first node of beam 1.

- RP2: A tie constraint is created between the 2nd node of beam 1 and the first mandrel ball while a pin constraint is created between the first node of beam 2 and the first mandrel ball.
- RP3: A tie constraint is created between the 2nd node of beam 2 and the second mandrel ball while a pin constraint is created between the first node of beam 3 and the second mandrel ball.
- RP4: A tie constraint is created between the 2nd node of beam 3 and the third mandrel ball while a pin constraint is created between the first node of beam 4 and the third mandrel ball.
- RP5: A tie constraint is created between the 2nd node of beam 4 and the fourth mandrel ball while a pin constraint is created between the first node of beam 5 and the fourth mandrel ball.
- RP6: A tie constraint is created between the 2nd node of beam 5 and the fifth mandrel ball.

On all above MPC constraints, the reference points act as control points while the beam nodes act as slave nodes. Consequently, it is very important to define the boundary conditions in such a way that the real manufacturing process is simulated. RP7, as shown in Figure 8, is the point that refers to the bend die and is responsible for the bending process as there the bending angle is applied. All dies and the tube shall conform to this bending angle. As a result, rotation angles of 30, 60 and 90 degrees are imposed on RP7.

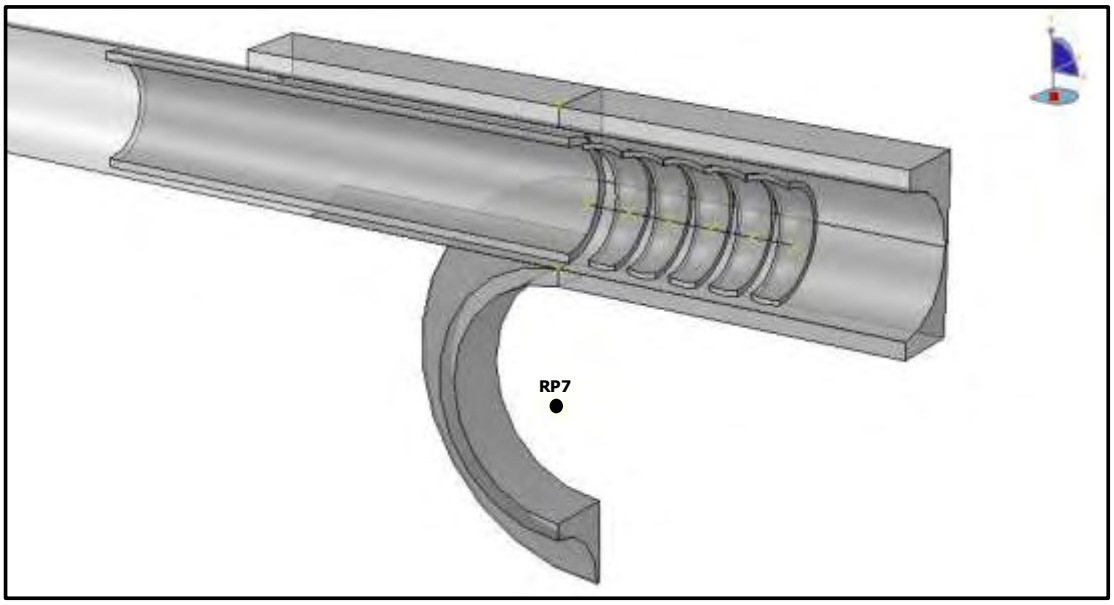

Figure 8: Point of bending angle application

The tube follows exactly the bend die movement. For this reason, displacements along x-axis and y-axis as well as rotations around all axes are restricted. Movement on z-axis is permitted. The mandrel shank during the process is immovable. Movements and rotations are restricted.

Concerning the mandrel balls, they are free to move on y-axis and z-axis as well as to rotate on x-axis. All other boundary conditions are restricted.

The wiper die is fixed to the tangent point, and no rotation or displacement is allowed.

The pressure die follows the motion of the bend die.

Finally, for the whole model x-symmetry condition is imposed. As a result, displacement on x-axis and rotations on y-axis and z-axis are restricted.

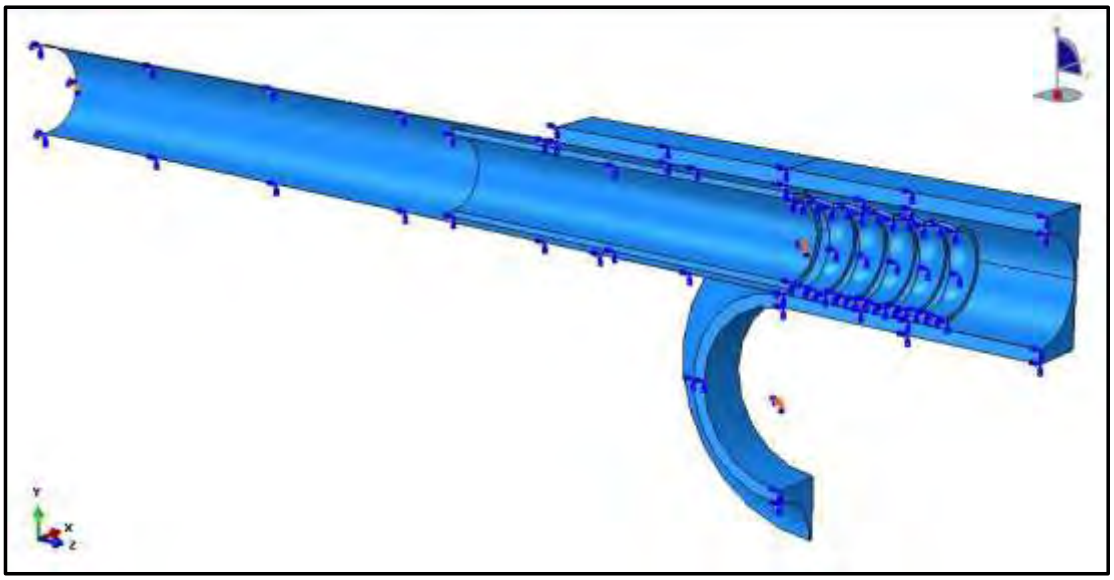

Figure 9: Boundary conditions

Chapter 3

Numerical results on pipe cold bending

The first objective of this study is to simulate bending of an initially straight tube (Figure 10) to different angles and evaluate the geometrical deviations from a tube without geometric defects. Three angles of bending are considered, 30, 60 and 90 degrees as shown in Figure 11, Figure 12, Figure 13. For all bending angles results for out-of straightness and out-of roundness were extracted. In addition, wall thickness variation in the bend area and stress distribution is examined for the same three generators.

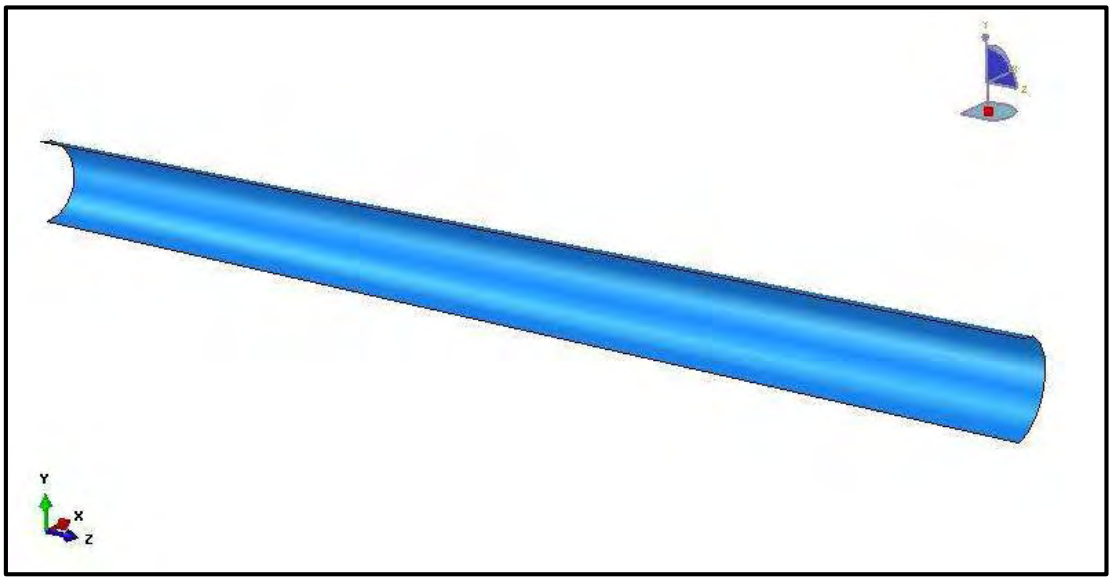

Figure 10: Straight tube subjected to bending

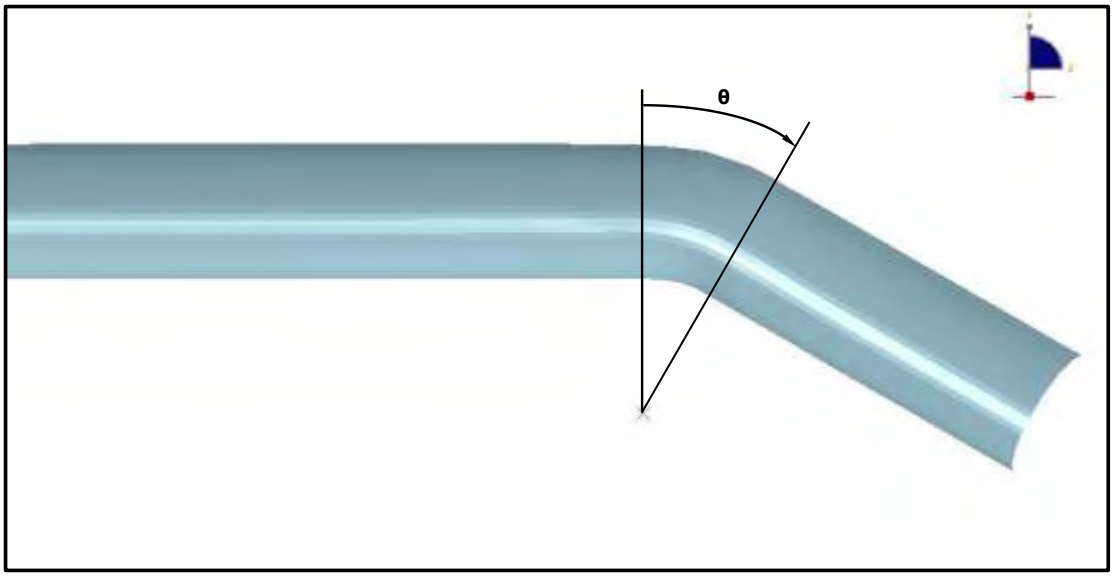

Figure 11: 30 degrees tube bending

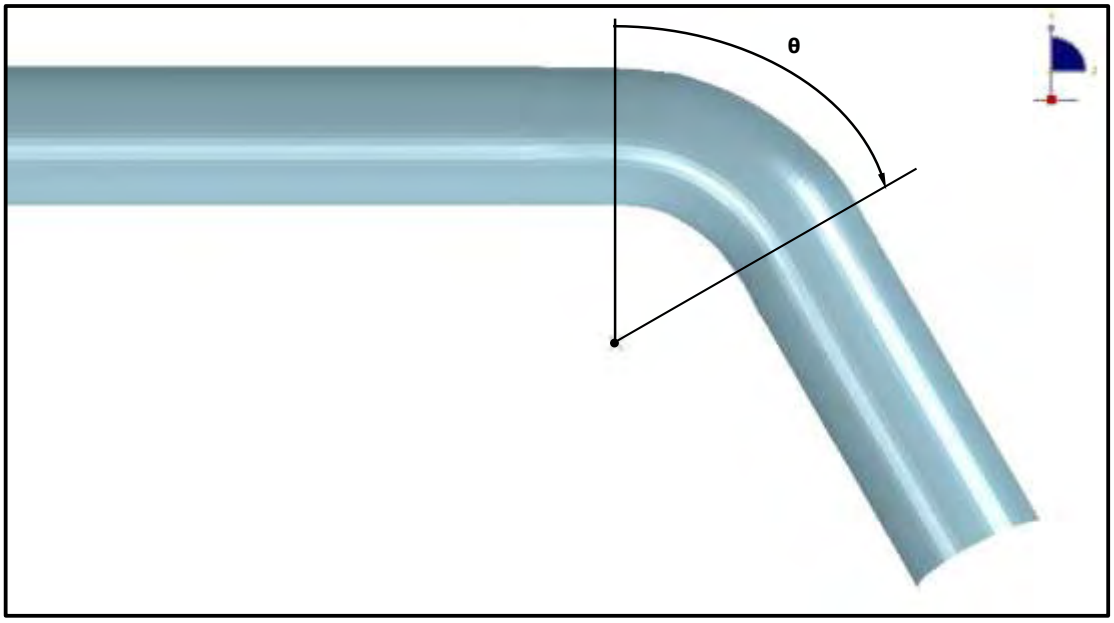

Figure 12: 60 degrees tube bending

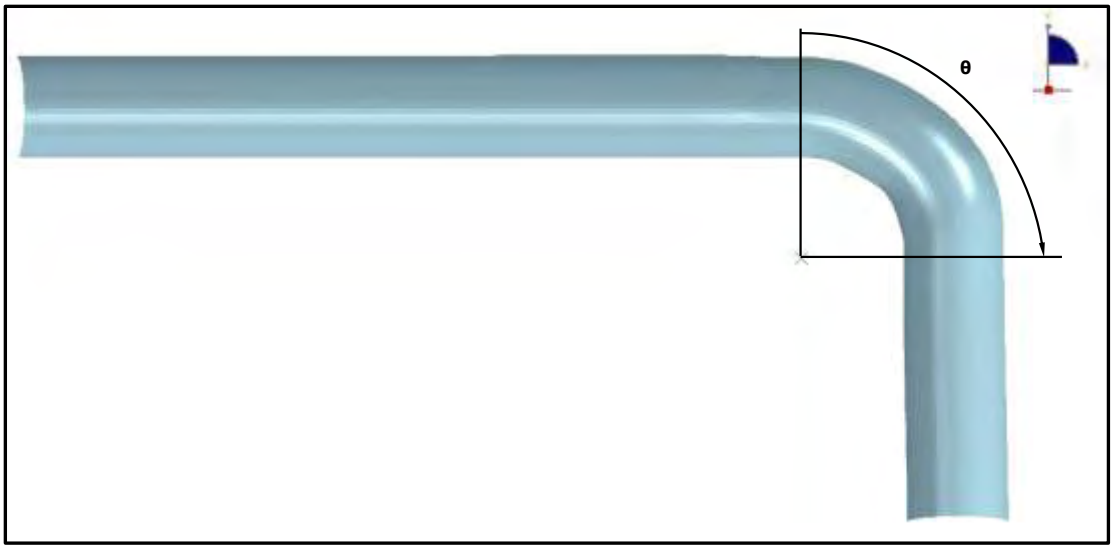

Figure 13: 90 degrees tube bending

3.1 Out-of "straightness"

Out-of "straightness", for all bending angles, is calculated for three tube generators in the bend area, the upper, the middle and the lower. The examined segments of the three generators consist of a number of nodes as shown in Figure 14Figure 15Figure 16. Each node at the end of the bending process is displaced with respect to its initial position. The final position of every node on the generators is calculated by adding the y-axis and z-axis displacements to the initial y-axis and z-axis coordinates. To plot the out-of "straightness", the y and z displacement values are normalized with the bending radius of each generator. For the upper generator the radius is 76 mm, for the middle is 57 mm, while for the lower generator it is 38 mm. Results are compared with the 30, 60 and 90-degree circular segment of a perfect tube respectively.

In Figure 17Figure 18Figure 19 the out-of "straightness" of the 30-degree tube, in the upper, middle and lower generator respectively, is shown. The results depicted in those figures demonstrate that each generator behaves in a different way compared to the generators of a perfectly circular tube that follows the bend axis. The upper generator shows, at the early bending stage, a deviation from the perfect curve, but as the angle along the bend increases the deformed shape obtained is very similar to the perfect. The middle generator shows a steady deviation from the perfect curve while the lower

generator shows at first a good comparison with the perfect curve but as the angle along the bend increases the deviation increases.

In Figure 20Figure 21Figure 22 the out-of ‟straightness″ of the 60-degree tube, in the upper, middle and lower generator respectively, is shown. The results obtained show that the upper generator follows quite well the perfect behavior, the middle generator shows a steady deviation from the perfect curve, smaller than that observed in the 30-degree elbow, while the lower generator is quite close to the perfect curve at the beginning and at the end of the bend.

In Figure 23Figure 24Figure 25 the out-of ‟straightness″ of the 90-degree tube, in the upper, middle and lower generator respectively, is shown. The results obtained show that all generators have a quite similar behavior. The curve deviation increases as the angle along the bend increases.

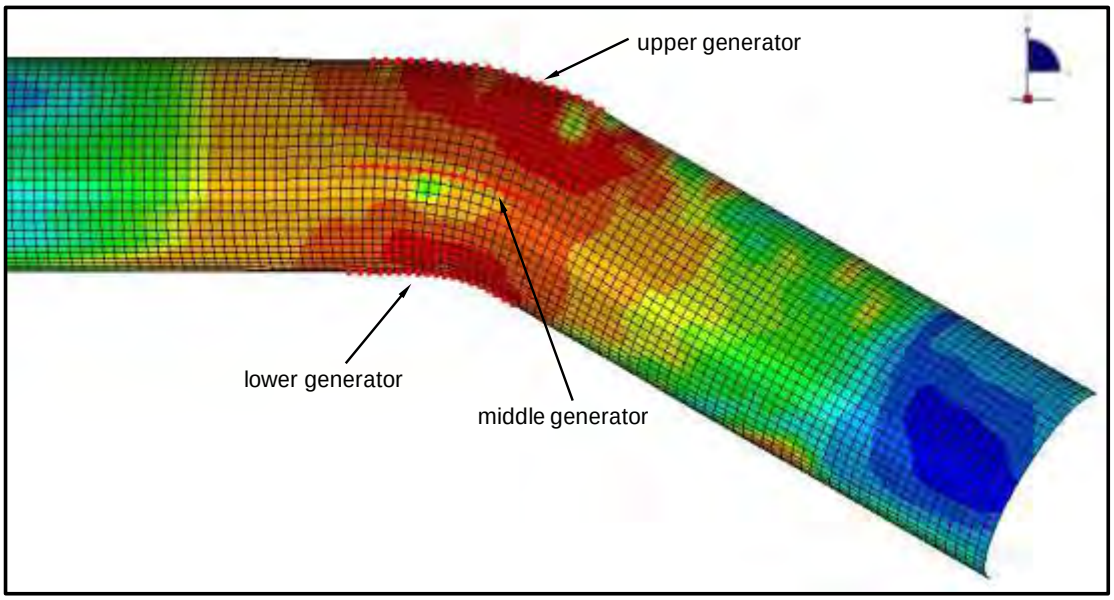

Figure 14: Upper, middle and lower generator of the 30-degree tube

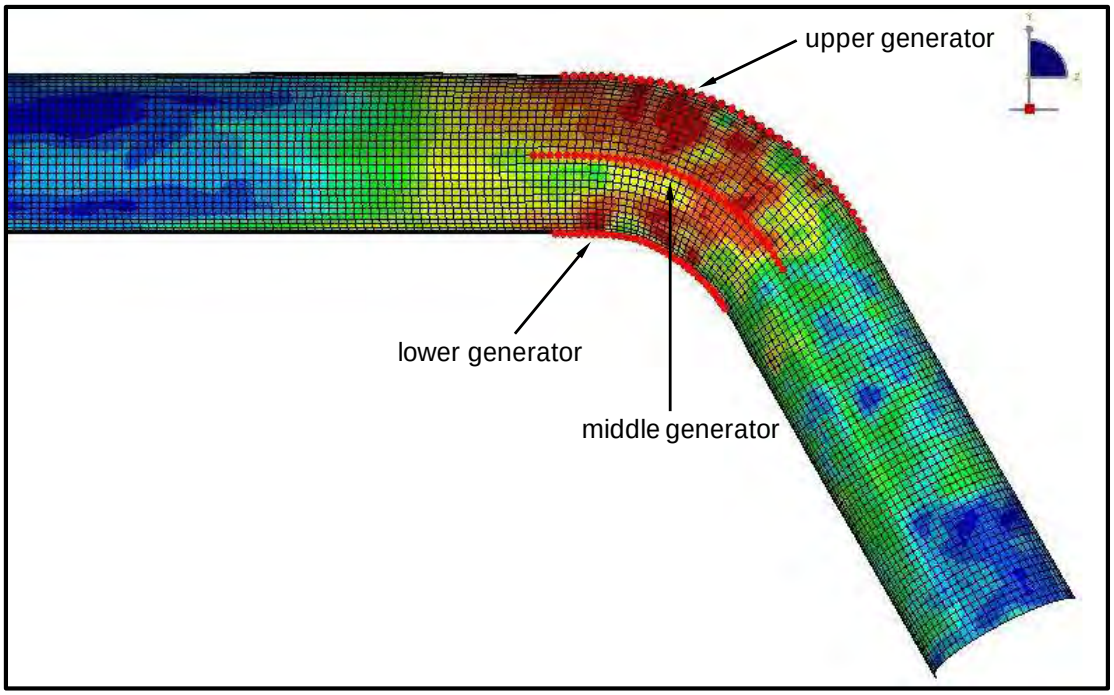

Figure 15: Upper, middle and lower generator of the 60-degree tube

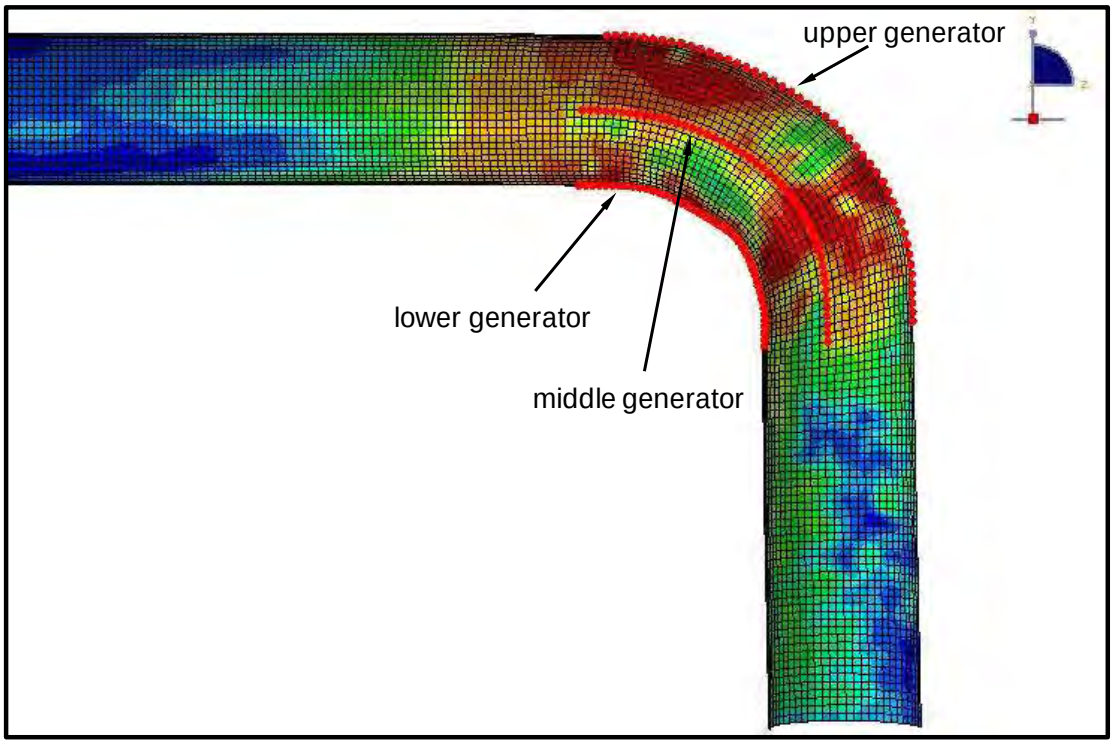

Figure 16: Upper, middle and lower generator of the 90-degree tube

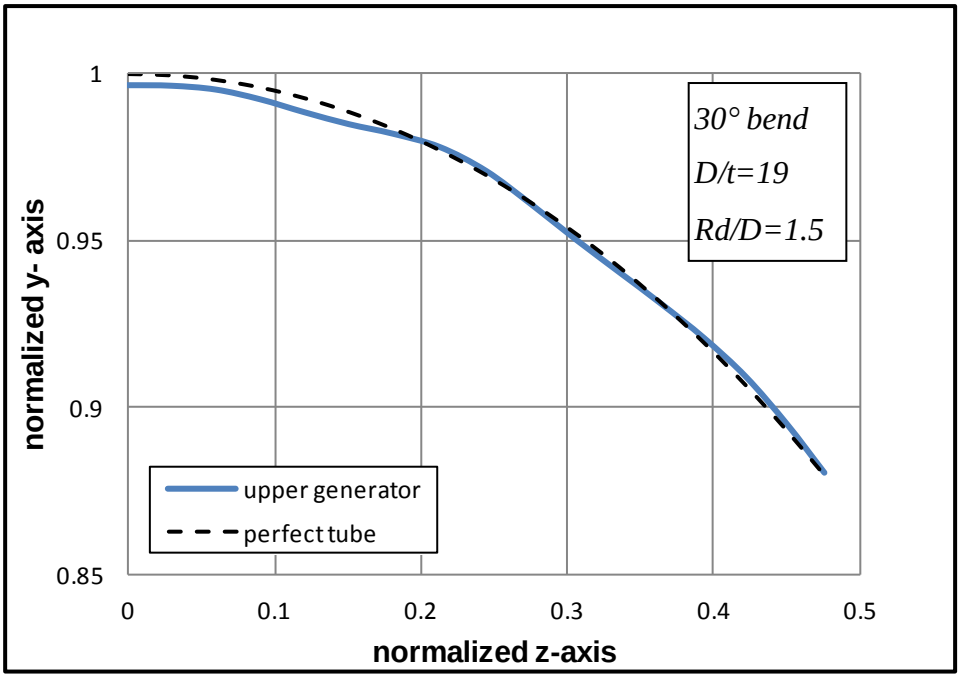

Figure 17: Out-of "straightness" of the 30-degree elbow upper generator

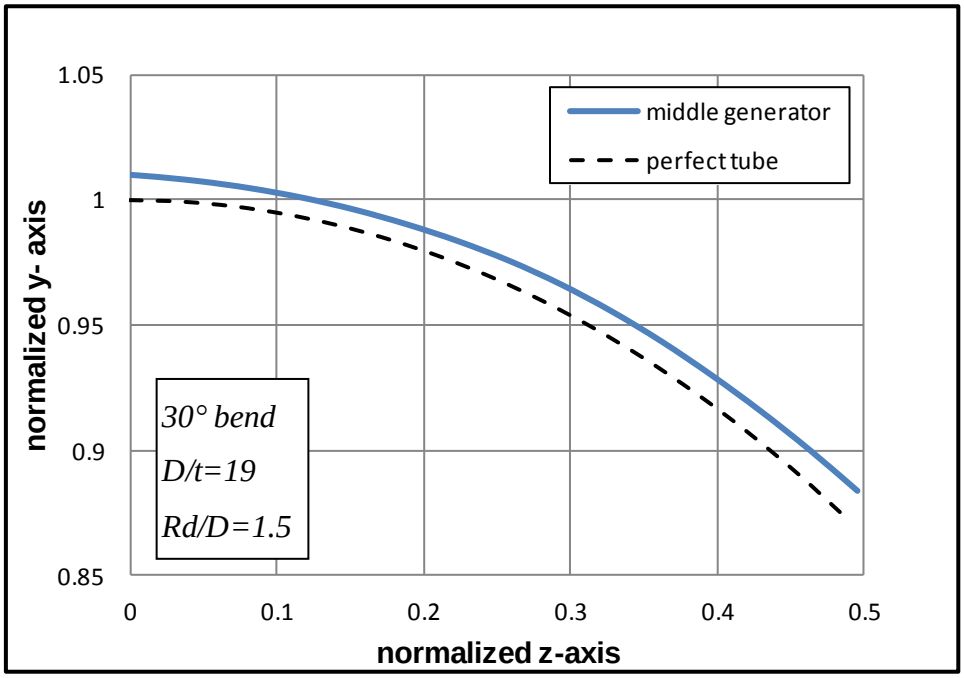

Figure 18: Out-of "straightness" of the 30-degree elbow middle generator

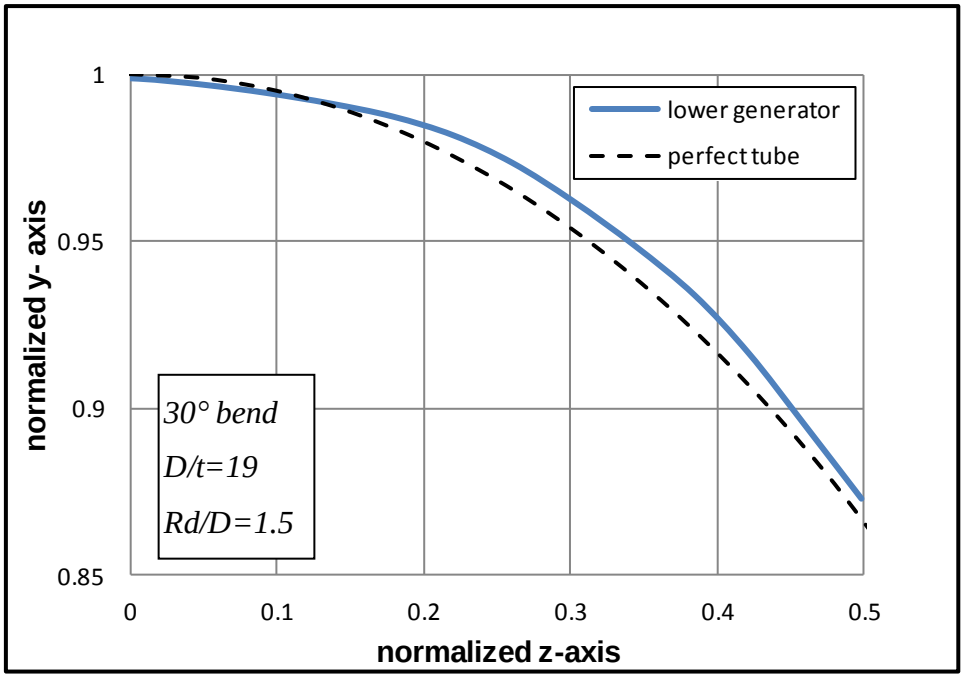

Figure 19: Out-of "straightness" of the 30-degree elbow lower generator

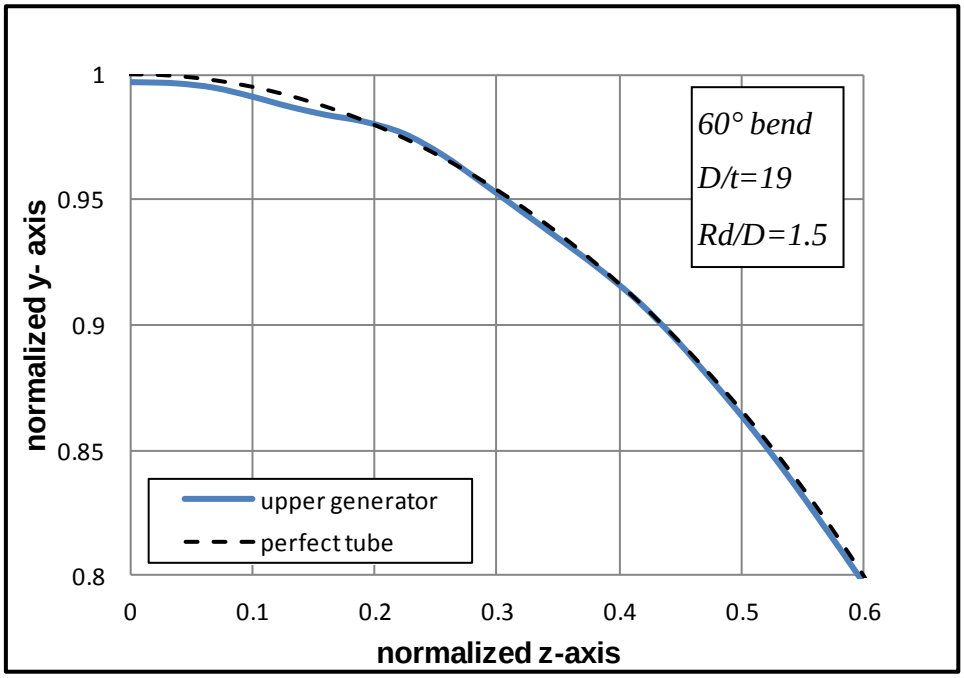

Figure 20: Out-of "straightness" of the 60-degree elbow upper generator

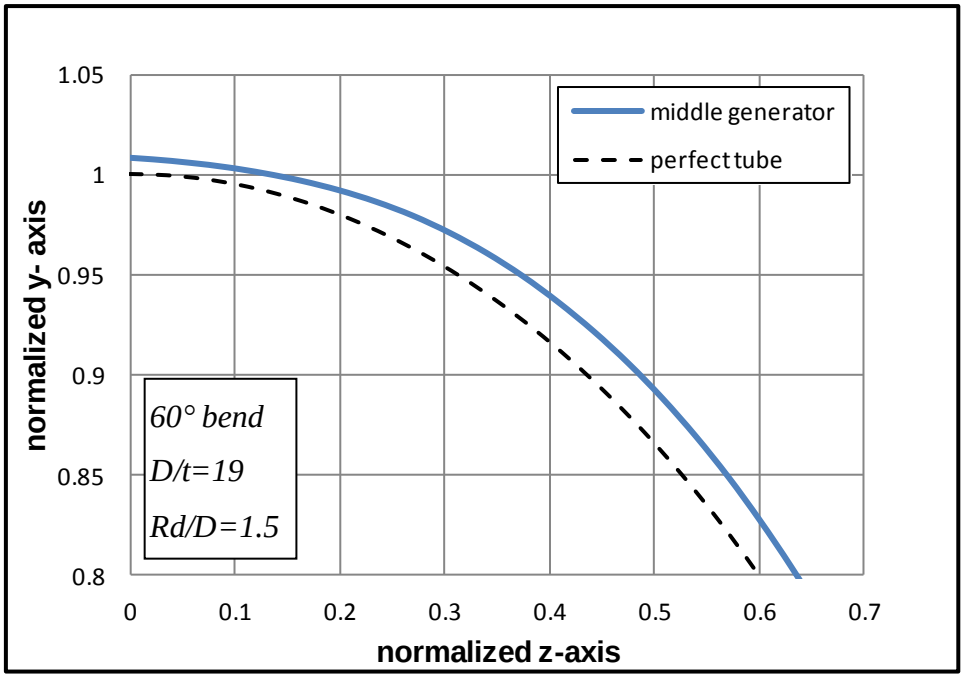

Figure 21: Out-of "straightness" of the 60-degree elbow middle generator

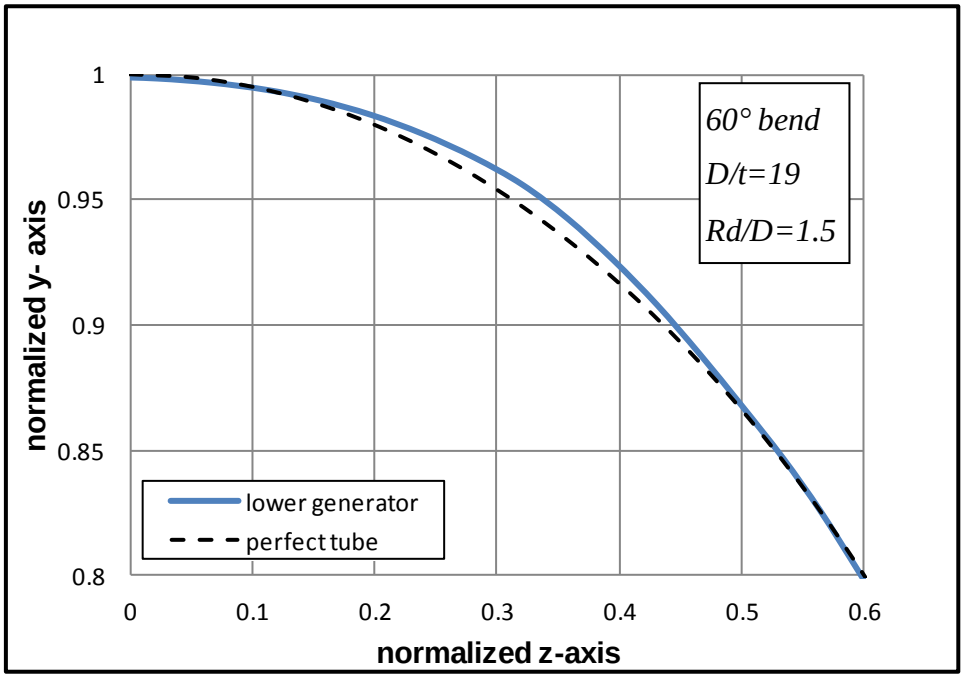

Figure 22: Out-of "straightness" of the 60-degree elbow lower generator

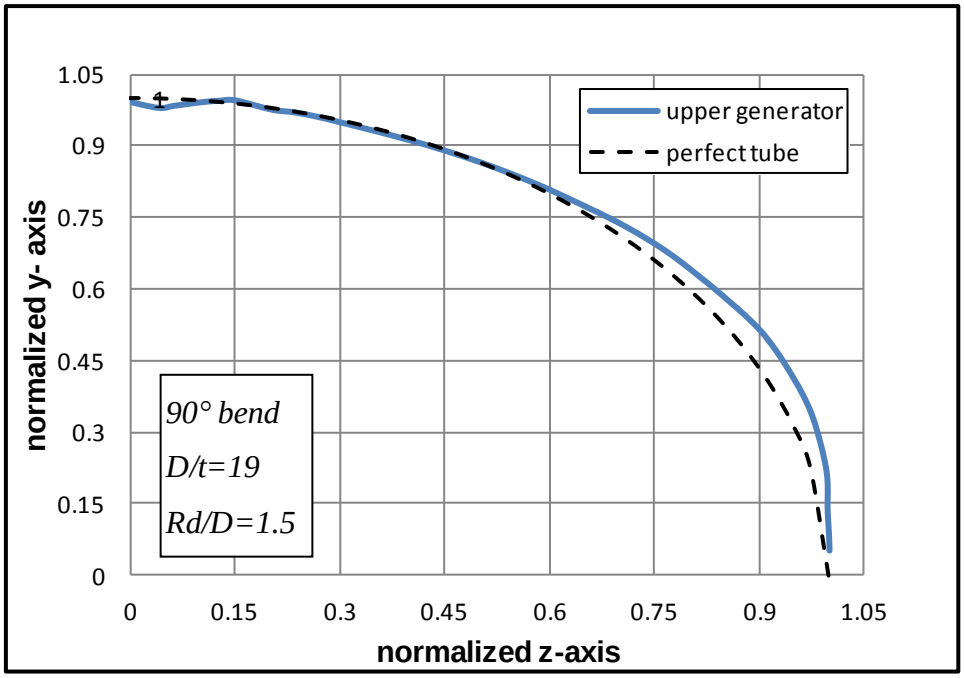

Figure 23: Out-of "straightness" of the 90-degree elbow upper generator

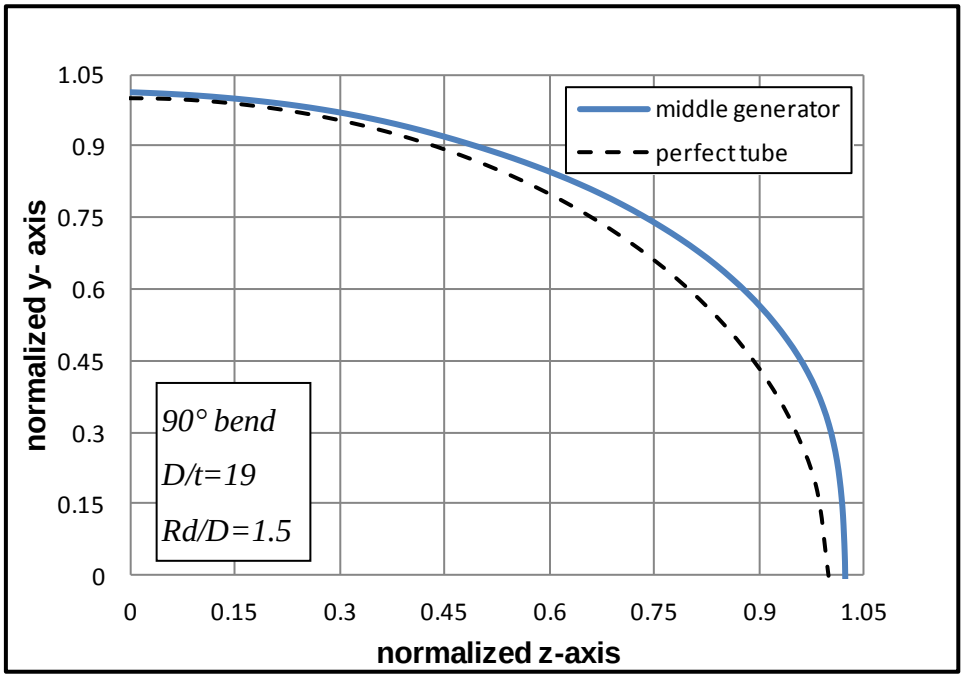

Figure 24: Out-of "straightness" of the 90-degree elbow middle generator

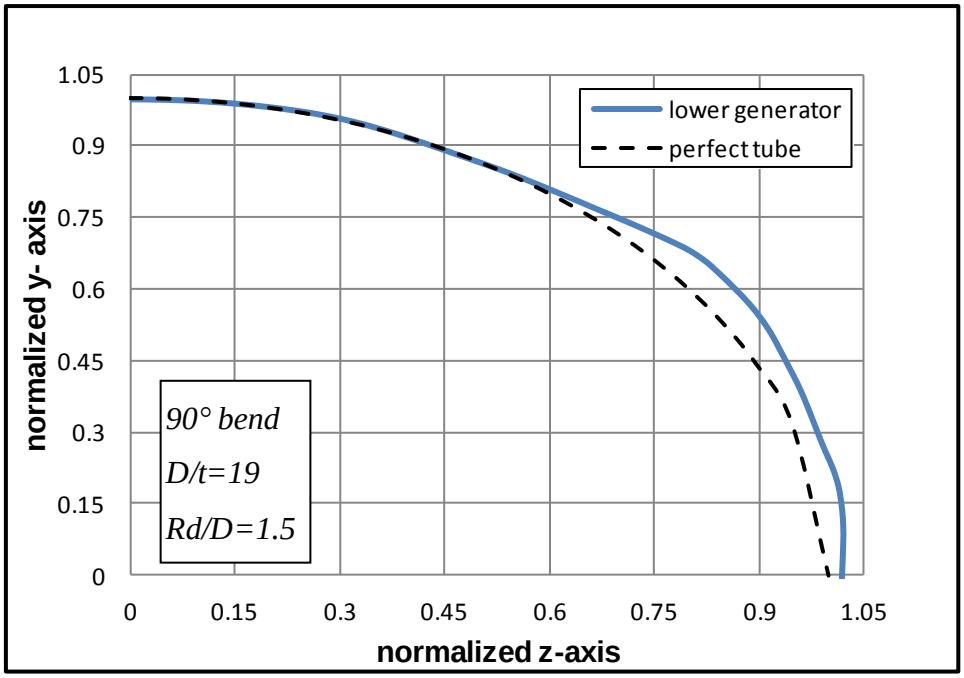

Figure 25: Out-of "straightness" of the 90-degree elbow lower generator

According to Figure 26, every node on the three generators is characterized by a radius r. We denote as r_{in} the radius of node k′ on the lower generator and as r_{out} the radius of node k on the upper generator. To calculate the value of radius r the y and z coordinates of every node are used. Then, for each generator, the deviation Δr is calculated from the difference Δr=r-R, where R is the radius of the generator of the perfect bend tube. Finally, the bending angle θ of every node is calculated by using the tangent from its y and z coordinates.

In Figure 27Figure 28Figure 29 the deviation Δr of each generator of the 30-degree tube from the geometry of the corresponding perfect tube with respect to the bend angle θ is plotted. The results depicted from the above figures demonstrate that the maximum diameter deviations from the perfect tube are localized in different bending angles for the three generators. More precisely, for the upper generator the maximum deviation of the deformed diameter is 0.3 mm and this occurs at bend angle equal to 7°. For the lower generator, the maximum deviation of the deformed diameter is 0.38 mm and this occurs at bend angle equal to 22° while for the middle generator the values change to 0.75 mm and 29° respectively.

In Figure 30Figure 31Figure 32 the deviation Δr of each generator of the 60-degree tube from the perfect geometry with respect to the bend angle θ is

plotted. The results show for the upper generator that the maximum deviation of the deformed diameter is 0.35 mm and this occurs at bend angle equal to 7°. For the lower generator, the maximum deviation of the deformed diameter is 0.32 mm and this occurs at bend angle equal to 18.5° while for the middle generator the values change to 1.34 mm and 58° respectively.

In Figure 33Figure 34Figure 35 the deviation Δr of each generator of the 90-degree tube from the perfect geometry with respect to the bend angle θ is plotted. The results show for the upper generator that the maximum deviation of the deformed diameter is 2.78 mm and this occurs at bend angle equal to 58°. For the lower generator, the maximum deviation of the deformed diameter is 2.1 mm and this occurs at bend angle equal to 50° while for the middle generator the values change to 3.59 mm and 53° respectively.

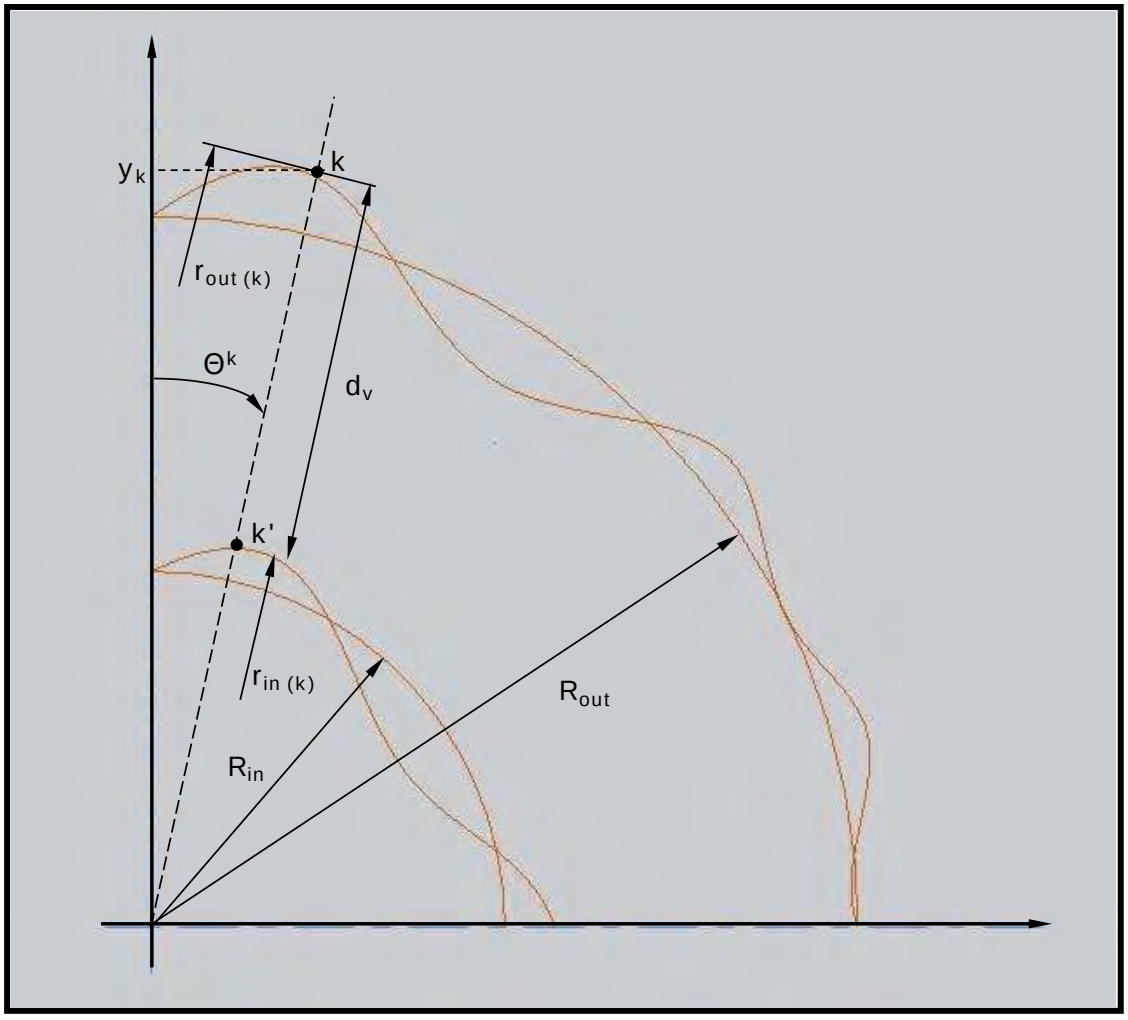

Figure 26: Geometric characteristics of upper and lower generators

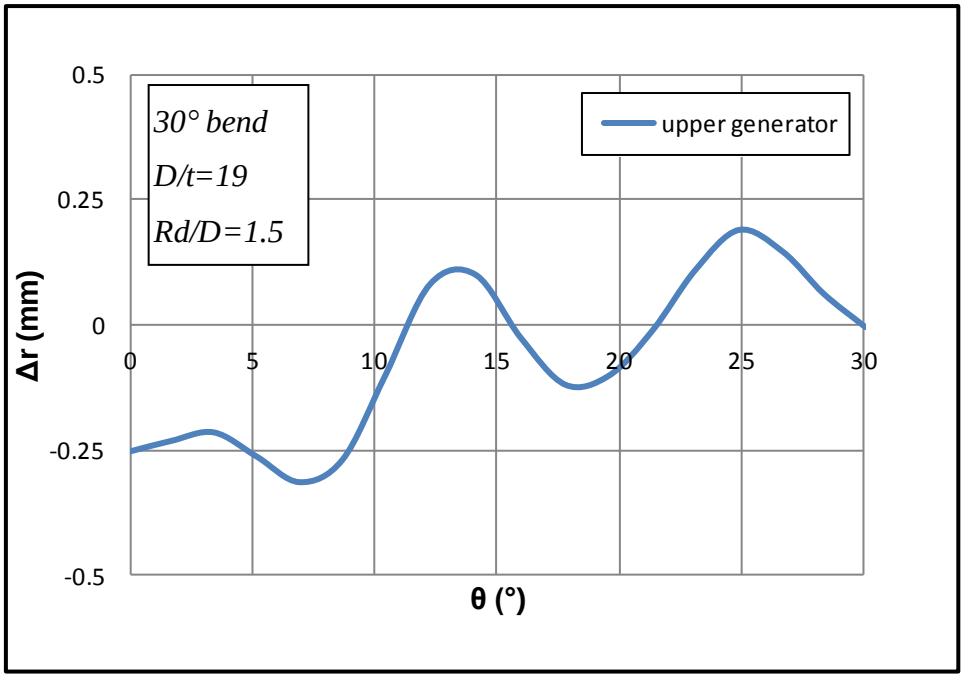

Figure 27: Radius deviation from perfect tube, for the 30-degree elbow upper generator

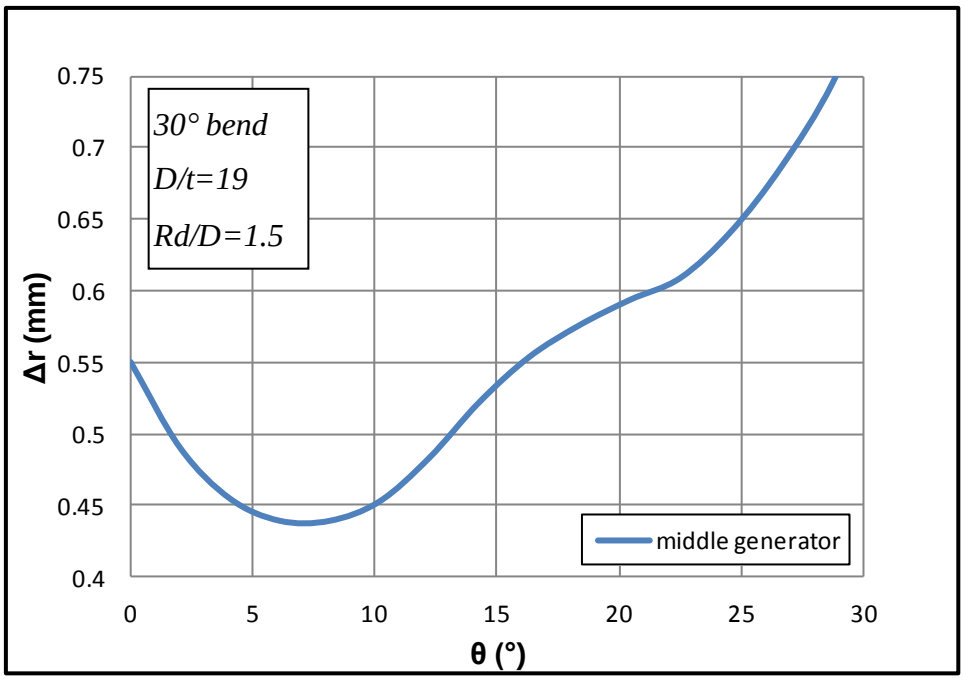

Figure 28: Radius deviation from perfect tube, for the 30-degree elbow middle generator

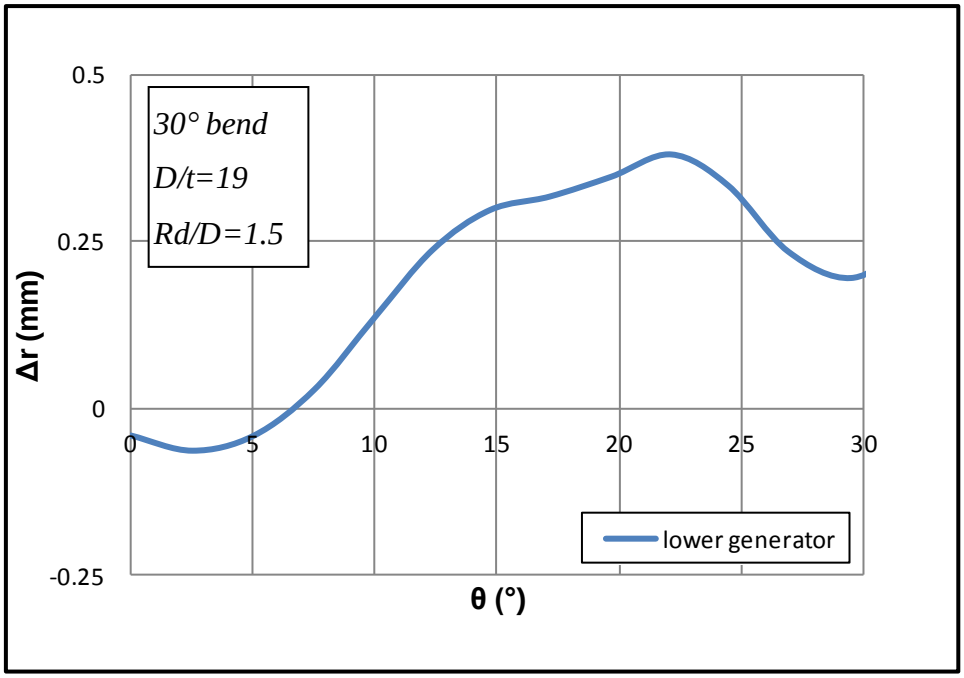

Figure 29: Radius deviation from perfect tube, for the 30-degree elbow lower generator

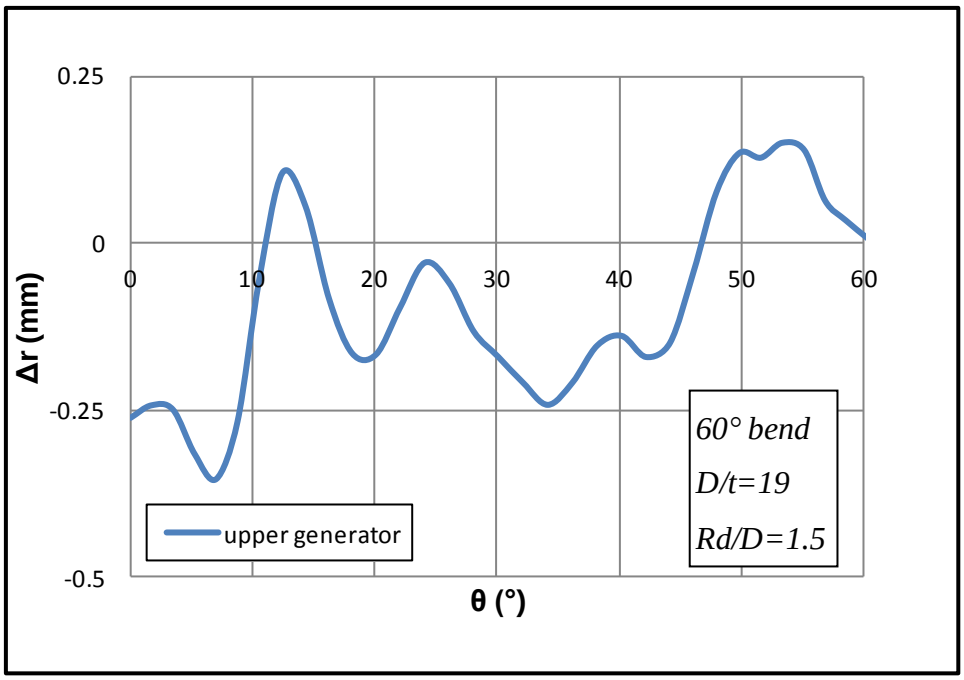

Figure 30: Radius deviation from perfect tube, for the 60-degree elbow upper generator

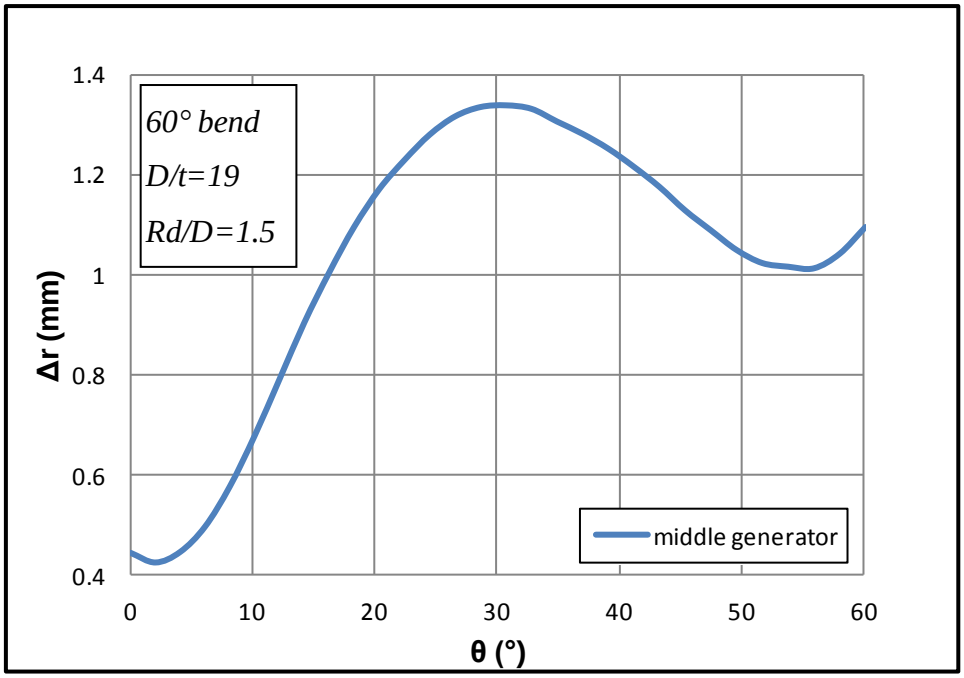

Figure 31: Radius deviation from perfect tube, the 60-degree elbow middle generator

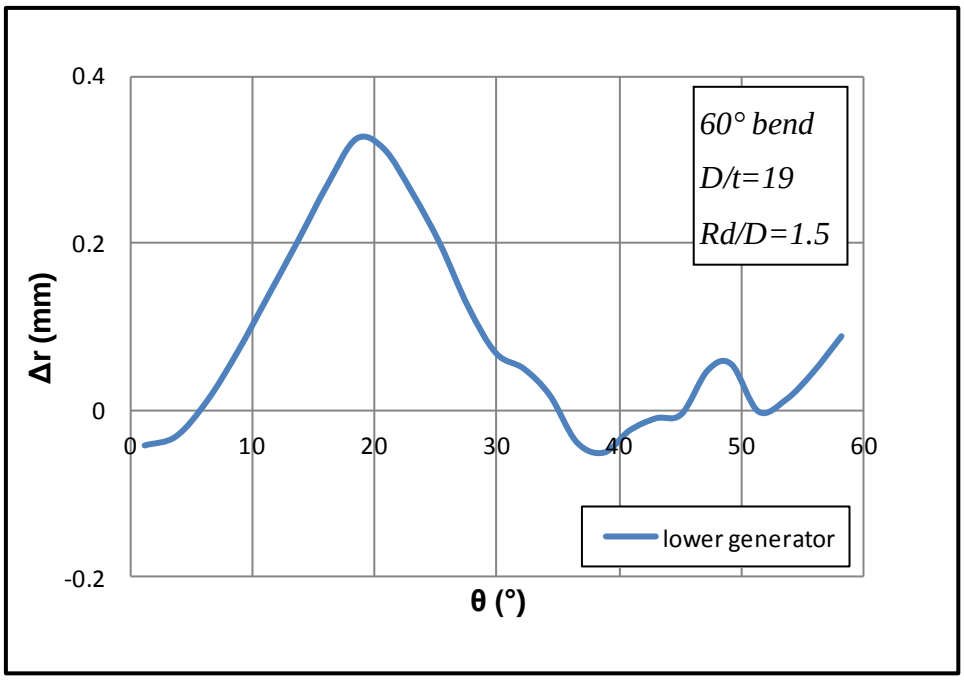

Figure 32: Radius deviation from perfect tube, the 60-degree elbow lower generator

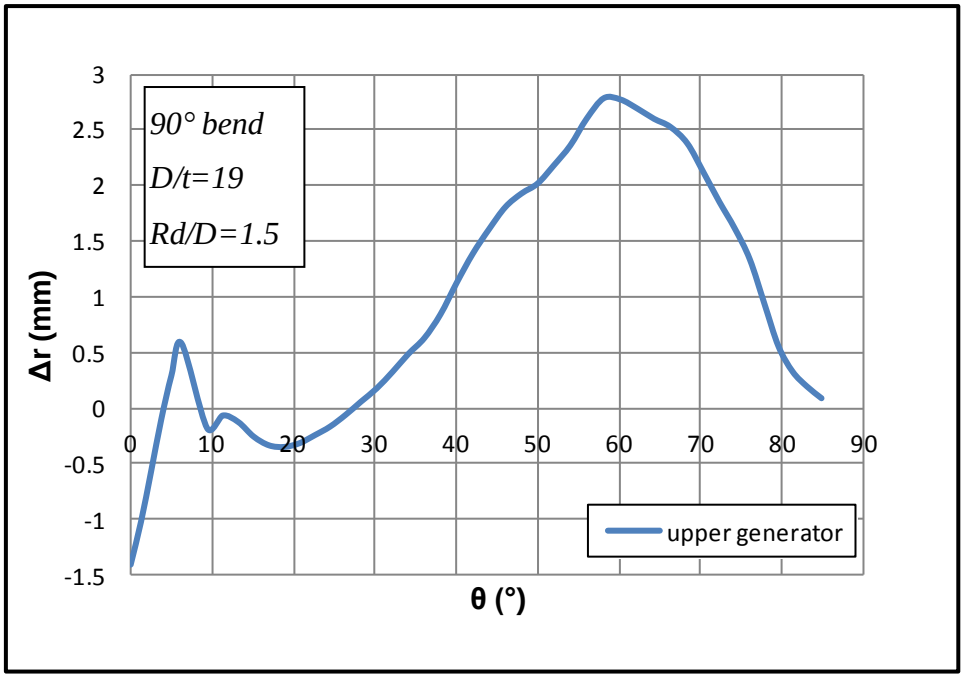

Figure 33: Radius deviation from perfect tube, the 90-degree elbow upper generator

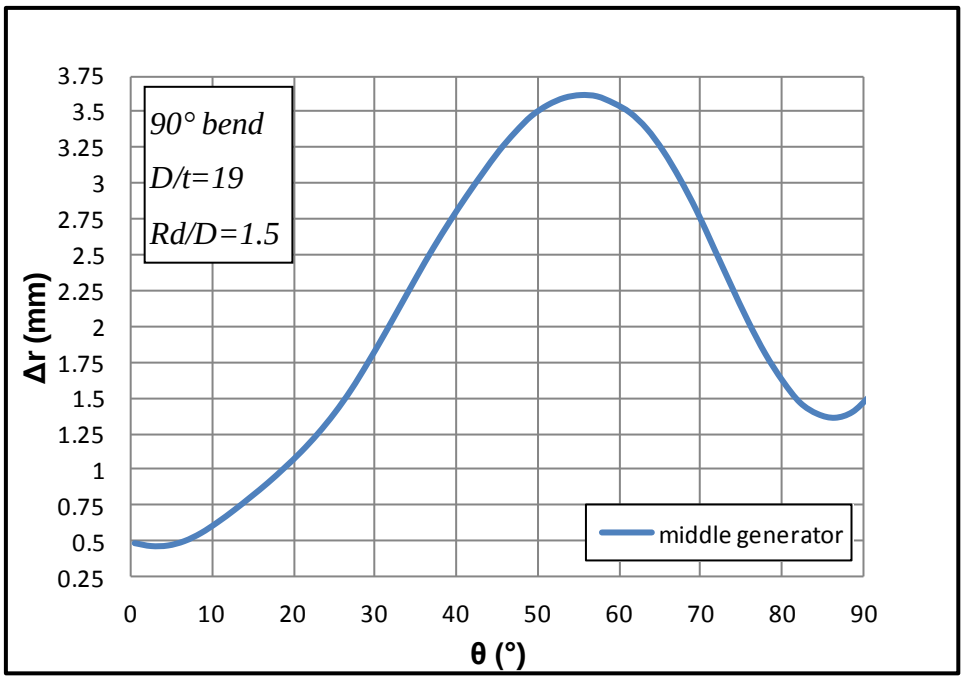

Figure 34: Radius deviation from perfect tube, the 90-degree elbow middle generator

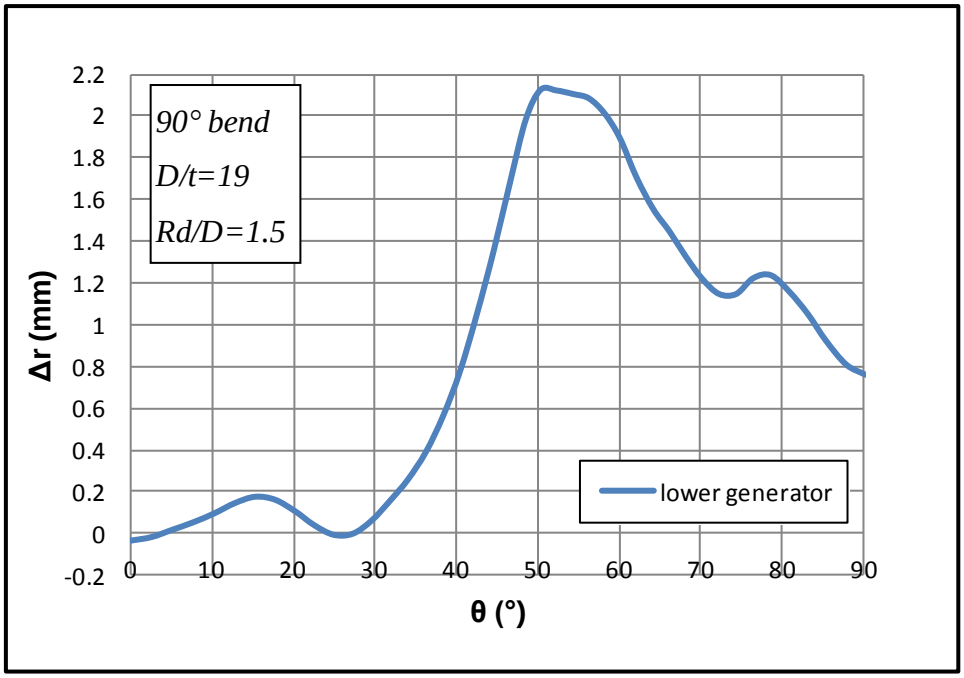

Figure 35: Radius deviation from perfect tube, the 90-degree elbow lower generator

In Figure 36Figure 37Figure 38 the diameter d_v of the deformed tube is compared to the diameter of the perfect tube and plotted in terms of the bending angle θ. As depicted in those figures, the tube diameter formed during the 30-degree elbow bending process ranges from 35.55 mm to 37.96 mm. For the 60 degrees ranges from 37.42 mm to 38.12 mm while for the 90 degrees from 36.63 mm to 39.55 mm.

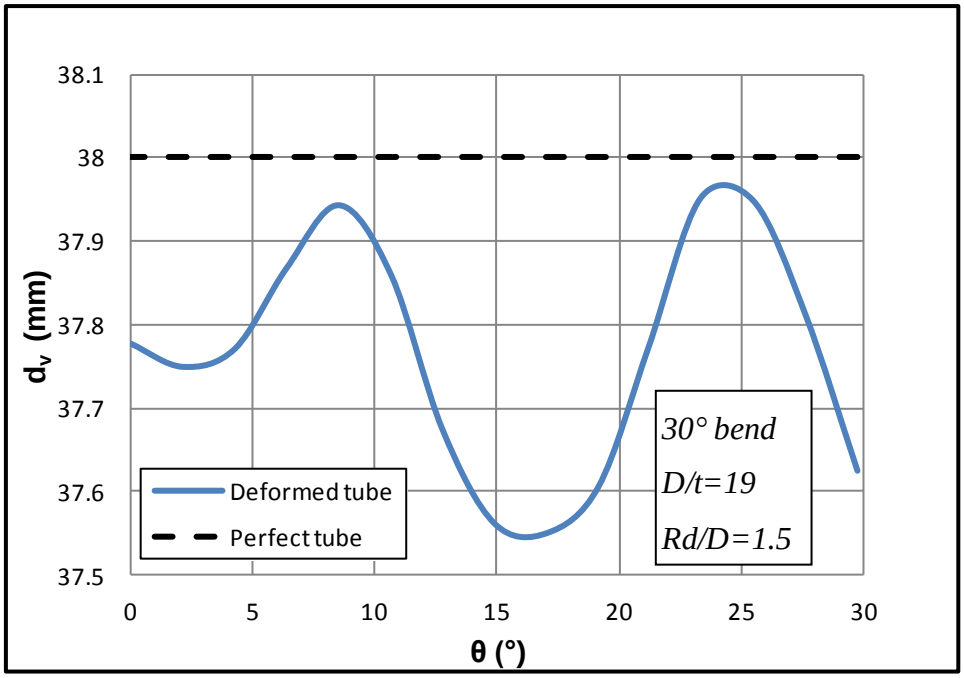

Figure 36: Diameter comparison of 30-degree elbow and perfect tube

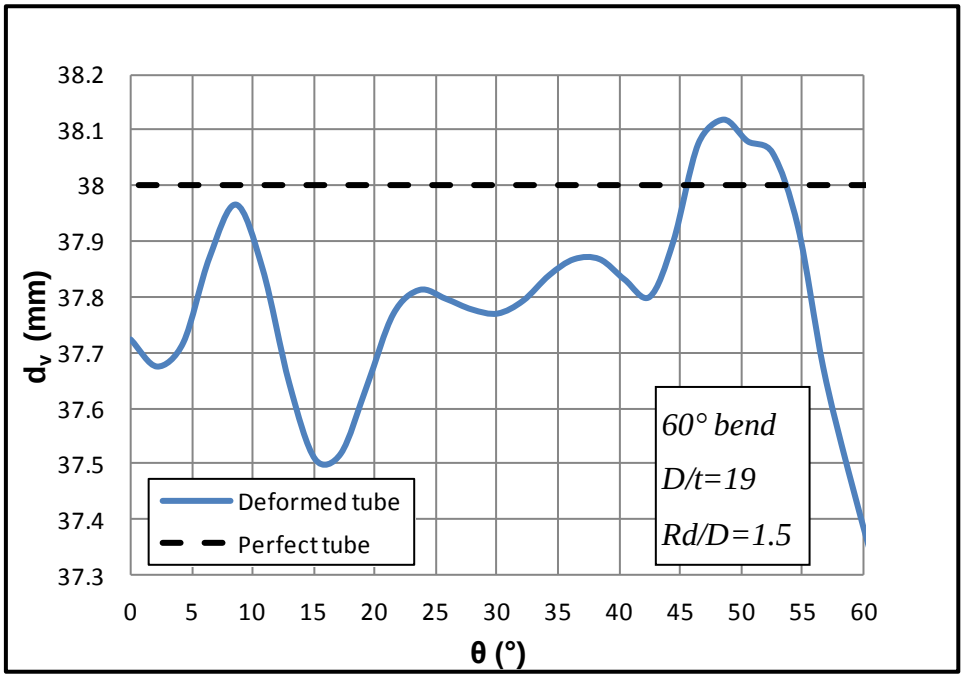

Figure 37: Diameter comparison of 60-degree elbow and perfect tube

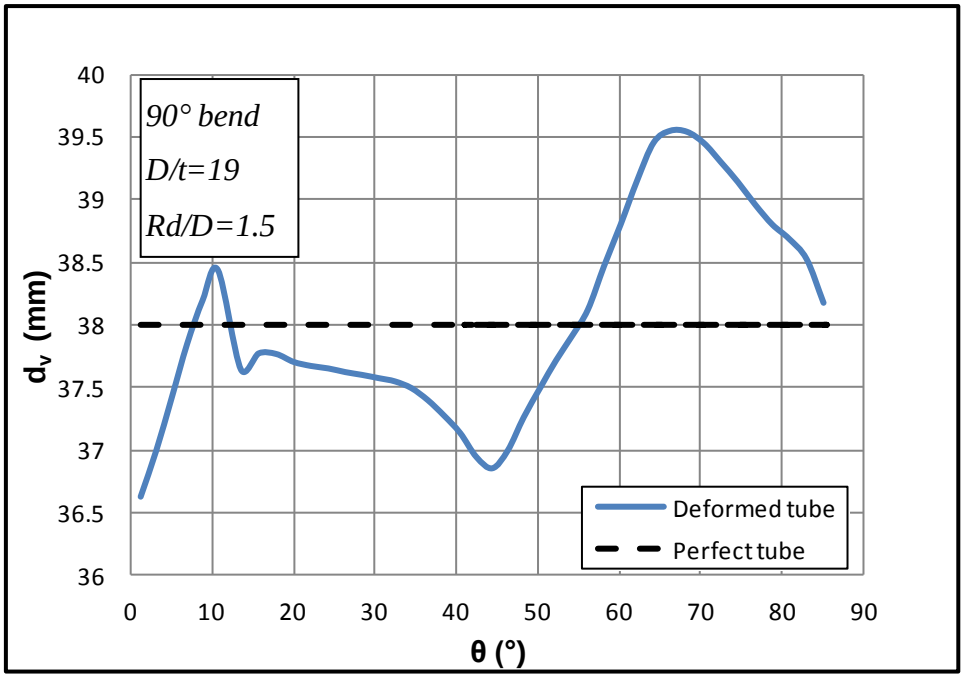

Figure 38: Diameter comparison of 90-degrees elbow and perfect tube

3.2 Out-of-roundness

Out-of roundness is calculated at several tube cross-sections (rings) after the deformation process. In Figure 39, Figure **40** and Figure **41**, several rings of the 30, 60 and 90-degree elbows, as well as the center of rotation are shown. For every ring the out-of roundness compared to the perfect tube rings is examined. It is worth mentioning that the choice of cross-sections is made under the assumption that the cross-sectional plane passes through the center of rotation. This is compatible with Bernoulli's assumption in classical beam theory. The final node position, on the x-y plane, is plotted by adding the displacement value of every node to its initial coordinates. In addition, a perfect ring of 38 mm diameter is considered as reference.

For the 30-degree elbow, rings are selected at the values of angle θ along the elbow corresponding at 7.5, 8.5, 14.5, 20, 24 and 25 degrees. In Figure 42Figure 47 the out-of roundness for every cross-section is plotted. The results depicted demonstrate that the cross-section distortion is more severe at the beginning and at the end of the bend with the diameter deviation reaching 0.8 mm less than the nominal diameter for the upper generator and 0.6 mm more for the lower generator.

For the 60-degree elbow, rings are selected at values of angle θ equal to 4, 8.5, 15 and 33 degrees. In Figure 48Figure 51 the out-of roundness for every ring is plotted. The results show that the cross-section distortion becomes more severe as the bending angle increases. At the cross-section located at 33 degrees along the bend the total cross-sectional deviation from the nominal diameter reaches the value of 2.87 mm. For further bending angles and till 60 degrees the cross-sections are significantly rotated with respect to the elbow axis and do not conform to the aforementioned assumption.

For the 90-degree elbow, rings are selected at angles of 10, 26 and 33 degrees. In Figure 52Figure 53 and Figure **54** the out-of roundness for every ring is plotted. The results show a rather severe cross-section distortion especially at the cross-section at 26 degrees. In the remaining sections up to 90 degrees the cross-sections do not conform to the aforementioned assumption.

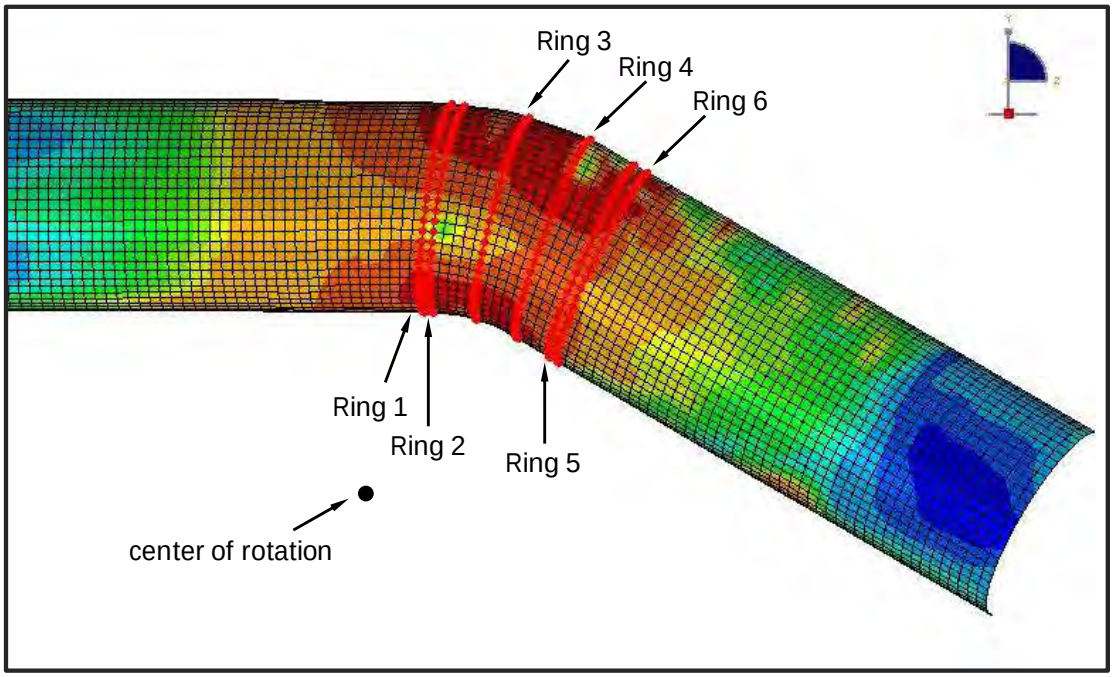

Figure 39: Cross-sections considered at the 30-degree elbow

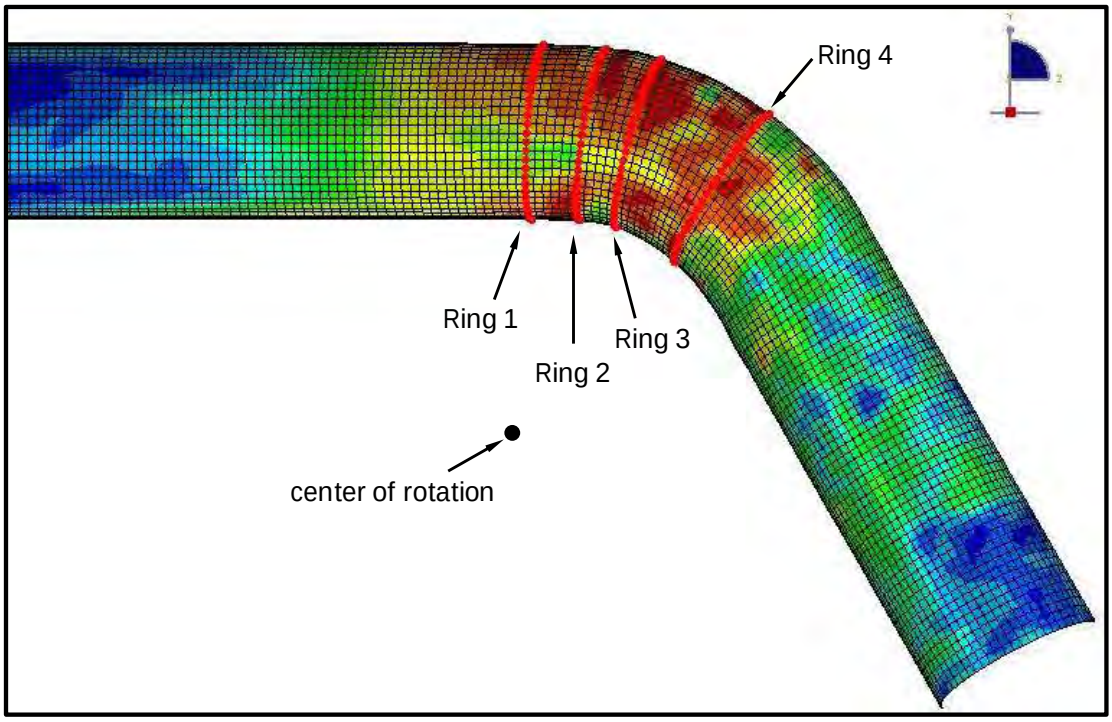

Figure 40: Cross-sections considered at the 60-degree elbow

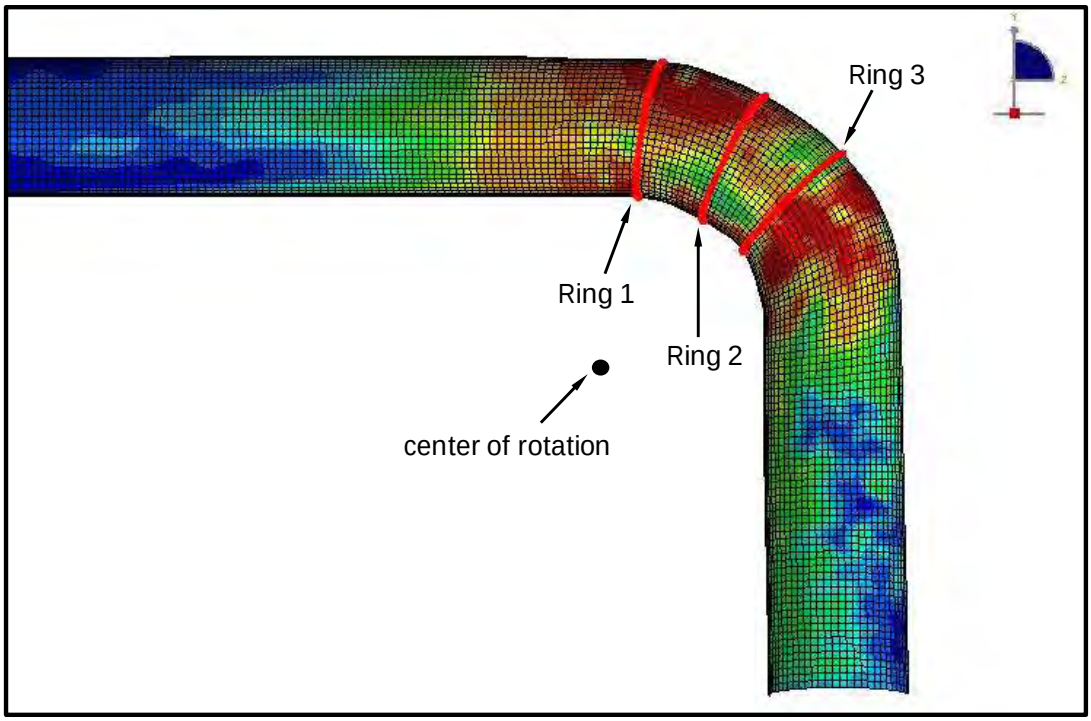

Figure 41: Cross-sections considered at the 90-degree elbow

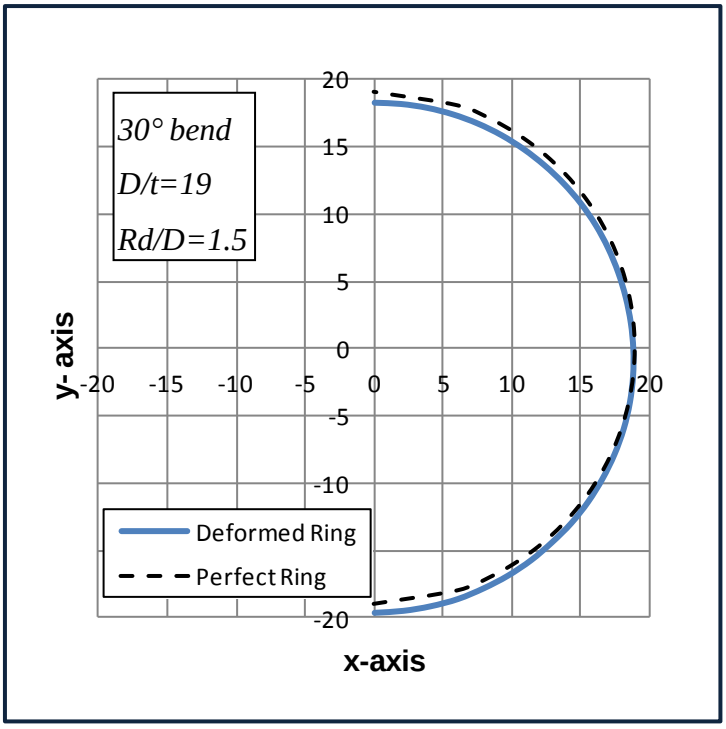

Figure 42: Out-of roundness of cross-section of 30-degree elbow ring 1

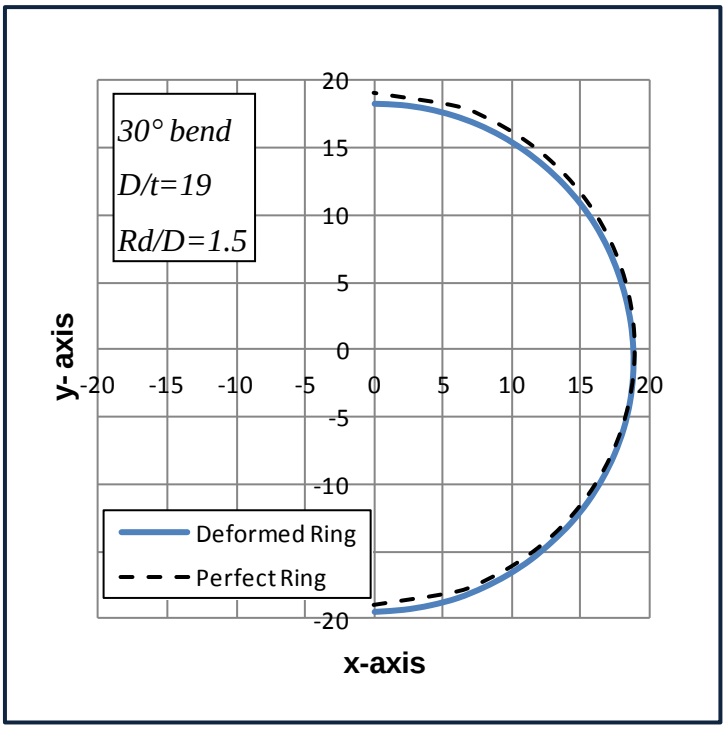

Figure 43: Out-of roundness of cross-section of 30-degree elbow ring 2

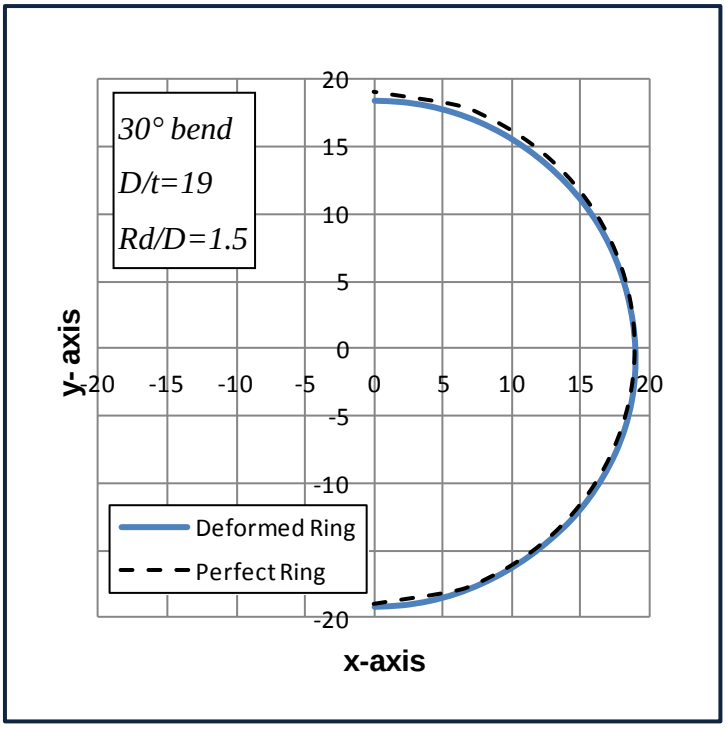

Figure 44: Out-of roundness of cross-section of 30-degree elbow ring 3

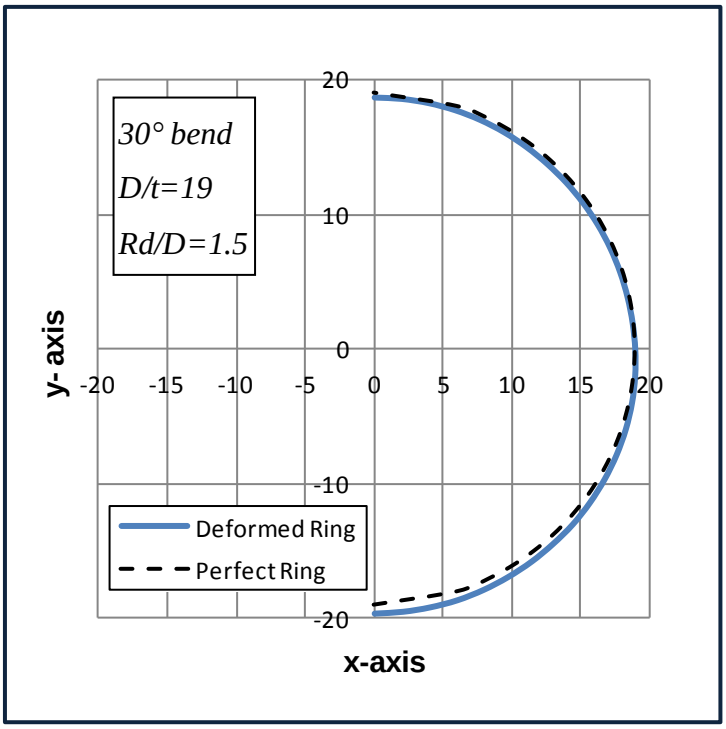

Figure 45: Out-of roundness of cross-section of 30-degree elbow ring 4

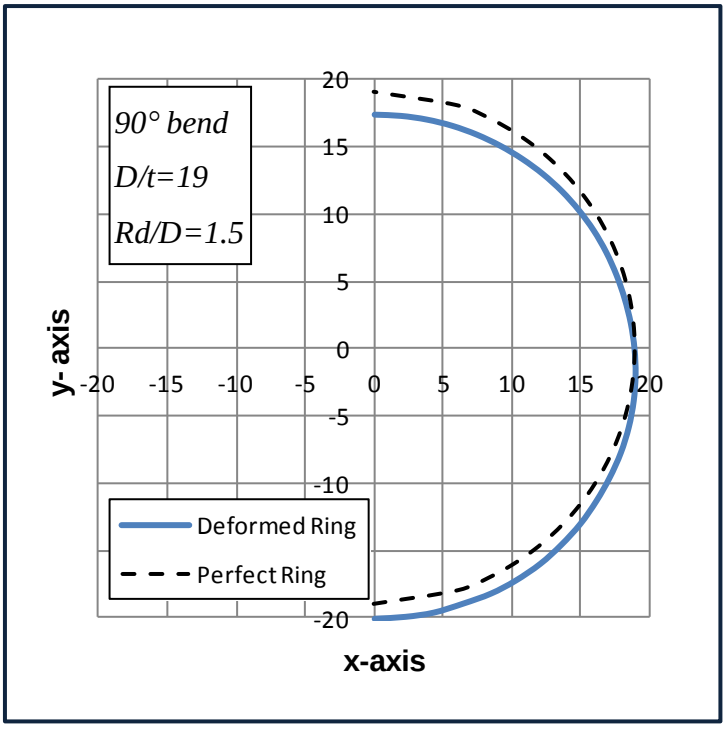

Figure 46: Out-of roundness of cross-section of 30-degree elbow ring 5

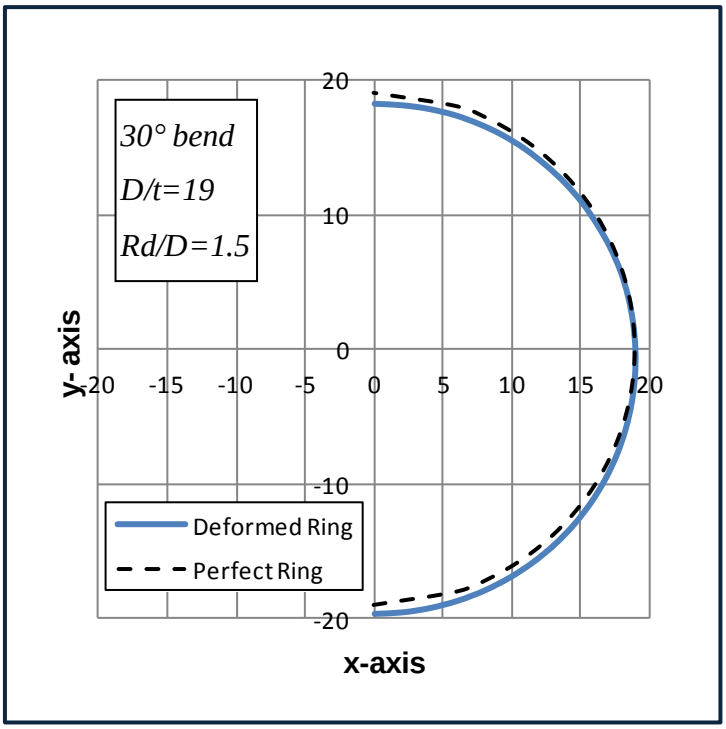

Figure 47: Out-of roundness of cross-section of 30-degree elbow ring 6

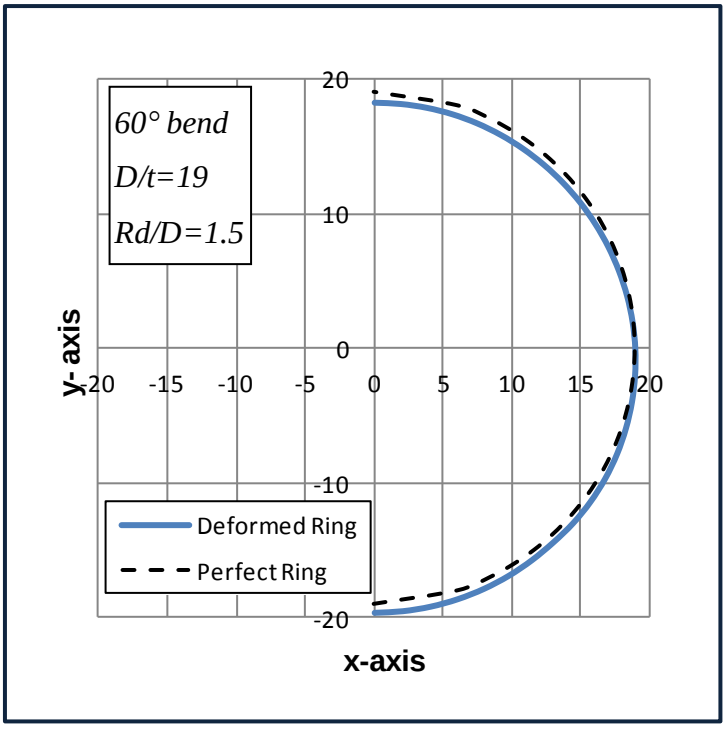

Figure 48: Out-of roundness of cross-section of 60-degree elbow ring 1

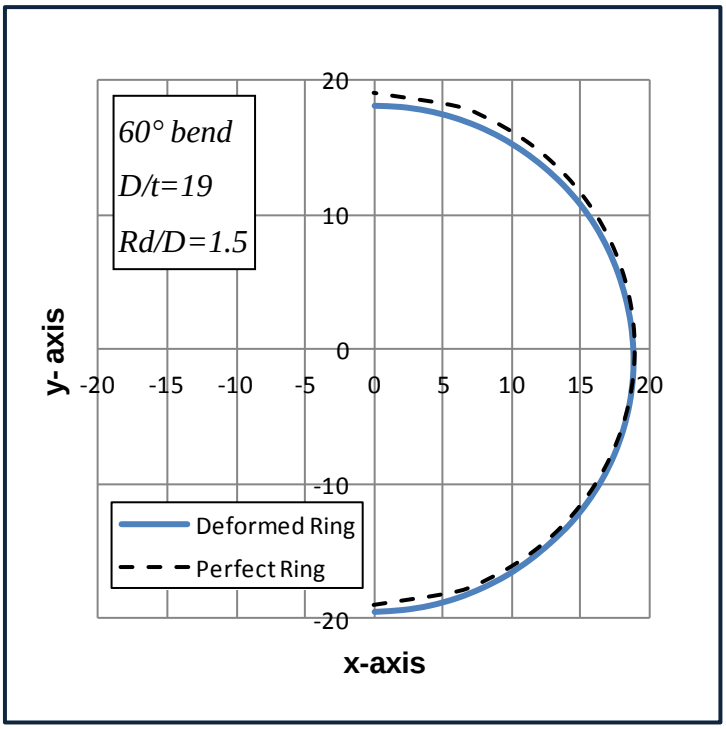

Figure 49: Out-of roundness of cross-section of 60-degree elbow ring 2

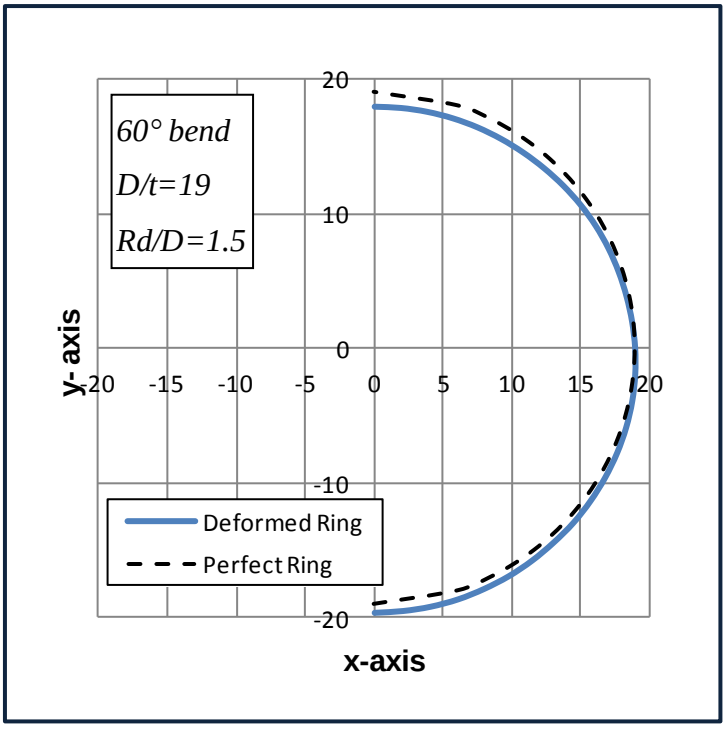

Figure 50: Out-of roundness of cross-section of 60-degree elbow ring 3

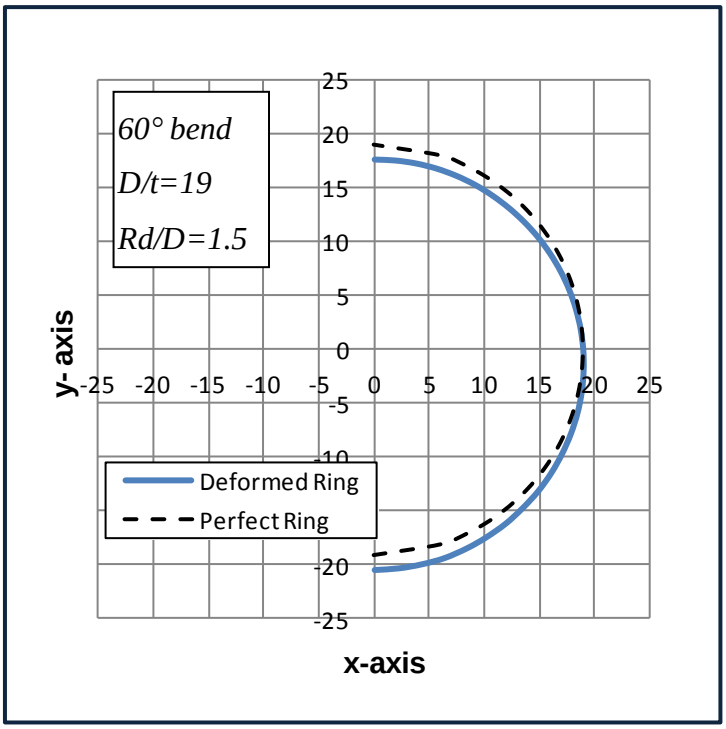

Figure 51: Out-of roundness of cross-section of 60-degree elbow ring 4

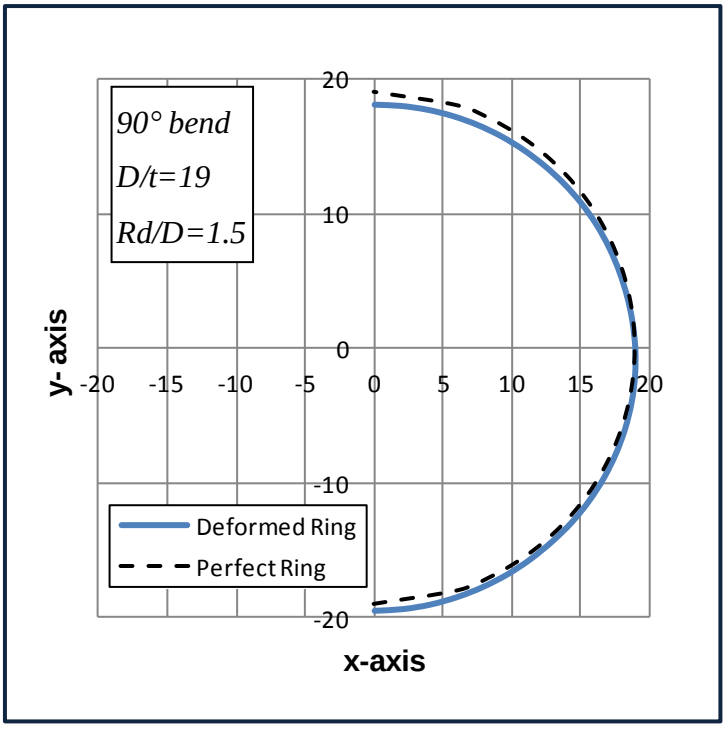

Figure 52: Out-of roundness of cross-section of 90-degree elbow ring 1

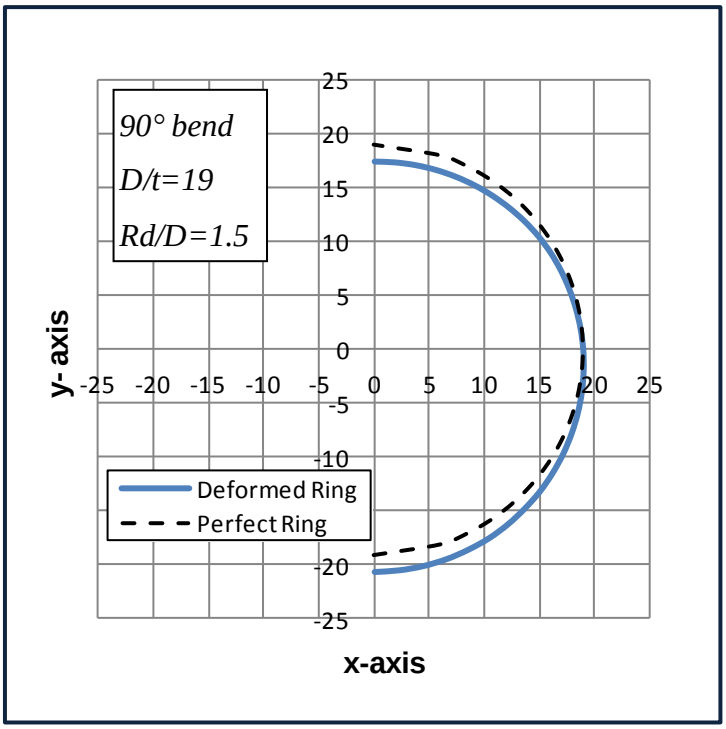

Figure 53: Out-of roundness of cross-section of 90-degree elbow ring 2

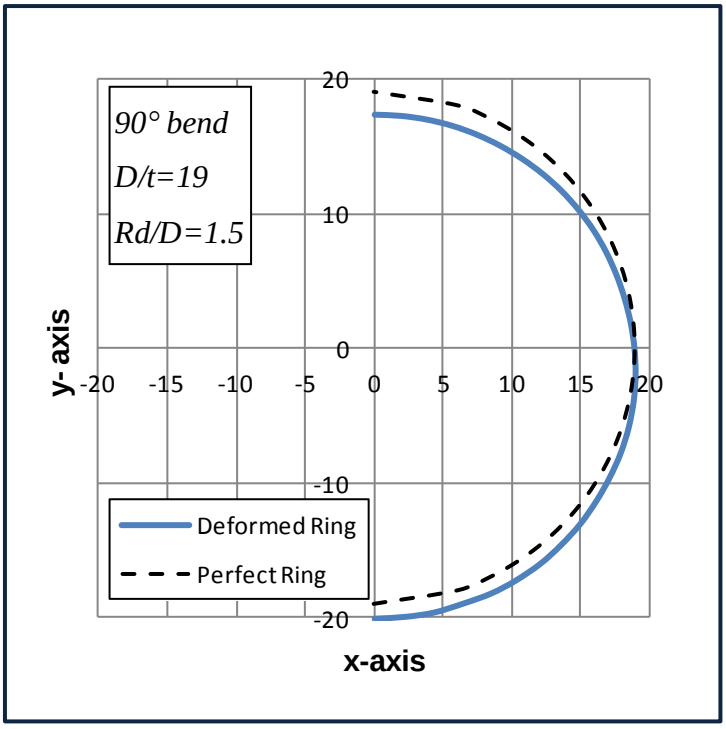

Figure 54: Out-of roundness of cross-section of 90-degree elbow ring 3

3.3 Wall thickness variation

As mentioned in chapter 1, for any bending process, upon bending deformation, complex tension and compression stress distributions are induced at the extrados and intrados of bend tube respectively, which may cause multiple defects. In this section, results for thickness variation were obtained for the upper, middle and lower generator of all bending degrees.

In Figure 55Figure 56Figure 57 cross-section thickness variation of the 30 degrees deformed tube is plotted in relation to angle θ along the bend. From the results depicted, it can be assumed that for the upper generator there is a cross-section thinning while for the lower generator there is a cross-section thickening. More precisely, the minimum thickness value obtained for the upper generator is 1.68 mm when the angle θ is 16 degrees while for the lower generator the maximum thickness value is 2.37 for an angle of 22 degrees. For the middle generator, the results demonstrate a variation in wall thickness but the numerical deviation from the initial value is quite small (approximately 0.06 mm pipe wall thinning for a cross-section at 25 degrees of angle θ).

In Figure 58Figure 59Figure 60 thickness variation of the 60-degree elbow is plotted in terms of the angle θ. From the results depicted, it can be assumed that the cross-section response is similar to that of the 30-degree elbow. In particular, the minimum thickness value obtained for the upper generator is 1.58 mm at angle θ equal to 43 degrees while for the lower generator the maximum thickness value is 2.55 at angle θ equal to 47 degrees. For the middle generator, the results demonstrate a variation in wall thickness but the numerical deviation from the initial value is quite small (approximately 0.07 mm cross-section thinning at 59 degrees of angle θ).

In Figure 61Figure 62Figure 63 thickness variation of the 90-degree elbow is plotted in terms of the angle θ. Same as with the previous bending angles, the minimum thickness value obtained for the upper generator is 1.4 mm when the angle is 71 degrees, while for the lower generator the maximum thickness value is 2.56 for angle θ equal to 58 degrees. For the middle generator, the results demonstrate a variation in wall thickness but the numerical deviation from the initial value is quite small (approximately 0.08 mm thinning at 83 degrees of angle θ).

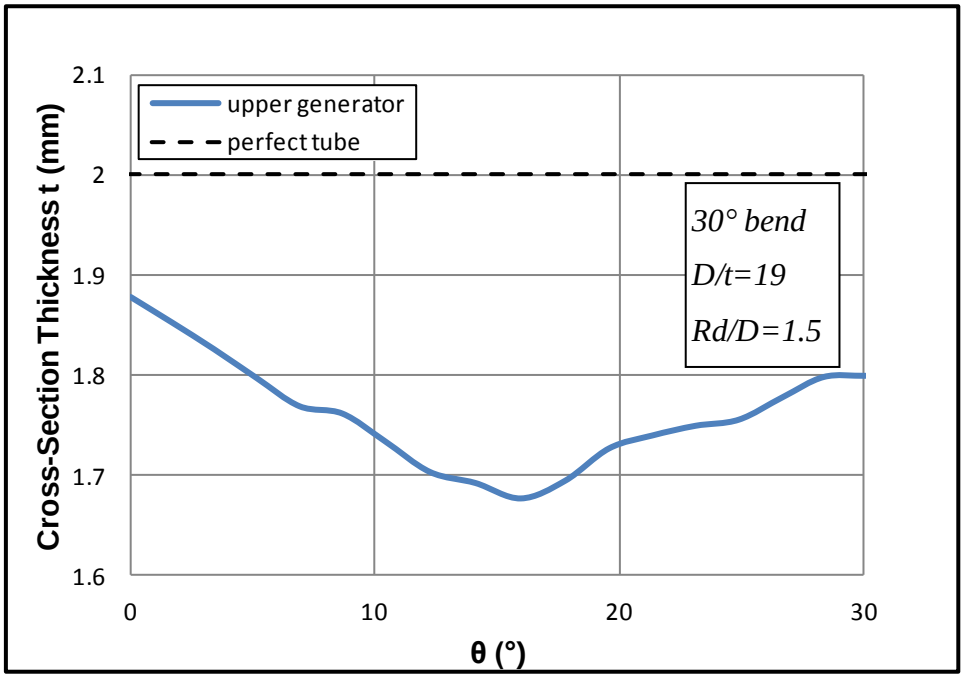

Figure 55: Thickness variation of 30-degree elbow along its upper generator

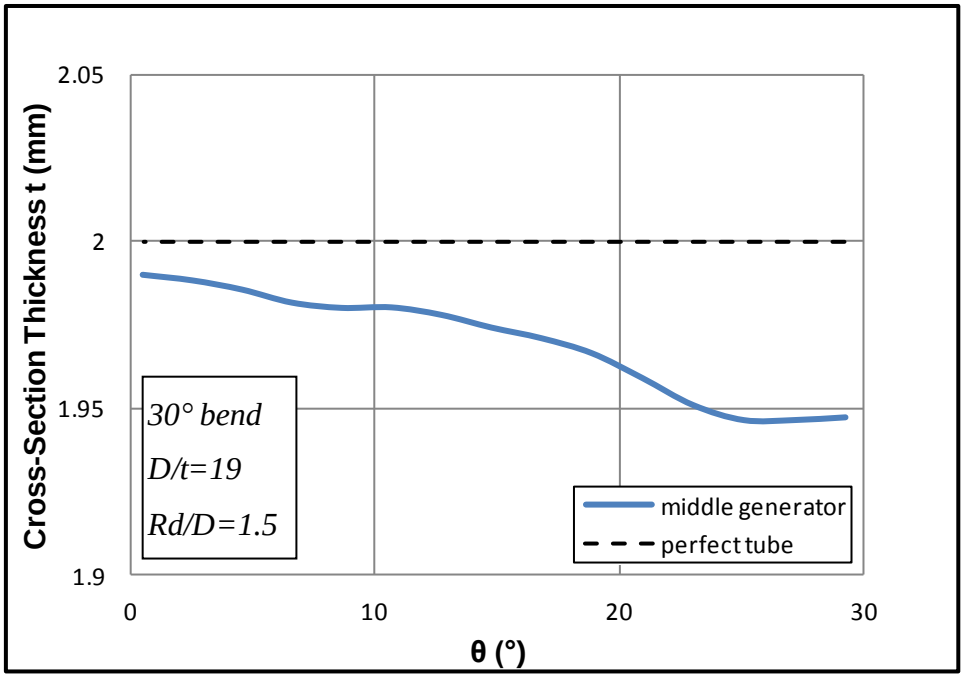

Figure 56: Thickness variation of 30-degree elbow along its middle generator

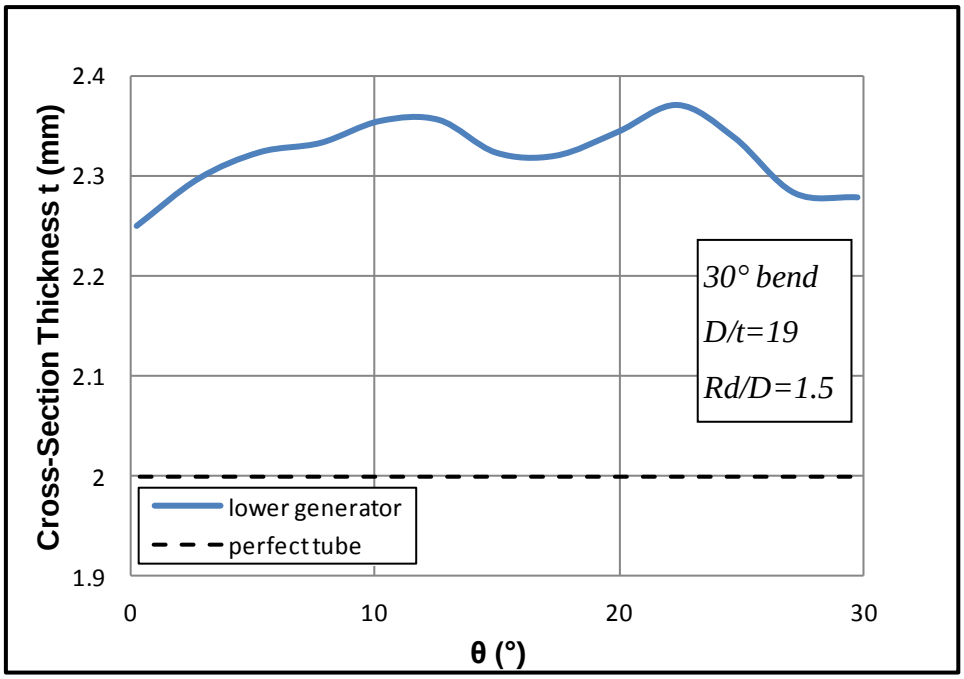

Figure 57: Thickness variation of 30-degree elbow along its lower generator

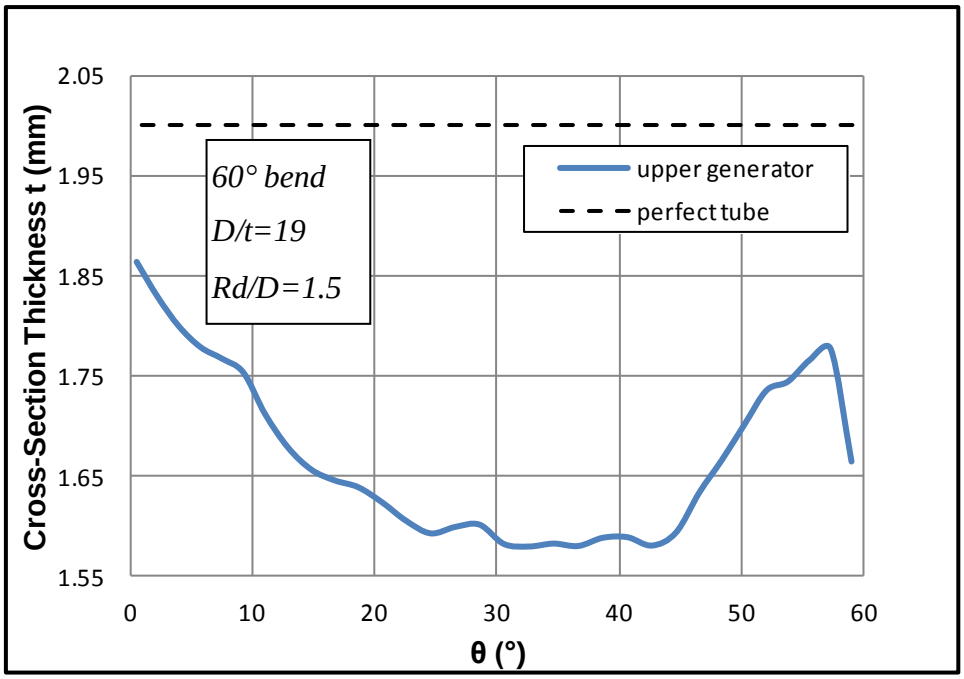

Figure 58: Thickness variation of 60-degree elbow along its upper generator

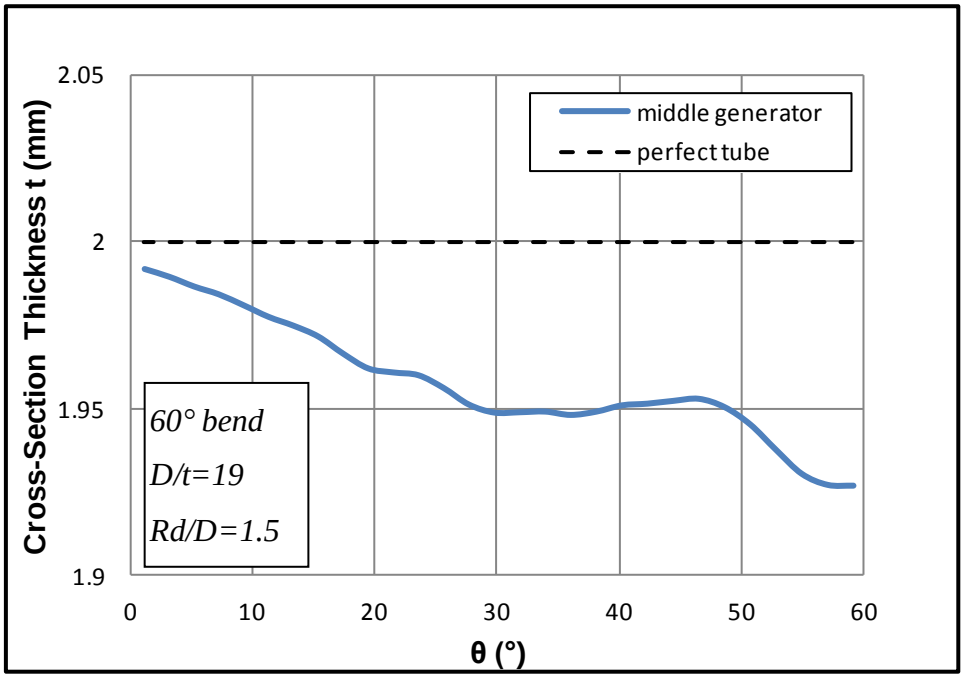

Figure 59: Thickness variation of 60-degree elbow along its middle generator

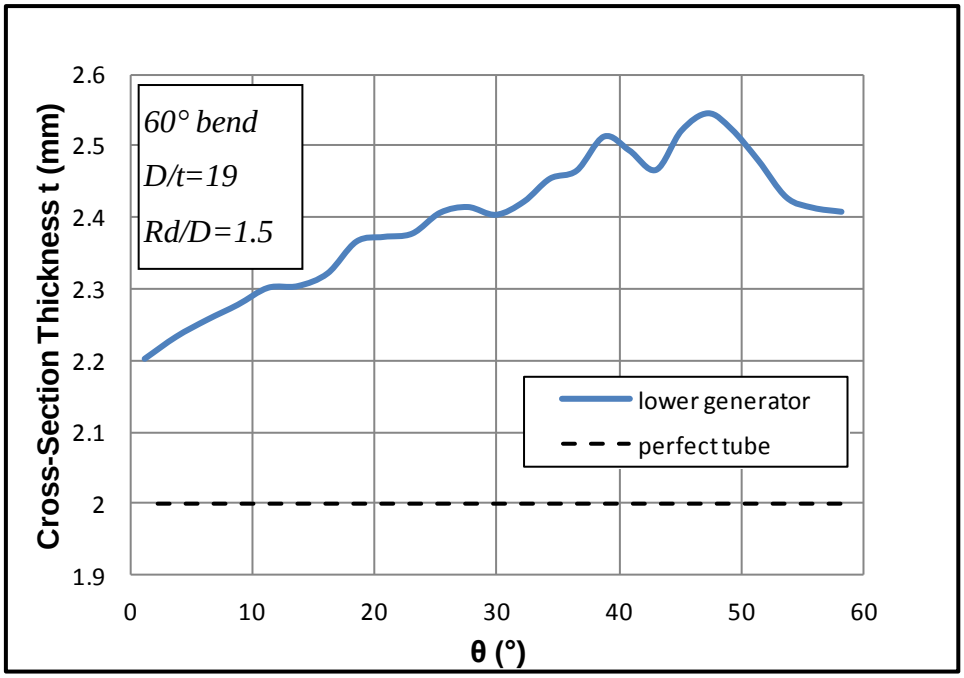

Figure 60: Thickness variation of 60-degree elbow along its lower generator

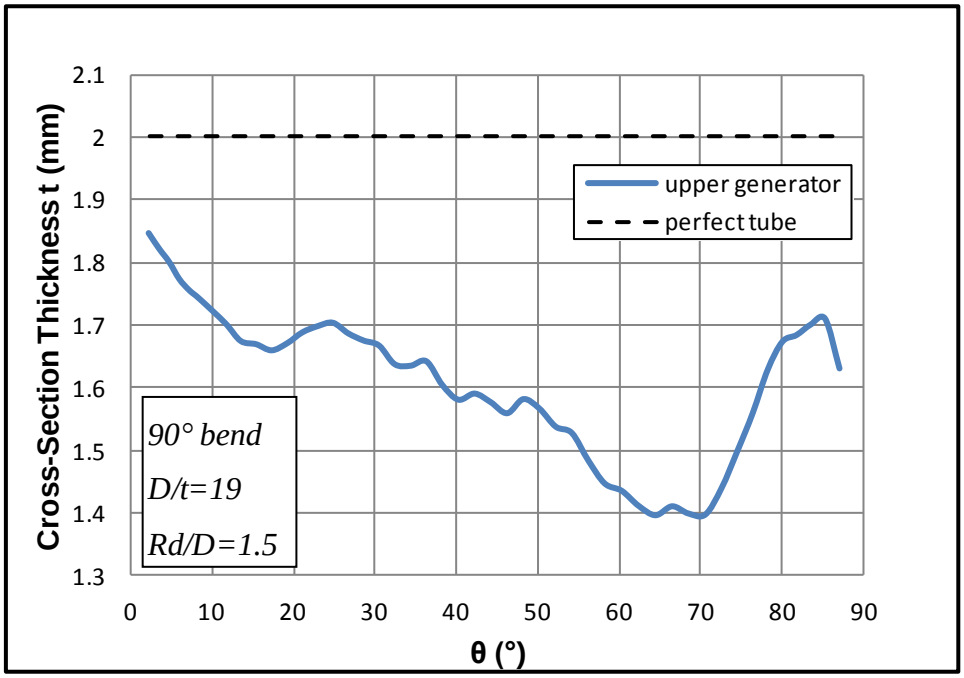

Figure 61: Thickness variation of 90-degree elbow along its upper generator

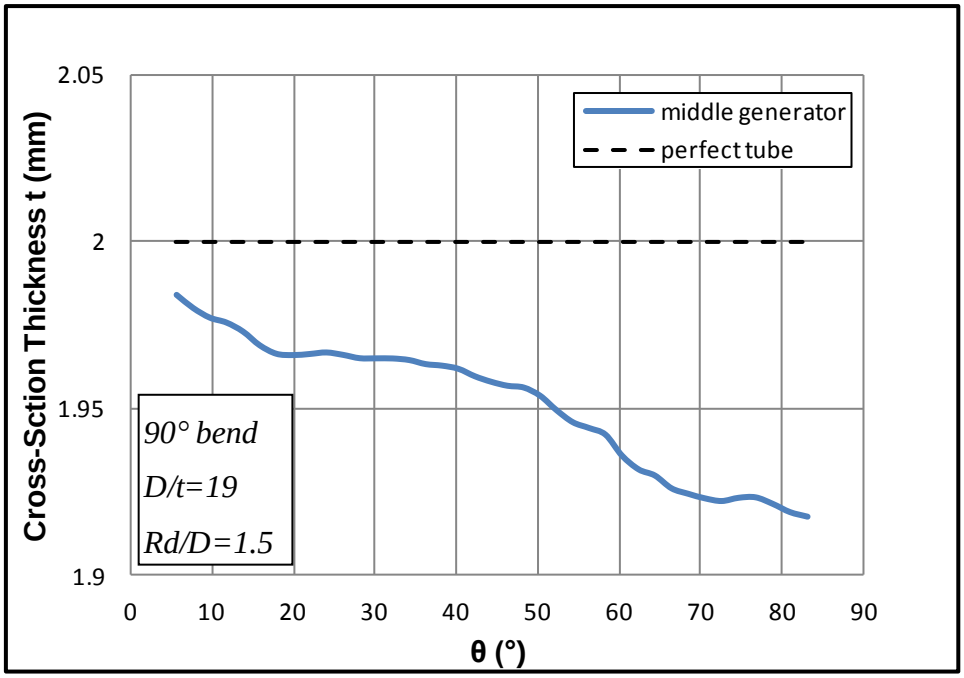

Figure 62: Thickness variation of 90-degree elbow along its middle generator

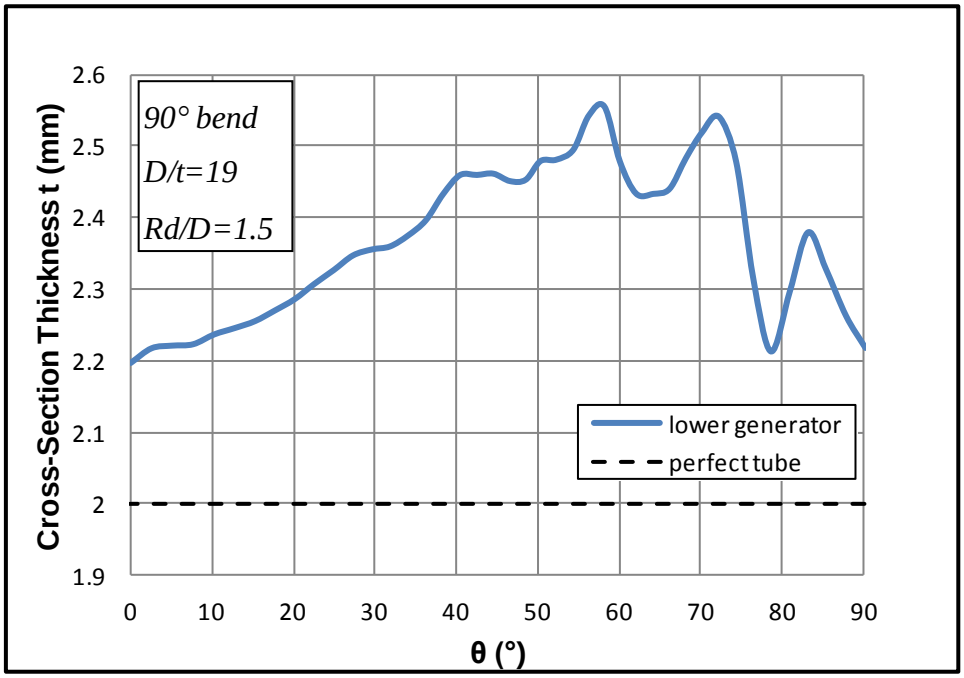

Figure 63: Thickness variation of 90-degree elbow along its lower generator

3.4 Stress distribution

During the manufacturing process a complex state of stresses across the thickness of the tubes are developed as a response to the bending angle imposed. These stresses remain on the tube even after the process affecting the elbows behavior. In the present study, five thickness integration points were used for the analysis. In this section, the so-called residual stresses are obtained for the first (SP1) and the fifth (SP5) integration point (Figure 64) of the upper, the lower and the middle generator.

In Figure 65Figure 70 the Von Mises stress in terms of the angle θ is plotted for the 30-degree elbow. The results depicted in those figures demonstrate that the maximum stress developed in the upper generator is 228.9 MPa for SP1 and 90 MPa for SP5. In the middle generator the stress values are 285 MPa for SP1 and 295 MPa for SP5 while in the lower generator 216 MPa and 178 MPa respectively.

In Figure 71Figure 76 the Von Mises stress in terms of the bending angle θ is plotted for the 60-degree elbow. The results depicted in those figures demonstrate that the maximum stress developed in the upper generator is 179 MPa for SP1 and 98 MPa for SP5. In the middle generator the stress values are 155 MPa for SP1 and 196 MPa for SP5 while in the lower generator 197 MPa and 147 MPa respectively.

In Figure 77Figure 82 the Von Mises stress in terms of the bending angle θ is plotted for the 90-degree elbow. The results depicted in those figures demonstrate that the maximum stress developed in the upper generator is 159 MPa for SP1 and 121 MPa for SP5. In the middle generator the stress values are 256 MPa for SP1 and 245 MPa for SP5 while in the lower generator 285 MPa and 154 MPa respectively.

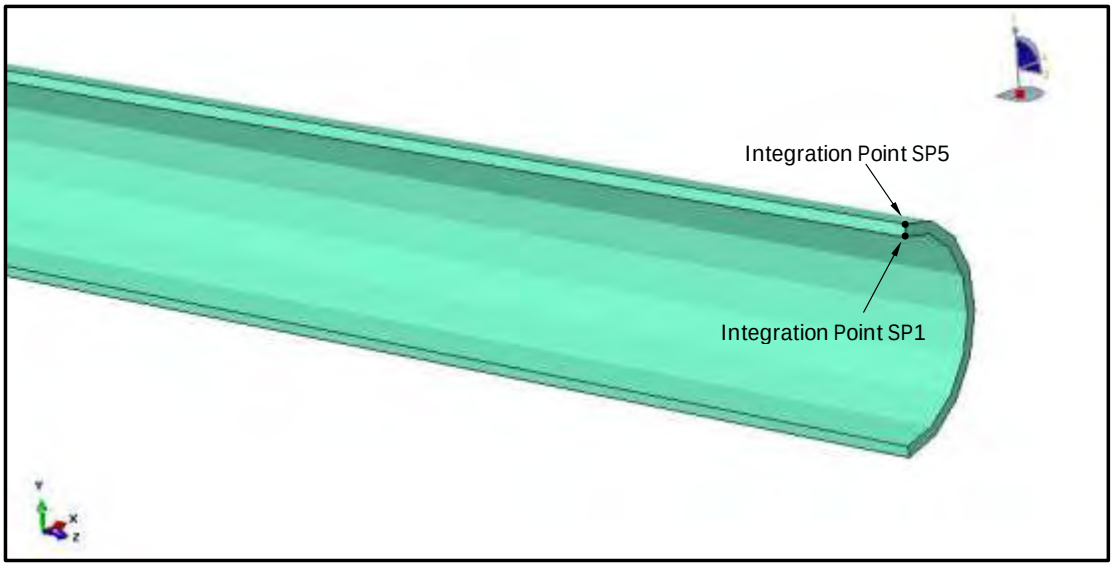

Figure 64: Integration points across the tube thickness

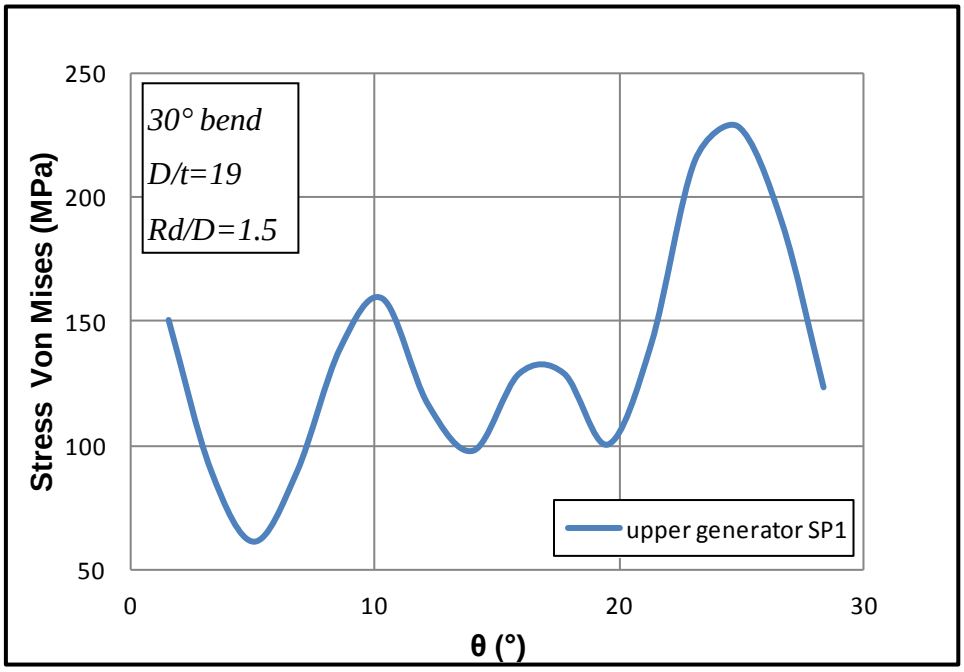

Figure 65: Von Mises stress distribution along the 30-degree elbow at the inner surface of the upper generator

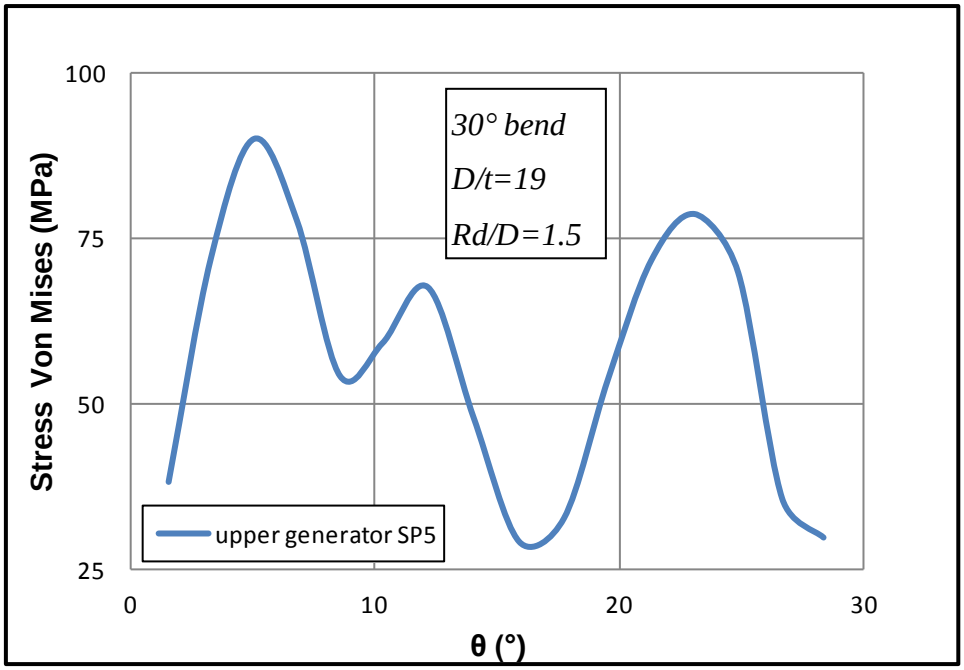

Figure 66: Von Mises stress distribution along the 30-degree elbow at the outer surface of the upper generator

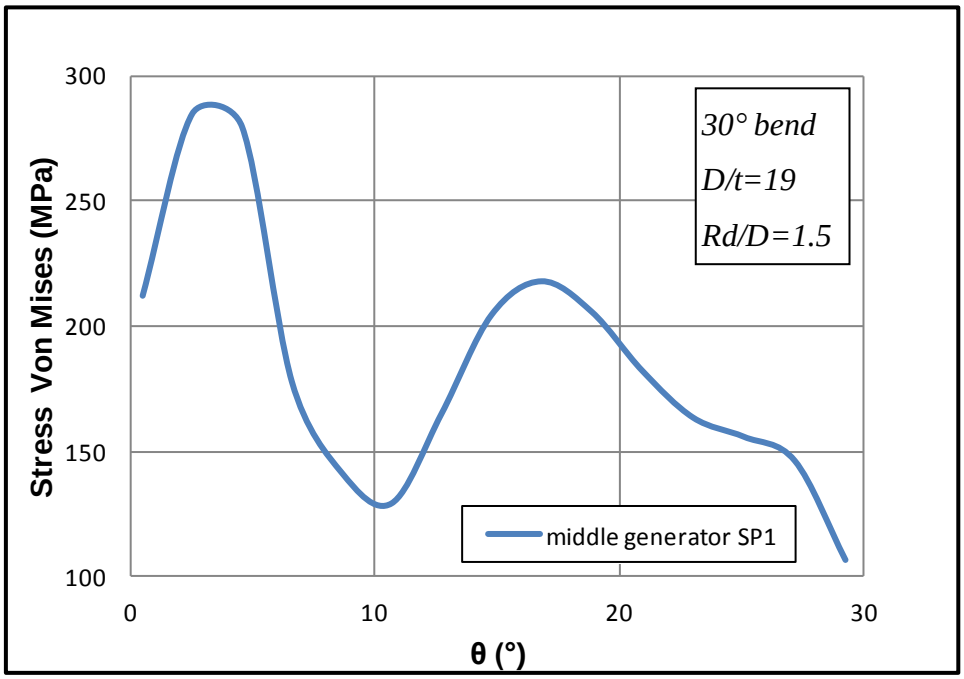

Figure 67: Von Mises stress distribution along the 30-degree elbow at the inner surface of the middle generator

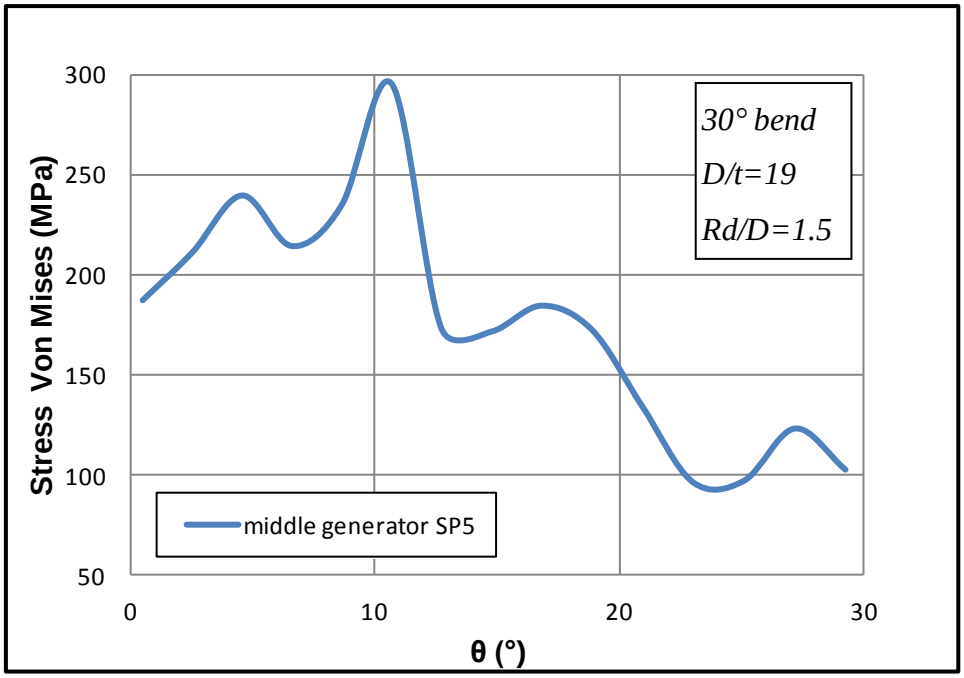

Figure 68: Von Mises stress distribution along the 30-degree elbow at the outer surface of the middle generator

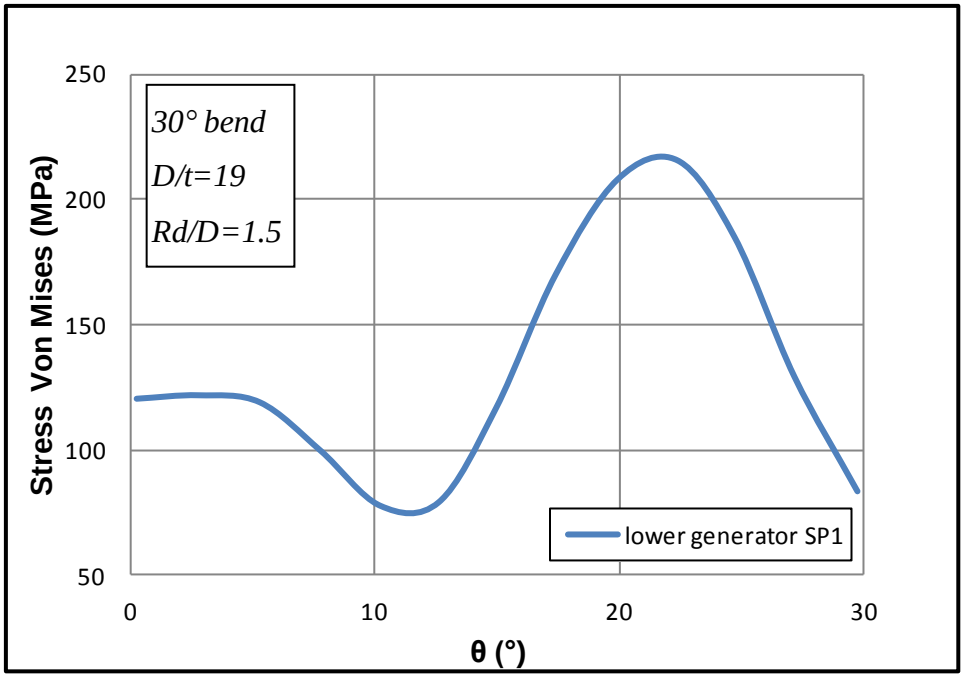

Figure 69: Von Mises stress distribution along the 30-degree elbow at the inner surface of the lower generator

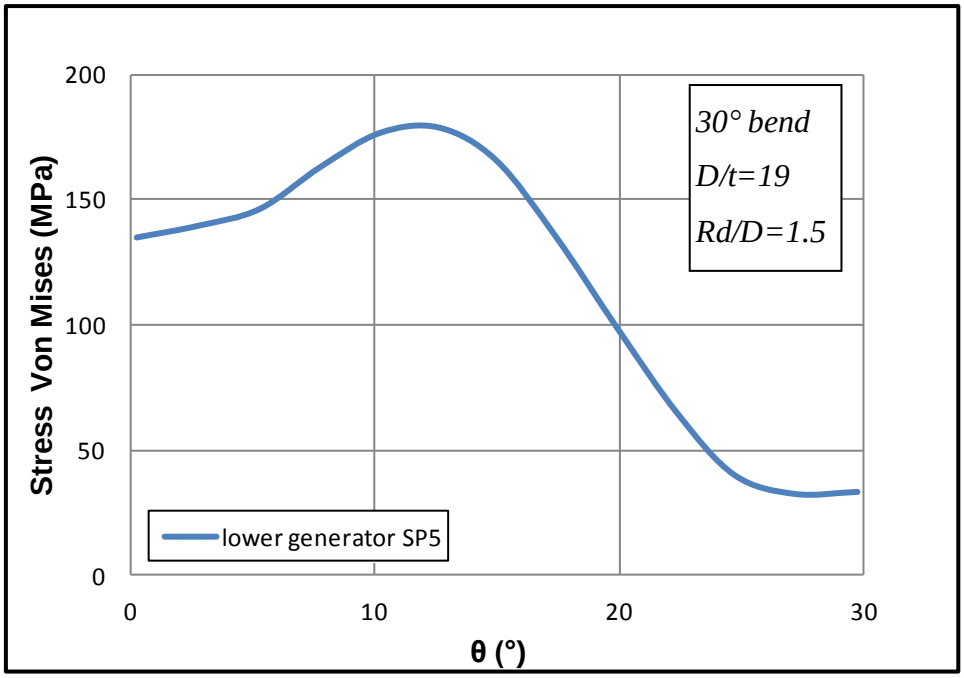

Figure 70: Von Mises stress distribution along the 30-degree elbow at the outer surface of the lower generator

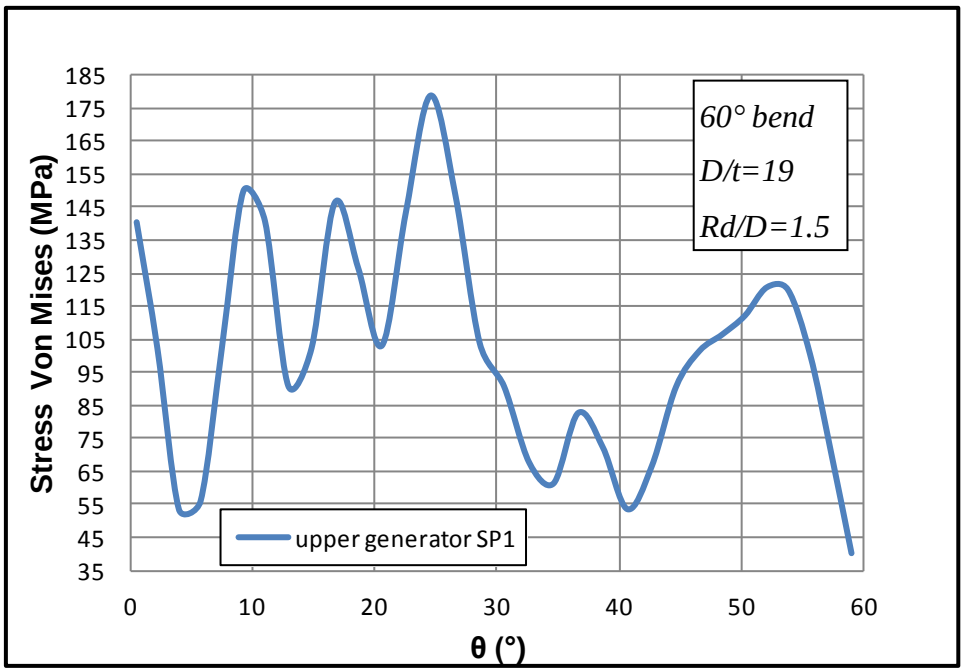

Figure 71: Von Mises stress distribution along the 60-degree elbow at the inner surface of the upper generator

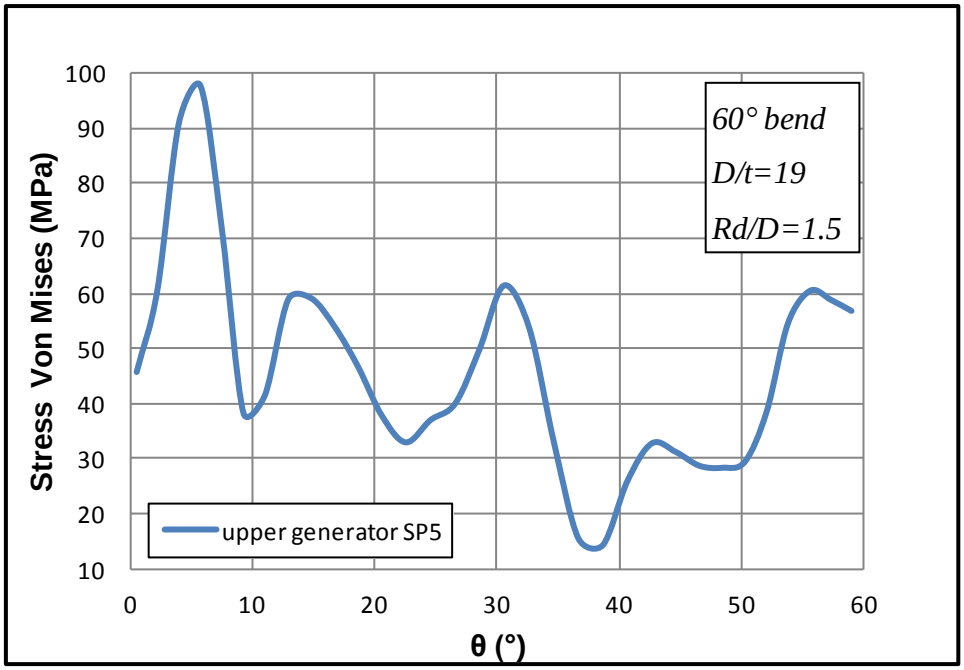

Figure 72: Von Mises stress distribution along the 60-degree elbow at the outer surface of the upper generator

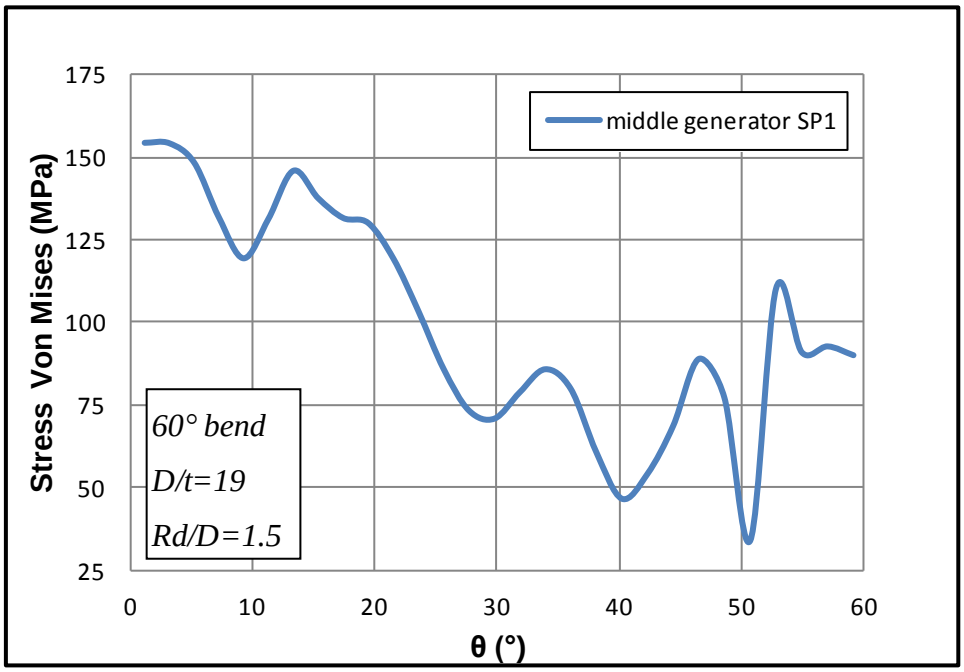

Figure 73: Von Mises stress distribution along the 60-degree elbow at the inner surface of the middle generator

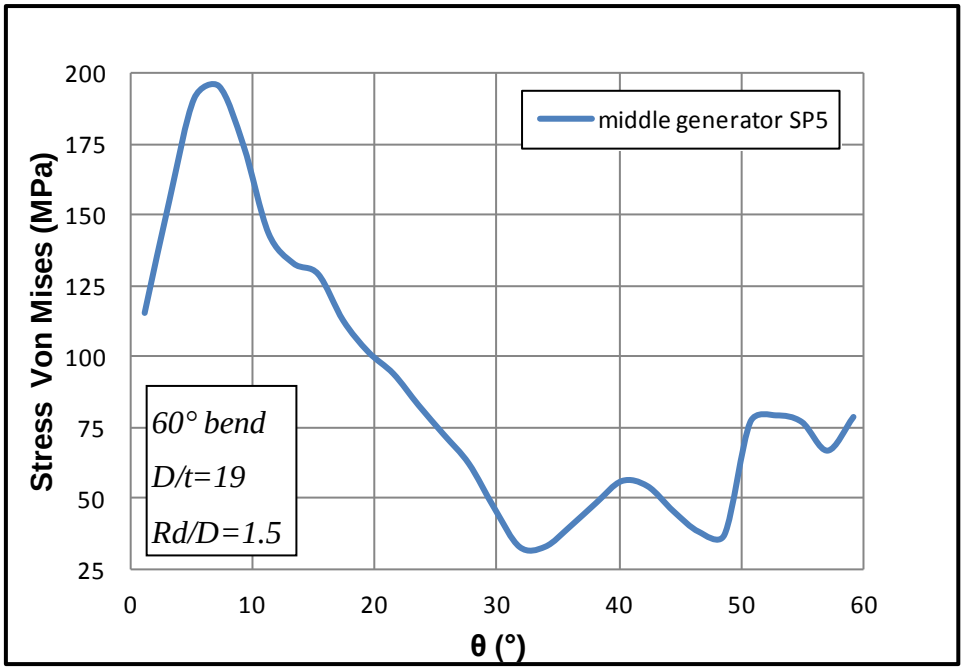

Figure 74: Von Mises stress distribution along the 60-degree elbow at the outer surface of the middle generator

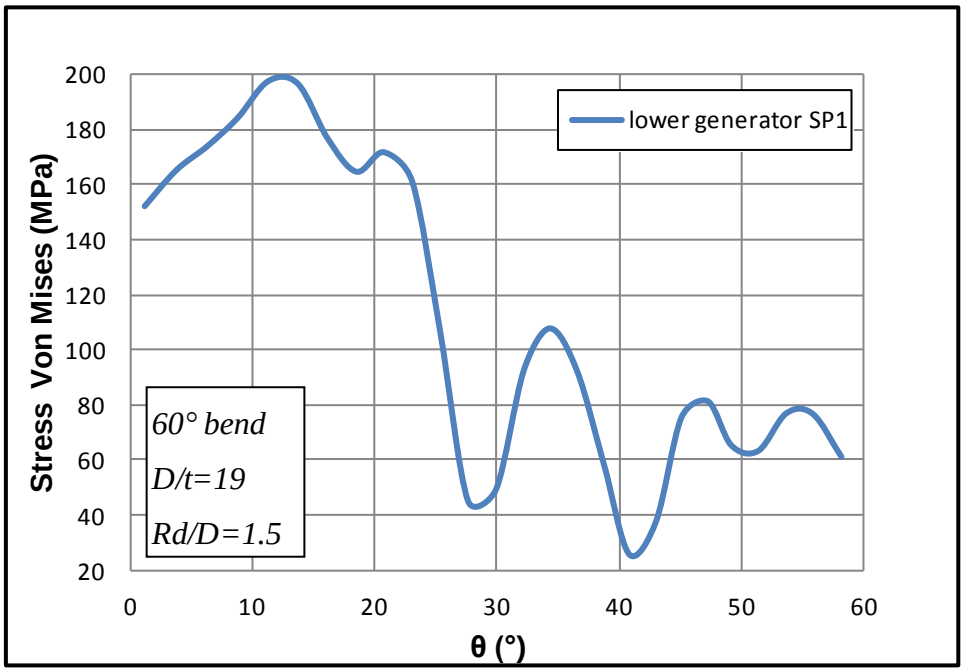

Figure 75: Von Mises stress distribution along the 60-degree elbow at the inner surface of the lower generator

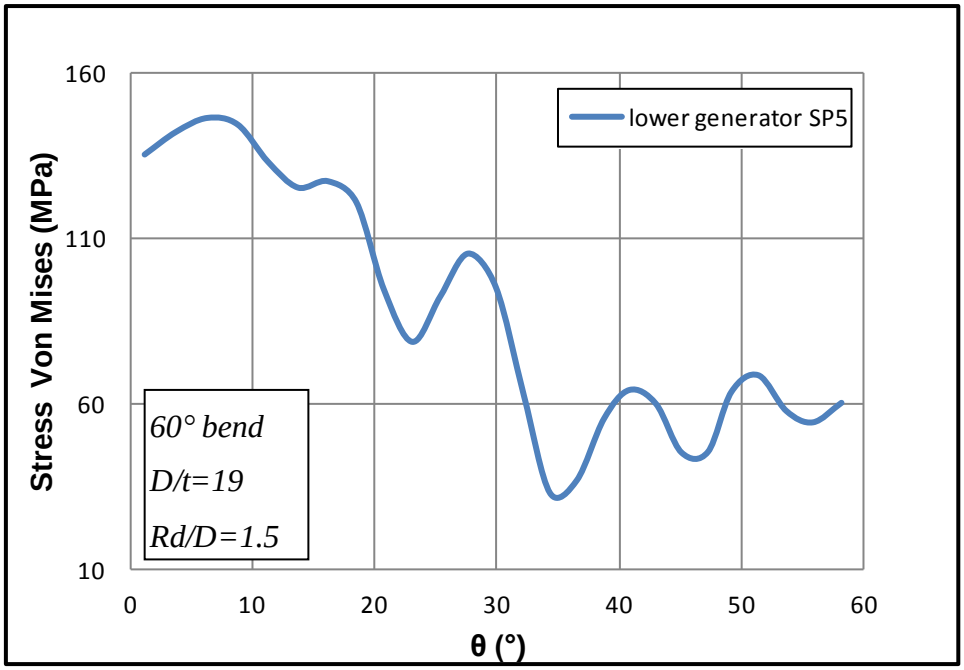

Figure 76: Von Mises stress distribution along the 60-degree elbow at the outer surface of the lower generator

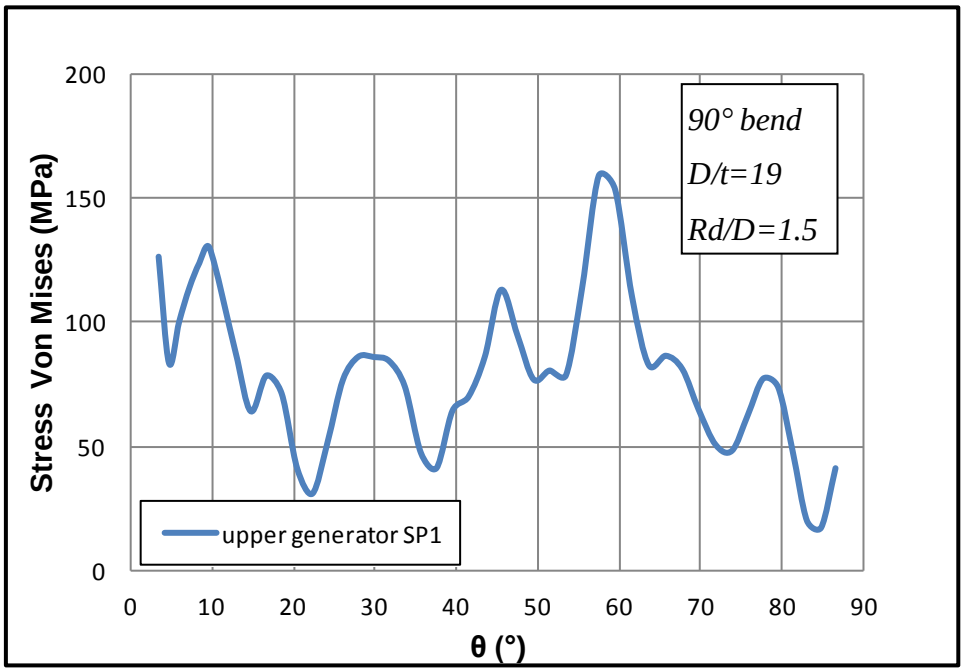

Figure 77: Von Mises stress distribution along the 90-degree elbow at the inner surface of the upper generator

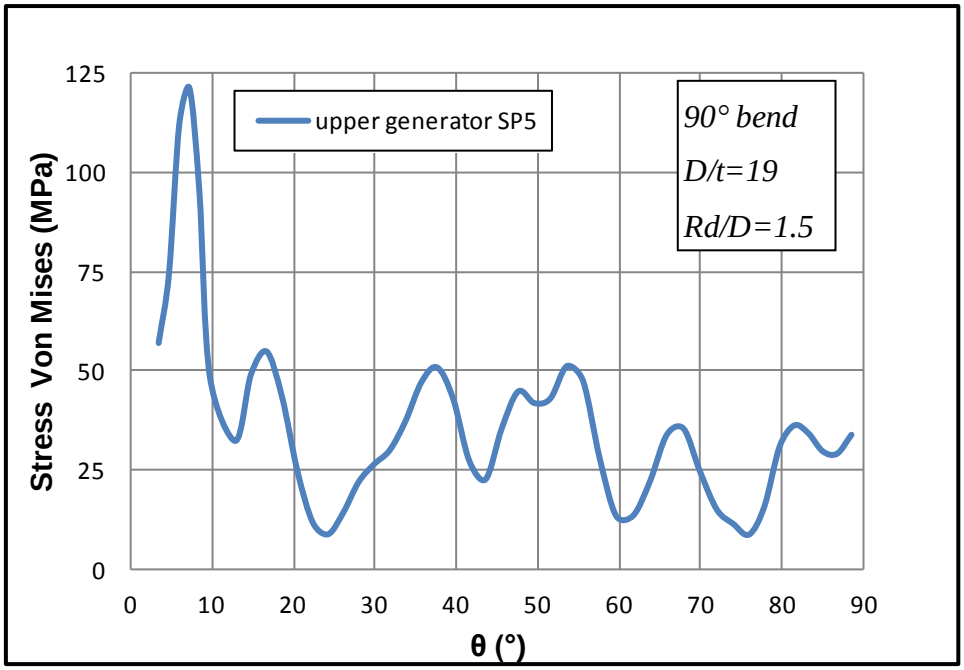

Figure 78: Von Mises stress distribution along the 90-degree elbow at the outer surface of the upper generator

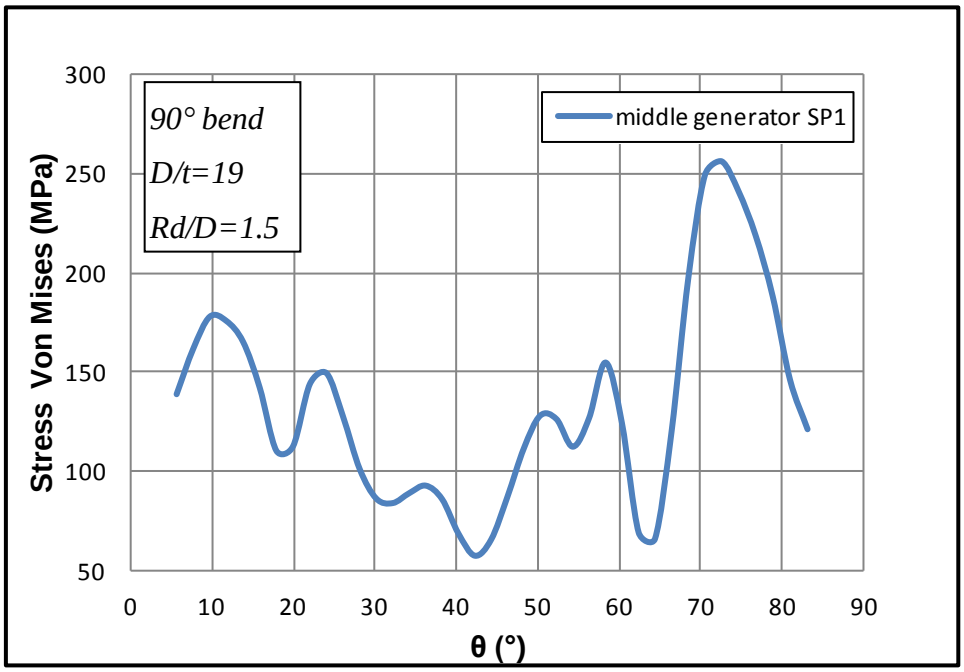

Figure 79: Von Mises stress distribution along the 90-degree elbow at the inner surface of the middle generator

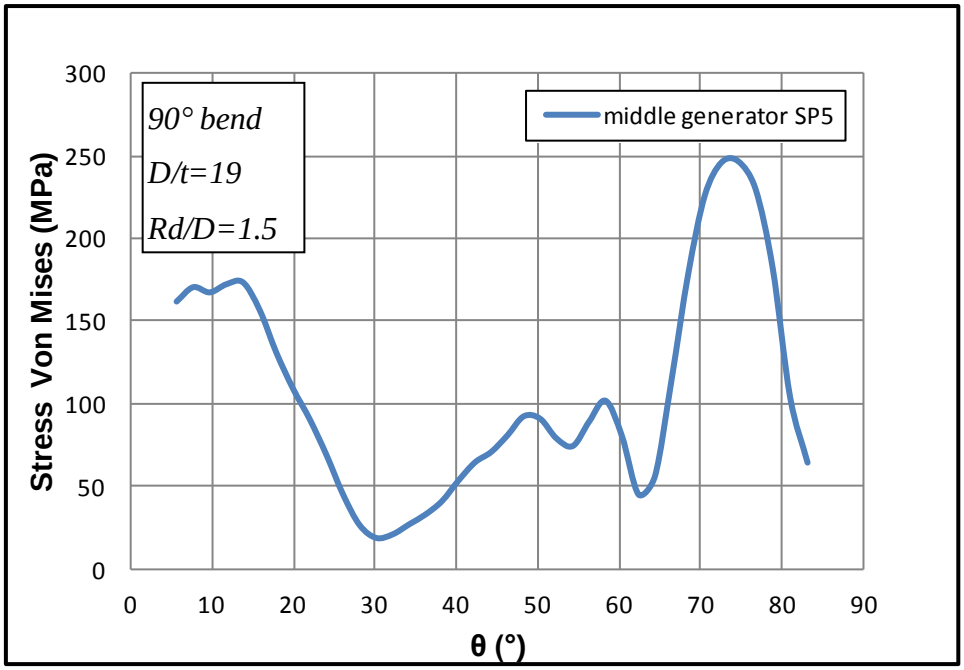

Figure 80: Von Mises stress distribution along the 90-degree elbow at the outer surface of the middle generator

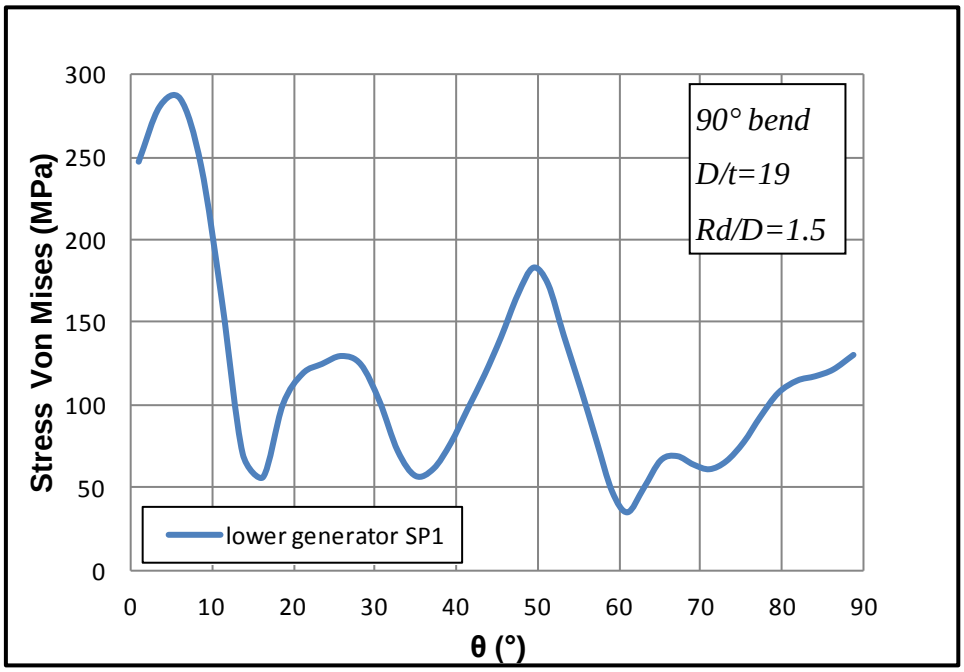

Figure 81: Von Mises stress distribution along the 90-degree elbow at the inner surface of the lower generator

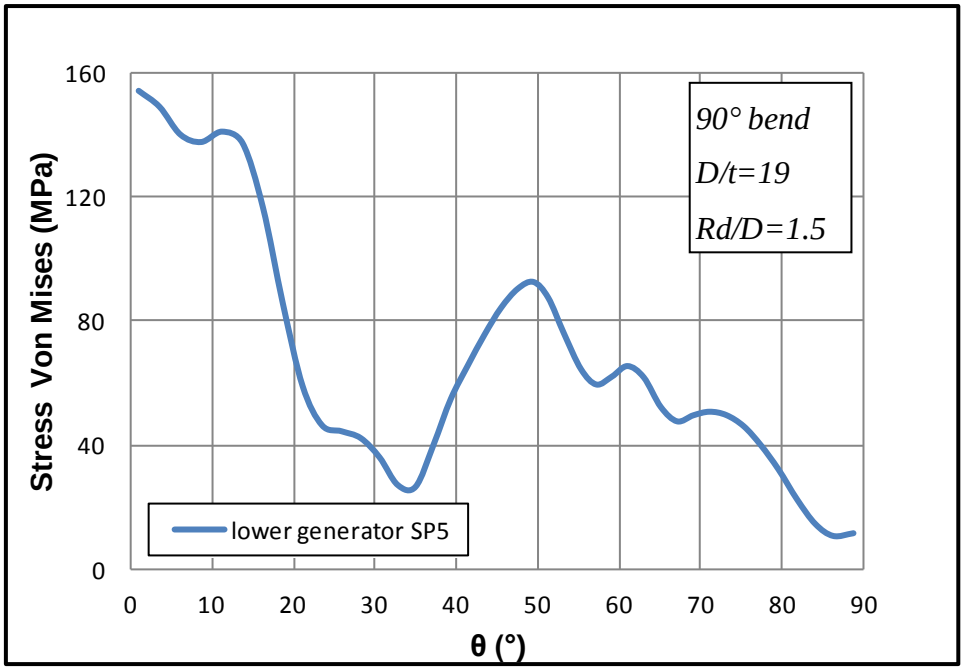

Figure 82: Von Mises stress distribution along the 90-degree elbow at the outer surface of the lower generator

Chapter 4

Numerical results on structural performance of cold-formed elbows

In this chapter, the structural performance of the bent, deformed tubes is investigated and the results are compared to those from perfect tubes. In Figure 83Figure 84Figure 85 the 30, 60 and 90-degree elbows after the manufacturing process are shown. Every tube is subjected successively to in-plane closing and opening bending moments. More precisely, the boundary conditions applied to the tube are as follows:

For the end sections A, all displacements and rotations are restrained while for the end sections B, displacements on y-axis and z-axis are permitted as well as rotation of ±0.5 rad about the x-axis. The remaining boundary degrees of freedom are restrained.

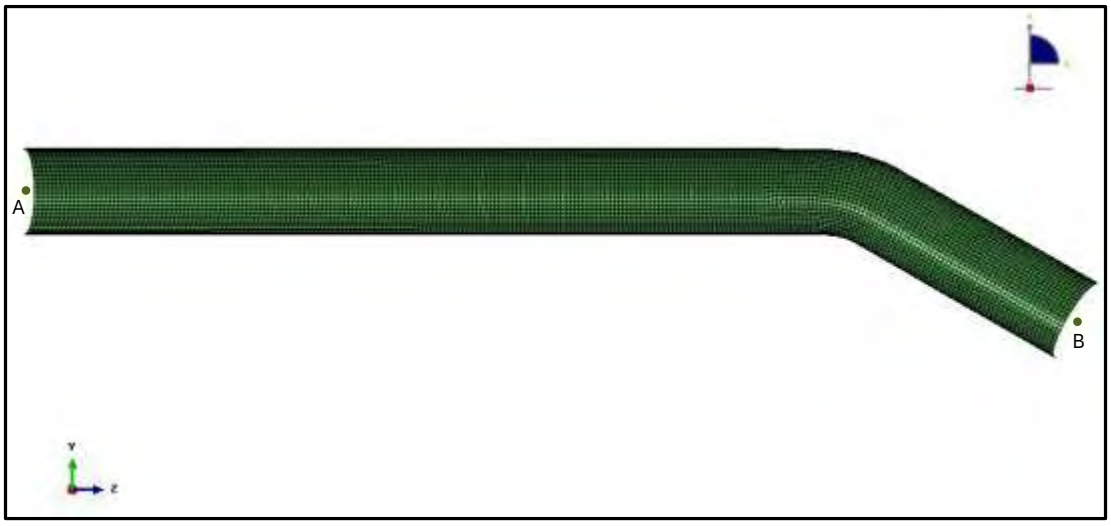

Figure 83: 30-degree elbow after manufacturing process

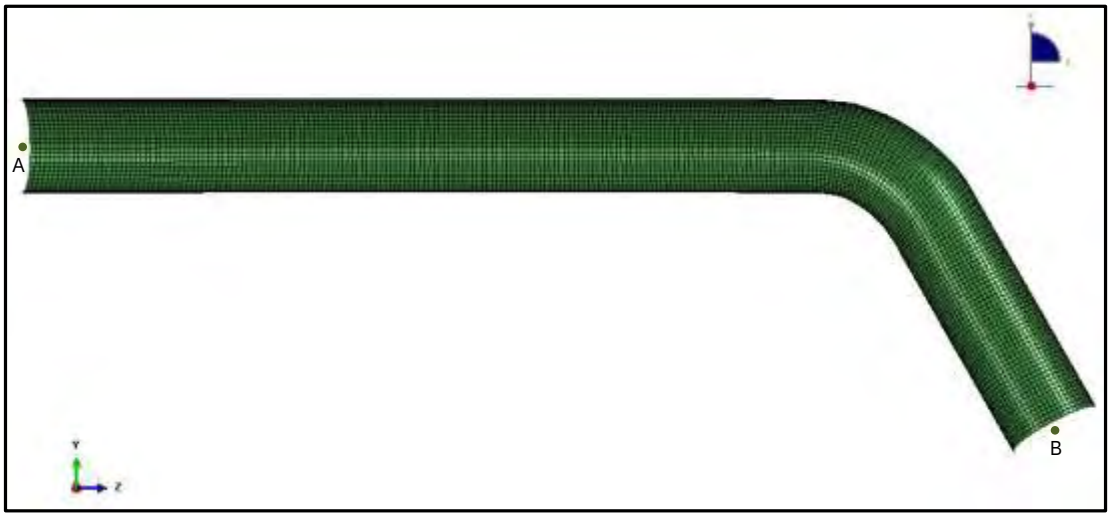

Figure 84: 60-degree elbow after manufacturing process

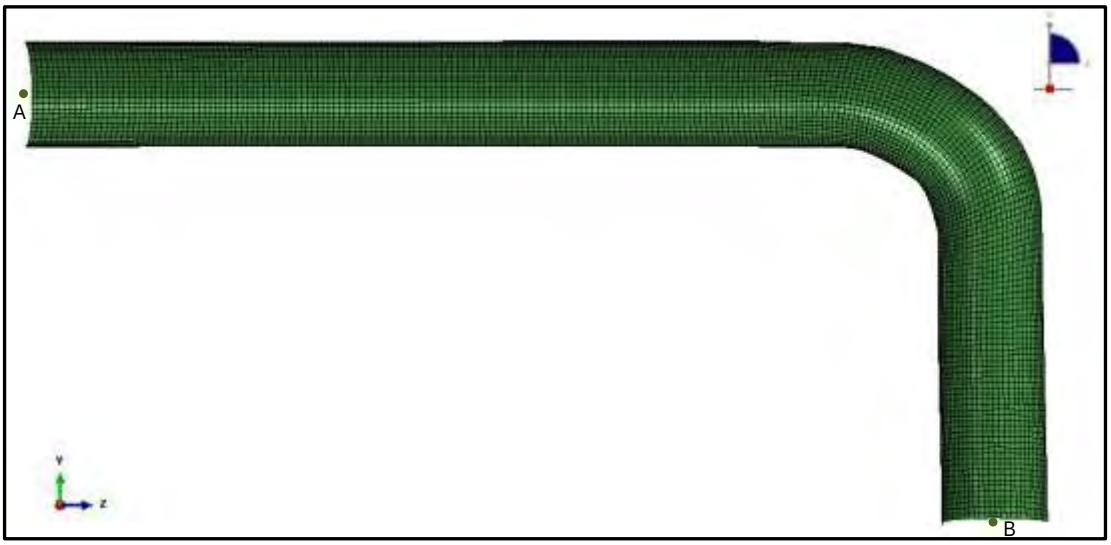

Figure 85: 90-degree elbow after manufacturing process

Elbow response under opening and closing bending moments

4.1 Closing bending moments

In this section the effect of closing bending moments to the 30, 60 and 90 degrees elbows are examined compared to the values of the perfect elbows. In Figure 89Figure 90 the applied in-plane closing bending moment of the 30-degree deformed and the 30-degree perfect elbow are plotted in terms of the end section B rotation φ about the x-axis, respectively. The reported moment is normalized by the fully-plastic moment ($M_p=\sigma_y D^2 t$). The results depicted in those figures demonstrate that the manufacturing process does not affect the value of the reaction moment on the end section B. The maximum normalized moment for both the deformed and the perfect elbow is 0.5 for 0.06 rad angle while the spring-back occurred is 0.011 rad (0.632 degrees).

In Figure 91Figure 92 the response under in-plane closing bending moment of the 60-degree deformed and the 60-degree perfect elbow is shown. The reported moment is normalized by the fully-plastic moment ($M_p=\sigma_y D^2 t$). Similar to 30 degrees the figures demonstrate that the manufacturing process does not affect the value of the reaction moment on the end section B. The maximum normalized moment for both the deformed and the perfect elbow is 0.38 for 0.08 rad angle while the spring-back occurred is 0.0115 rad (0.661 degrees).

In Figure 93Figure 94, the applied in-plane closing bending moment of the 90-degree deformed and the 90-degree perfect elbow is depicted. The reported moment is normalized by the fully-plastic moment ($M_p=\sigma_y D^2 t$). The maximum normalized moment for both the deformed and the perfect elbow is 0.35 for 0.09 rad angle while the spring-back occurred is 0.0117 rad (0.675 degrees).

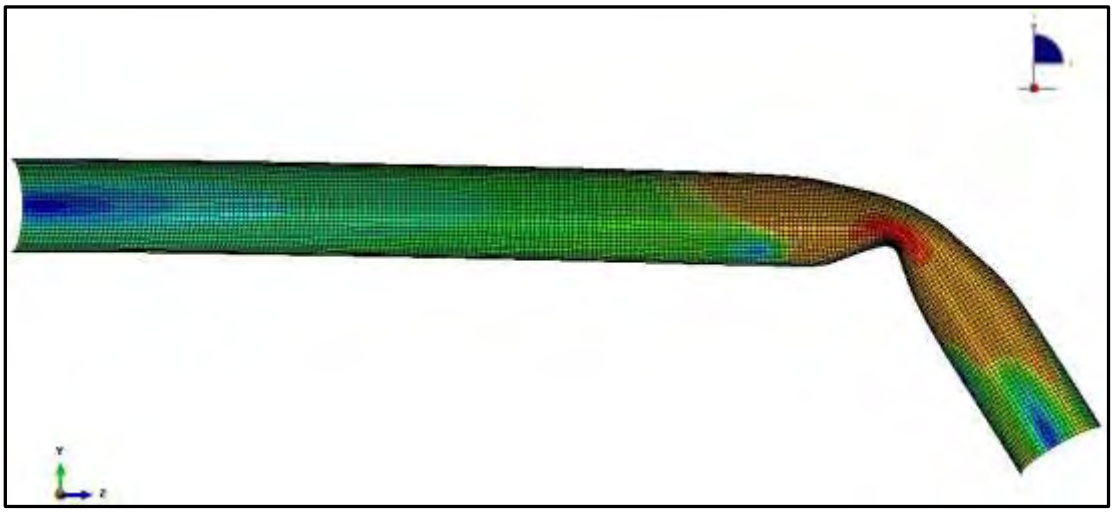

Figure 86: Elbow (30 degrees) deformation under in-plane closing bending moments

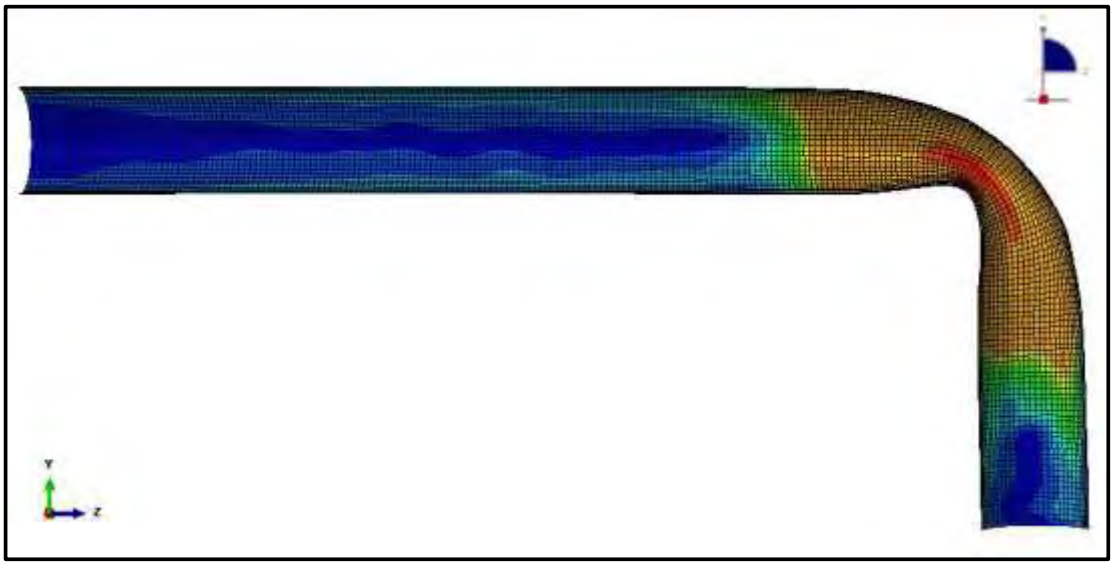

Figure 87: Elbow (60 degrees) deformation under in-plane closing bending moments

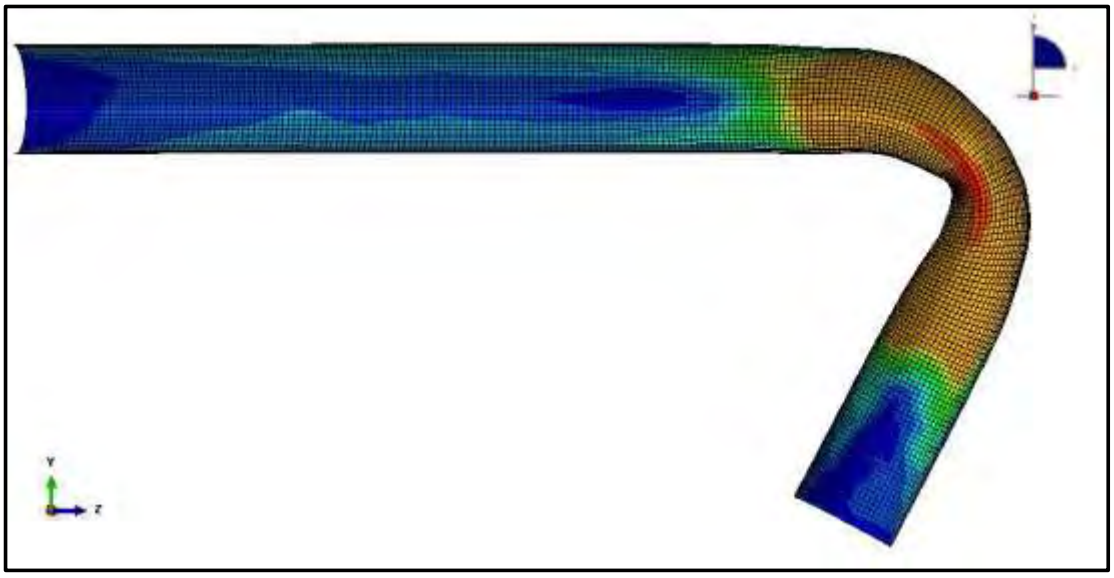

Figure 88: Elbow (90 degrees) deformation under in-plane closing bending moments

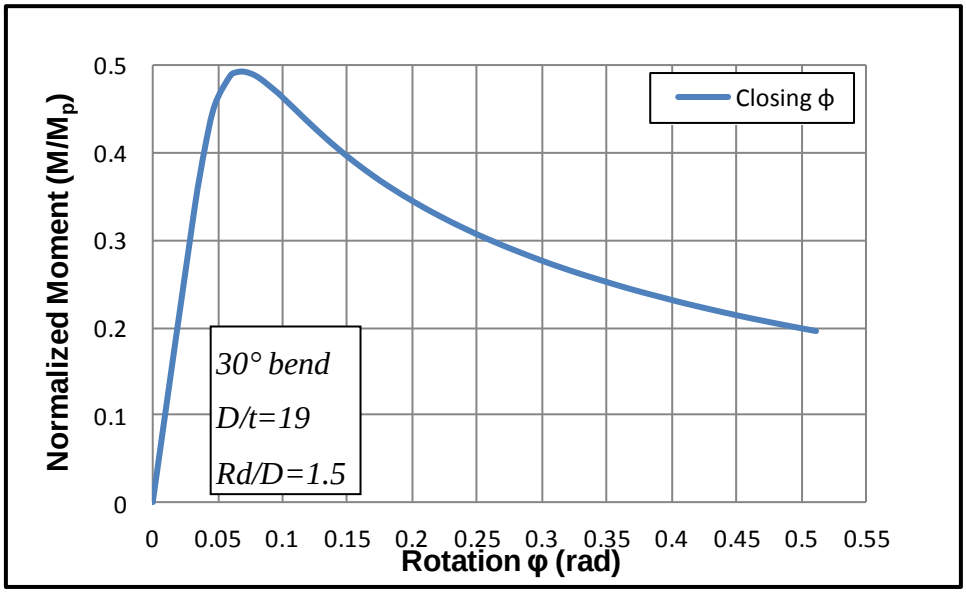

Figure 89: Elbow (30 degrees) response under in-plane closing bending moments

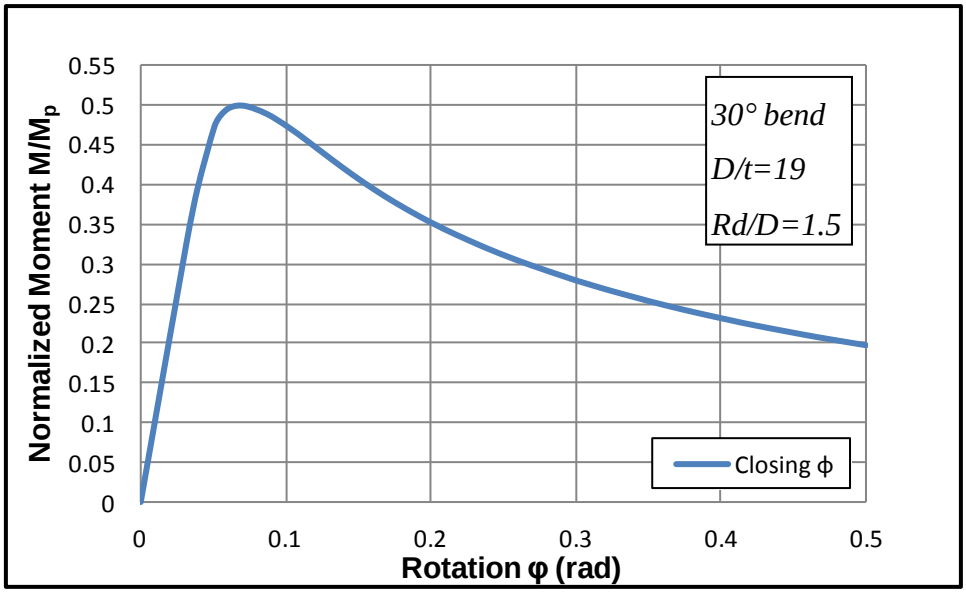

Figure 90: Perfect elbow (30 degrees) response under in-plane closing bending moments

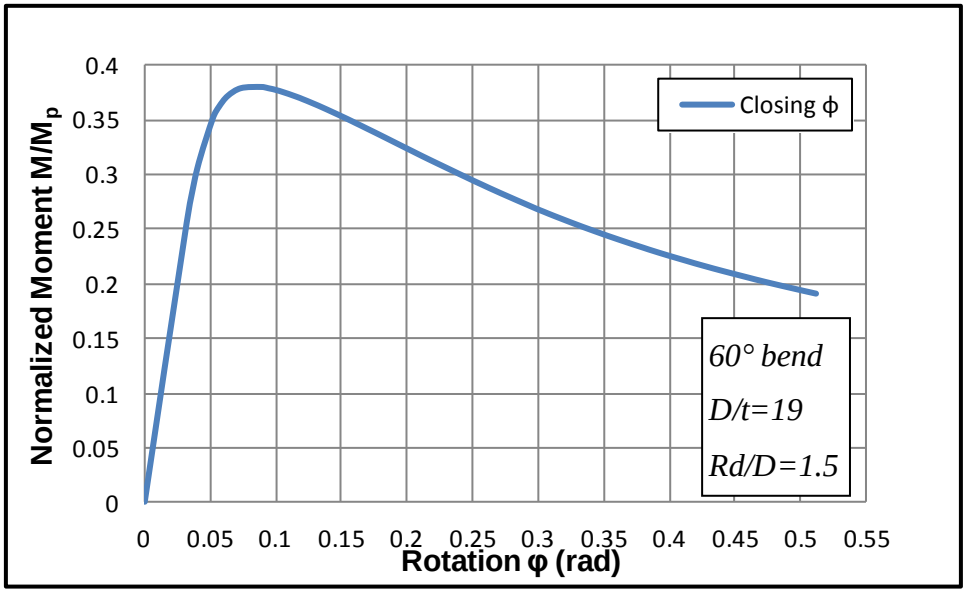

Figure 91: Elbow (60 degrees) response under in-plane closing bending moments

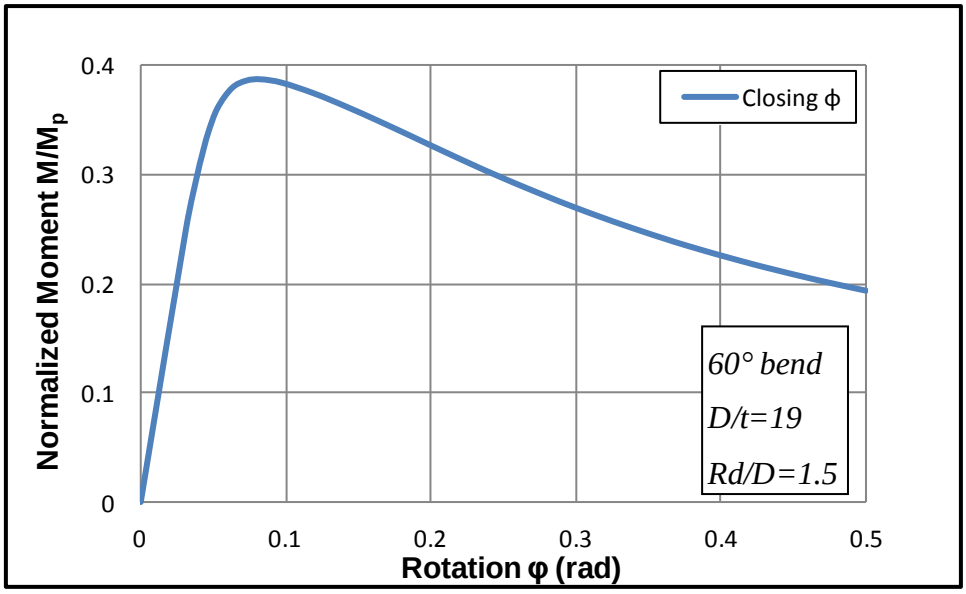

Figure 92: Perfect elbow (60 degrees) response under in-plane closing bending moments

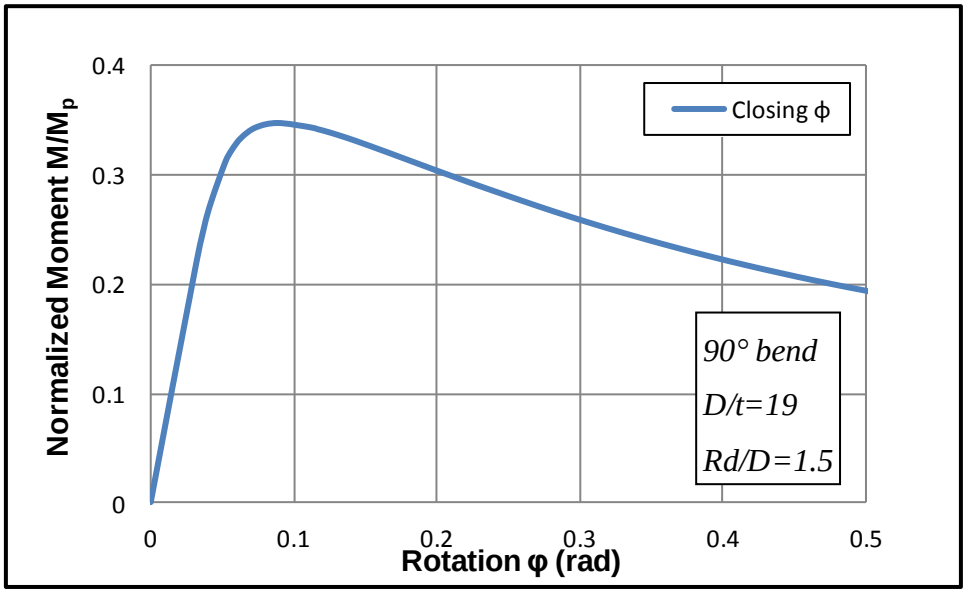

Figure 93: Elbow (90 degrees) response under in-plane closing bending moments

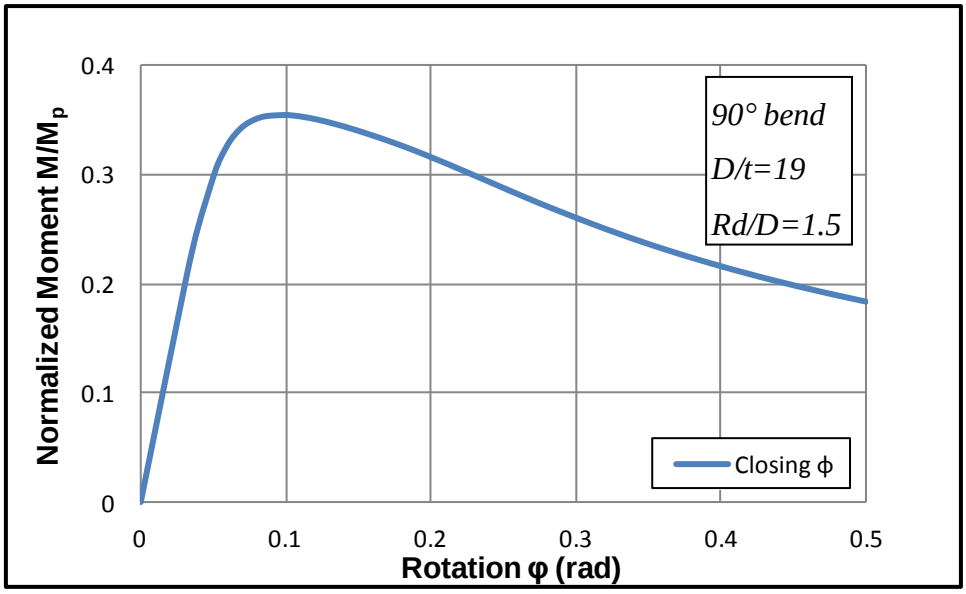

Figure 94: Perfect elbow (90 degrees) response under in-plane closing bending moments

4.2 Opening bending moments

In Figure 98Figure 103, the applied in-plane opening bending moments of the 30, 60 and 90-degree deformed and perfect elbows respectively, are plotted in terms of the end section B rotation φ about the x axis. The reported moments are normalized by the fully-plastic moment ($M_p=\sigma_y D^2 t$). Similarly to the closing bending moments, the results depicted in those figures demonstrate that the manufacturing process does not affect significantly the value of the reaction moment on the end section B.

More precisely, for the 30 degrees elbow the maximum opening normalized moment is 0.68 for 0.2 rad angle for both the deformed and the perfect elbow. For the 60 degrees tube the values change to 0.66 and 0.3 respectively. Finally, for the 90 degrees elbow the maximum opening normalized moment depicted is 0.5 for 0.3 rad.

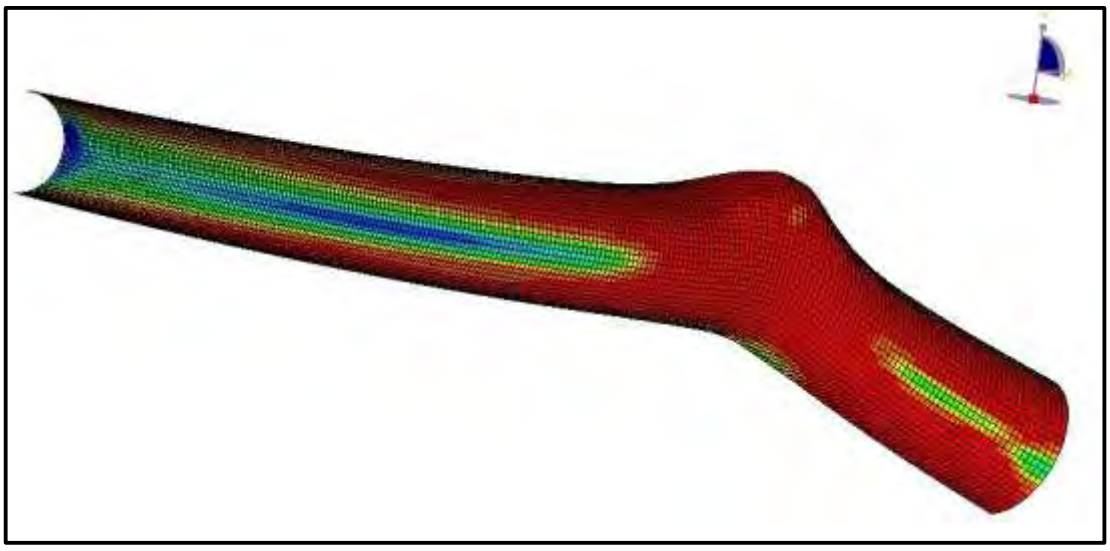

Figure 95: Elbow (30 degrees) deformation under in-plane opening bending moments

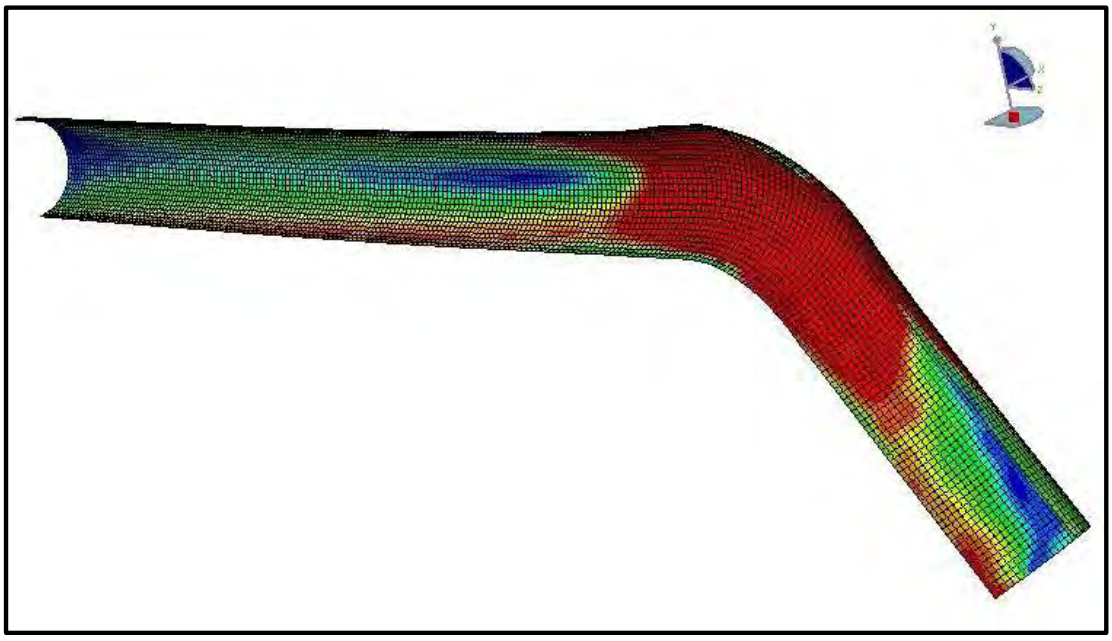

Figure 96: Elbow (60 degrees) deformation under in-plane closing bending moments

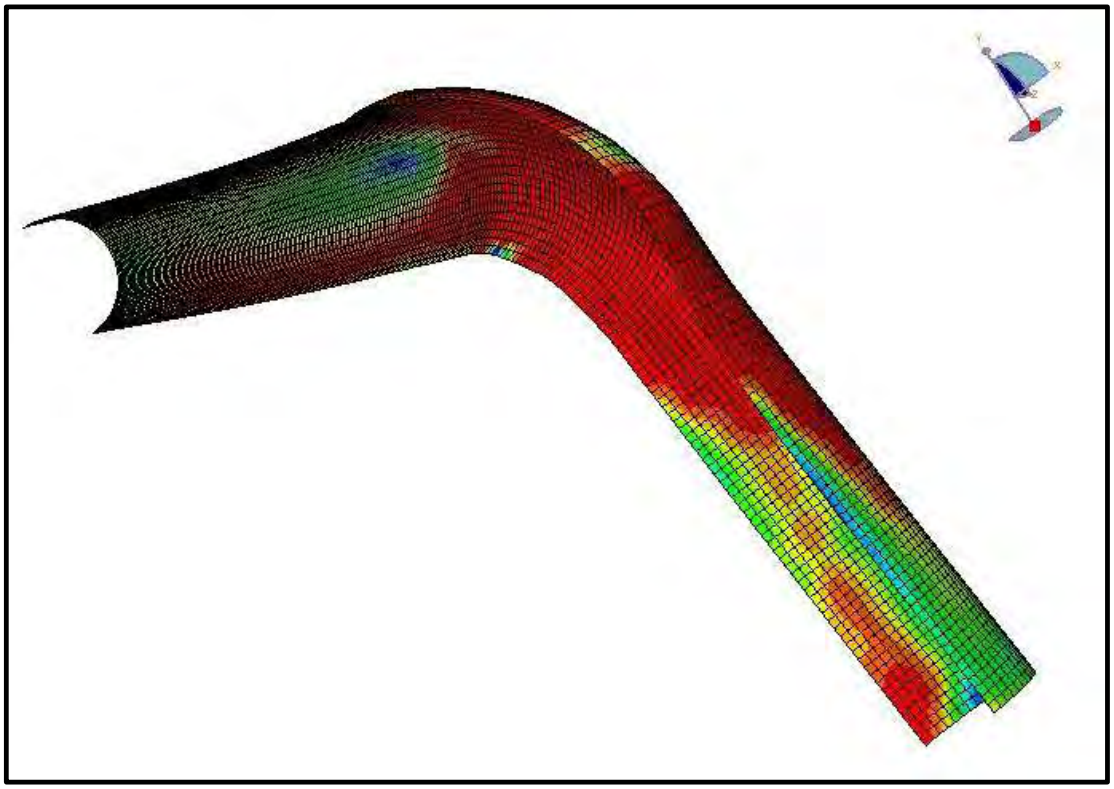

Figure 97: Elbow (90 degrees) deformation under in-plane opening bending moments

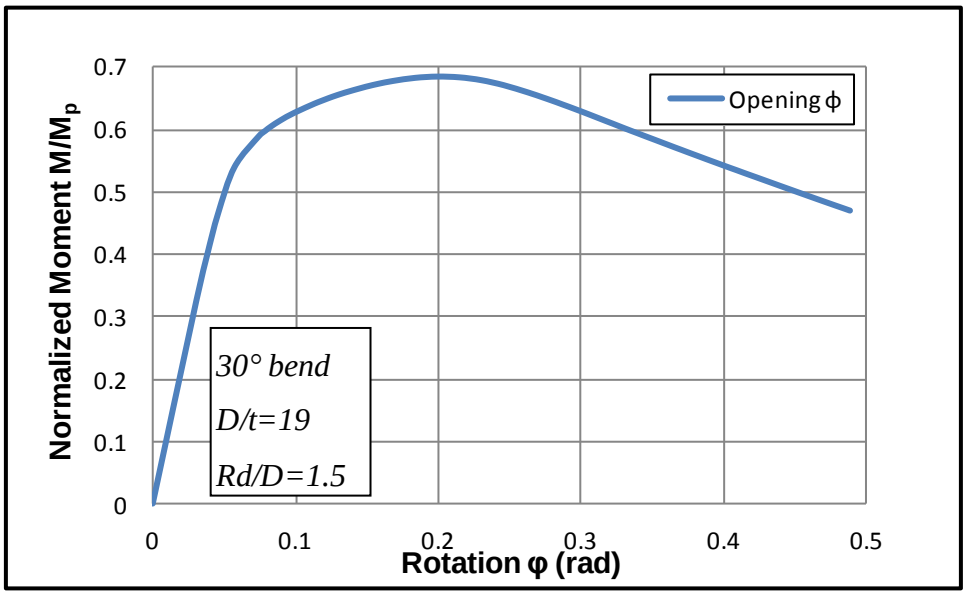

Figure 98: Elbow (30 degrees) response under in-plane opening bending moments

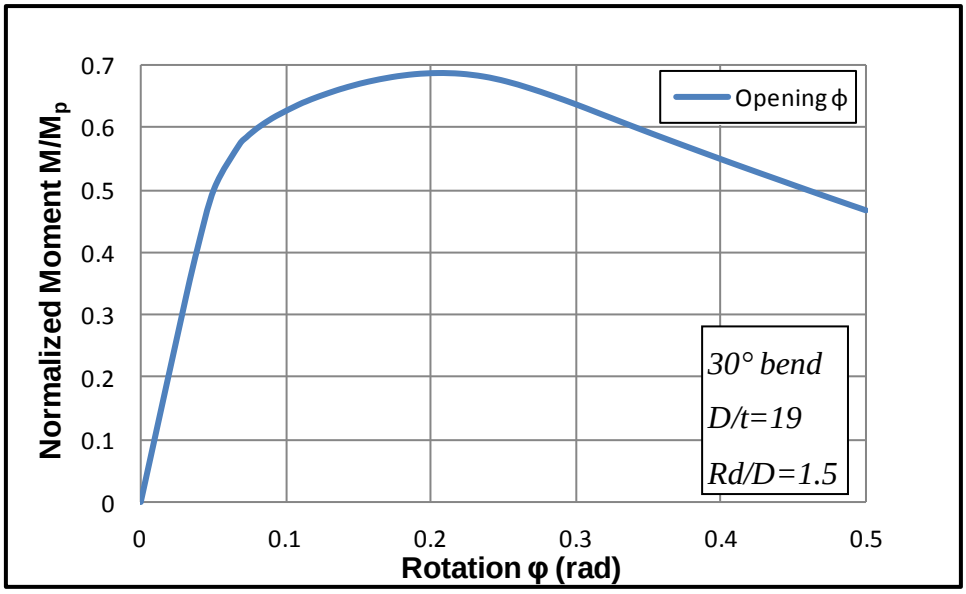

Figure 99: Perfect elbow (30 degrees) response under in-plane opening bending moments

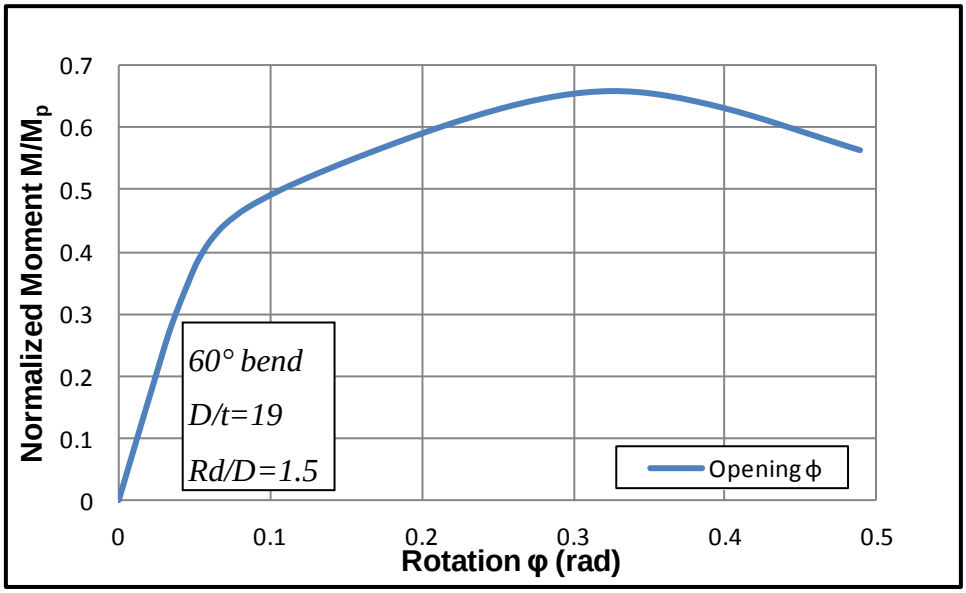

Figure 100: Elbow (60 degrees) response under in-plane opening bending moments

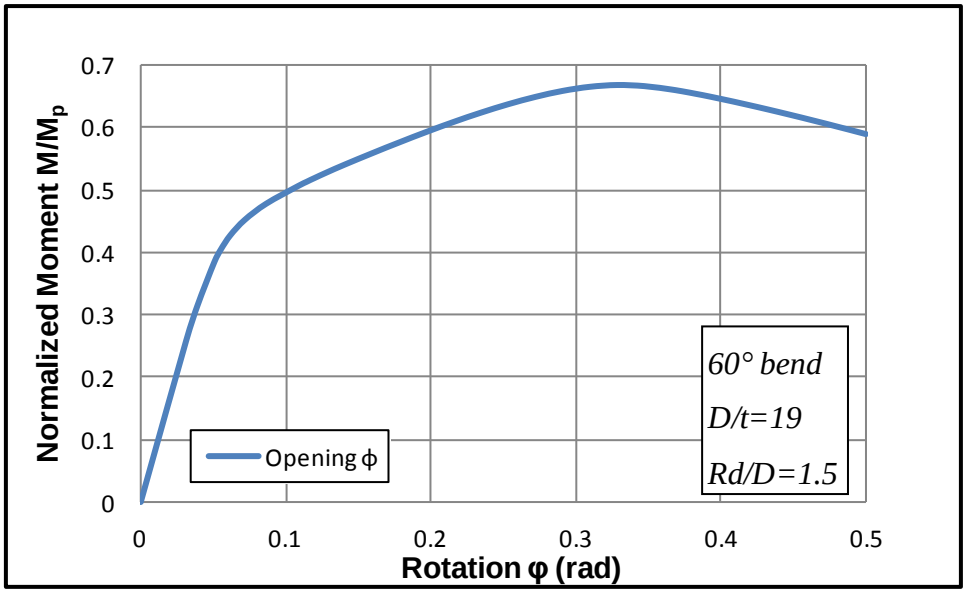

Figure 101: Perfect elbow (60 degrees) response under in-plane opening bending moments

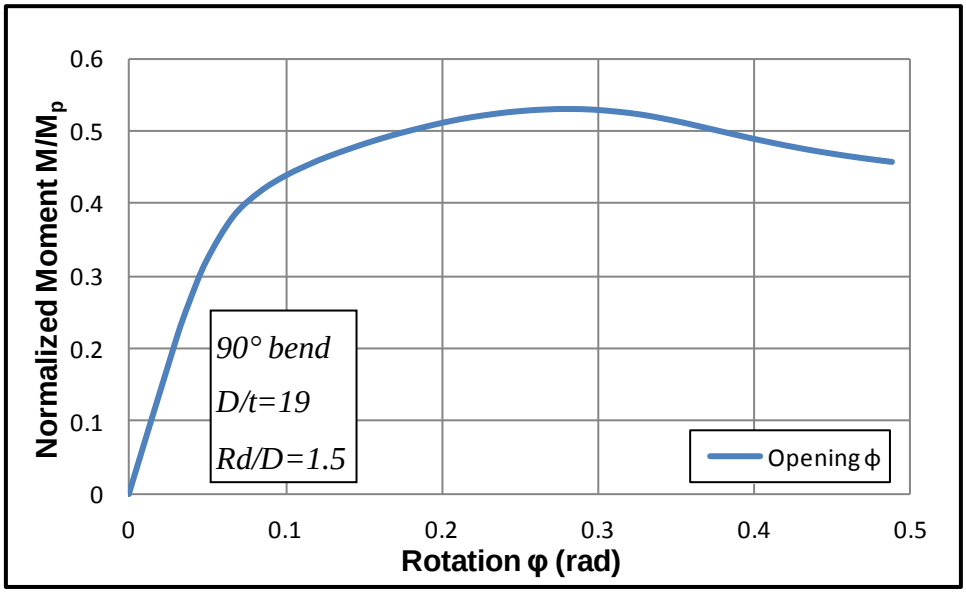

Figure 102: Elbow (90 degrees) response under in-plane opening bending moments

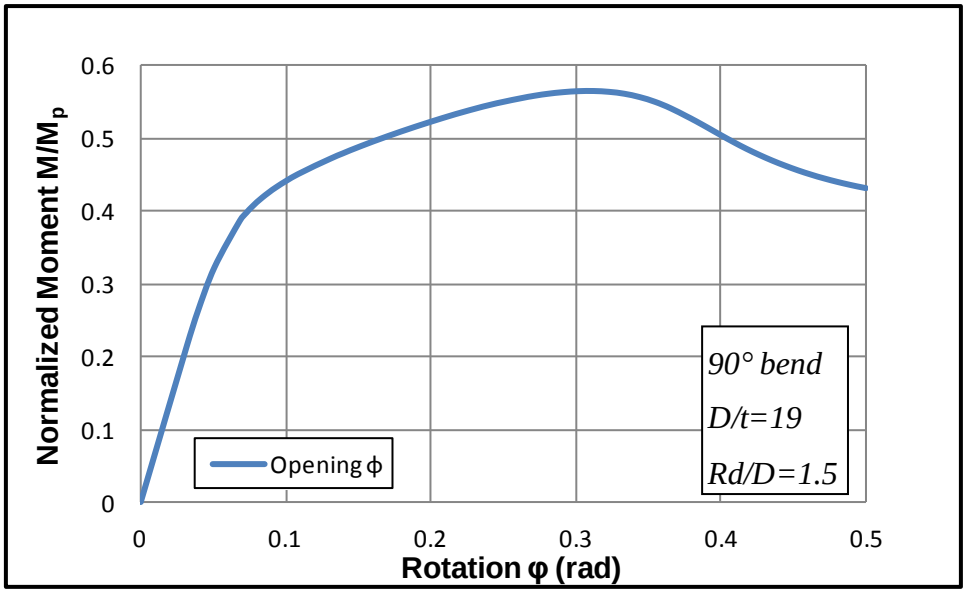

Figure 103: Perfect elbow (90 degrees) response under in-plane opening bending moments

4.3 Ovalization

The applied in-plane closing bending moment causes a rather severe ovalization to the cross-section of the tube, especially in the bend area.

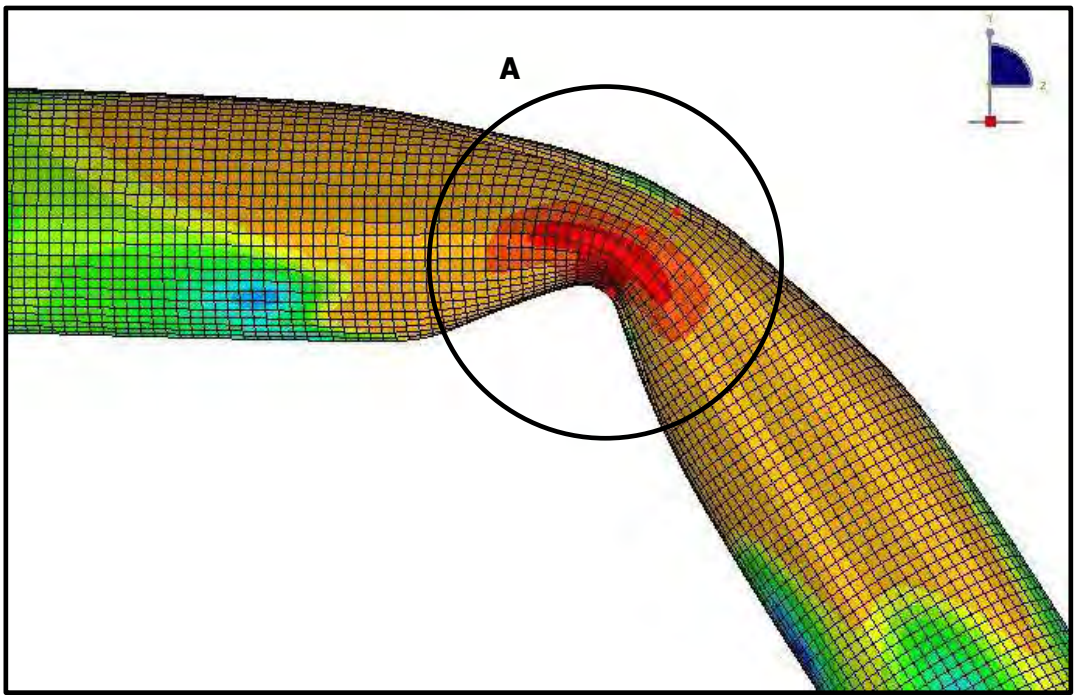

Figure 104: Cross-section A ovalization of 30-degree elbow under in-plane closing bending moment

Ovalization is expressed through the non-dimensional ovalization parameter $ov=|D_A-D_B| / D_m$, where DA is the length of the deformed diameter on the plane of bending and DB is the length of deformed diameter perpendicular to the plane of bending, both measured at the cross-section under consideration (Figure 104). In Figure 105Figure 106, the ovalization is plotted in terms of the applied bending angle φ.

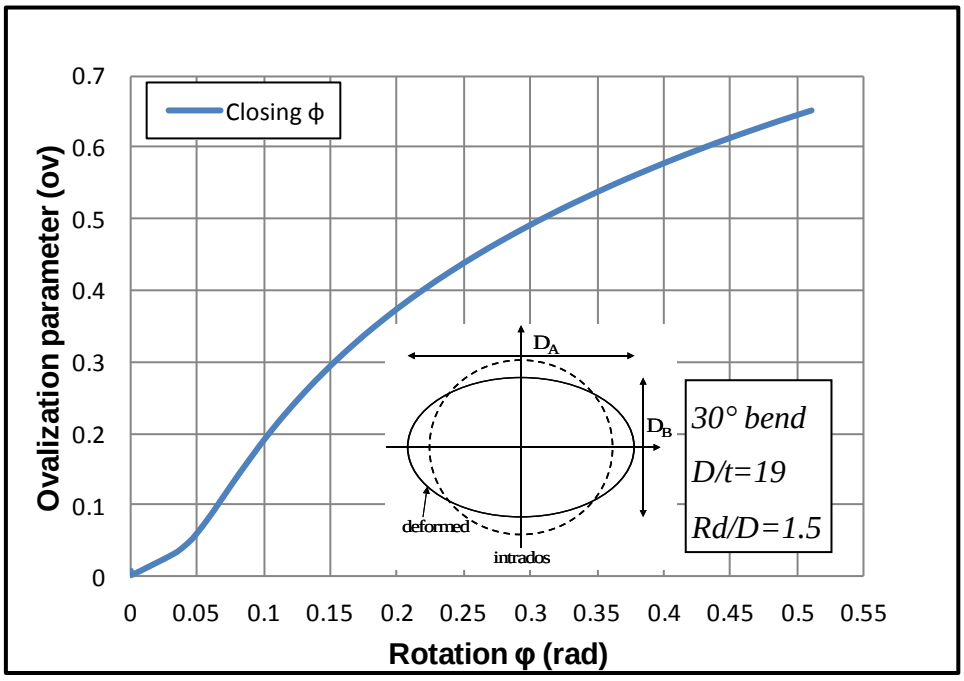

Figure 105: Ovalization of cross-section A of 30-degree elbow

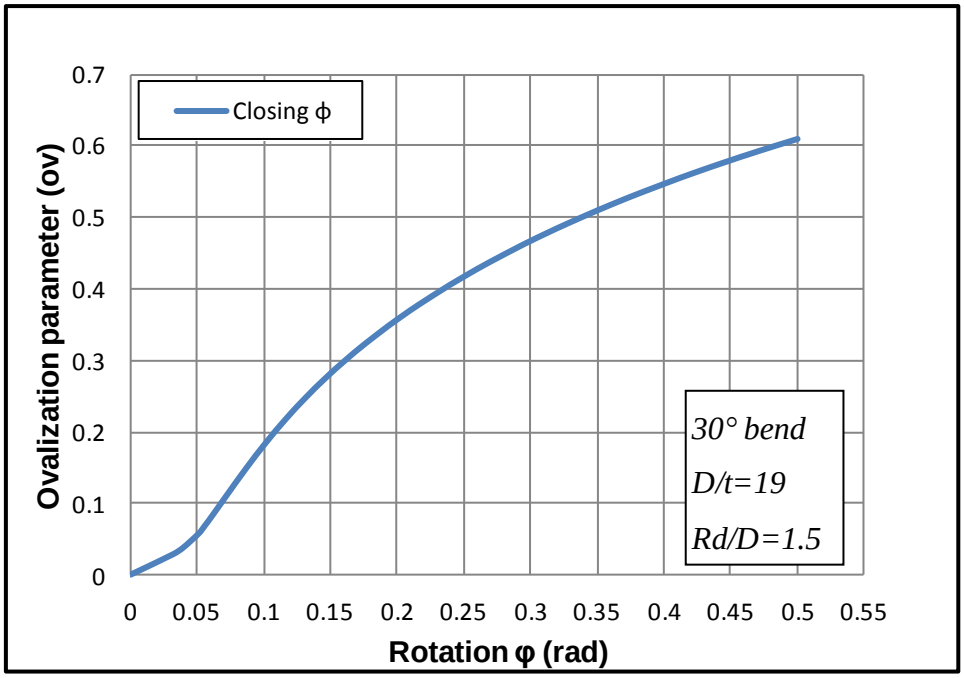

Figure 106: Cross-section ovalization of 30-degree perfect elbow

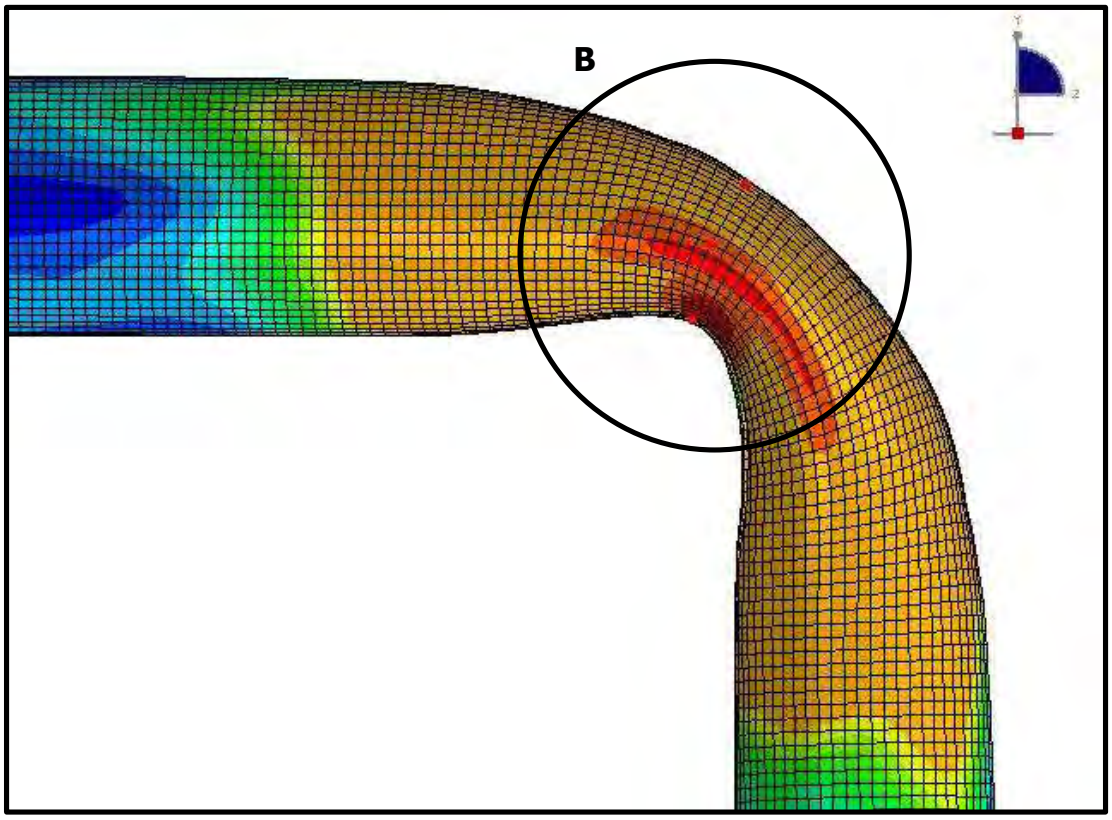

Figure 107: Cross-section B ovalization of 60-degree elbow under in-plane closing bending moment

In Figure 107 the ovalization caused due to bending is shown. In Figure 108Figure 109, the ovalization of the ring B is plotted in terms of the applied bending angle φ.

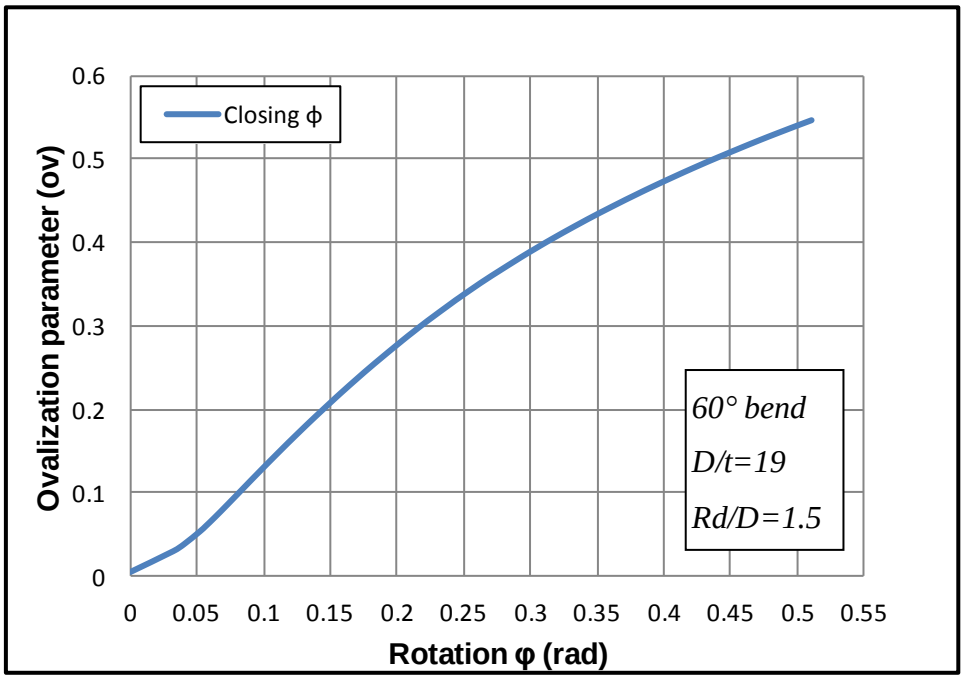

Figure 108: Ovalization of cross-section B of 60-degree elbow

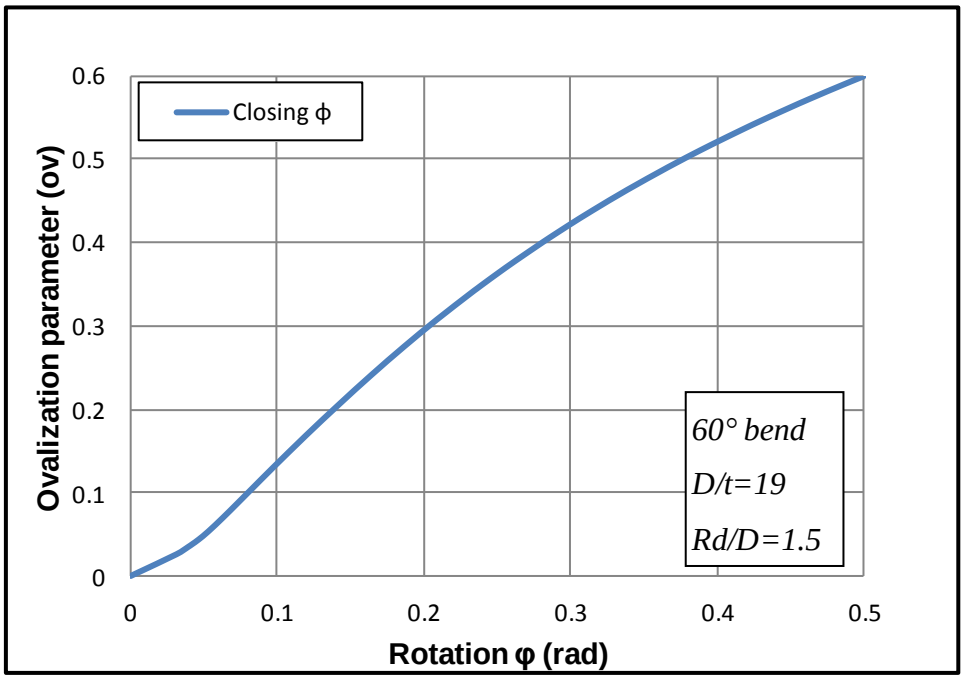

Figure 109: Ovalization of cross-section of 60-degree perfect elbow

In Figure 110 the ovalization caused due to bending is shown. In Figure 111Figure 112, the ovalization of the ring B is plotted in terms of the applied bending angle φ.

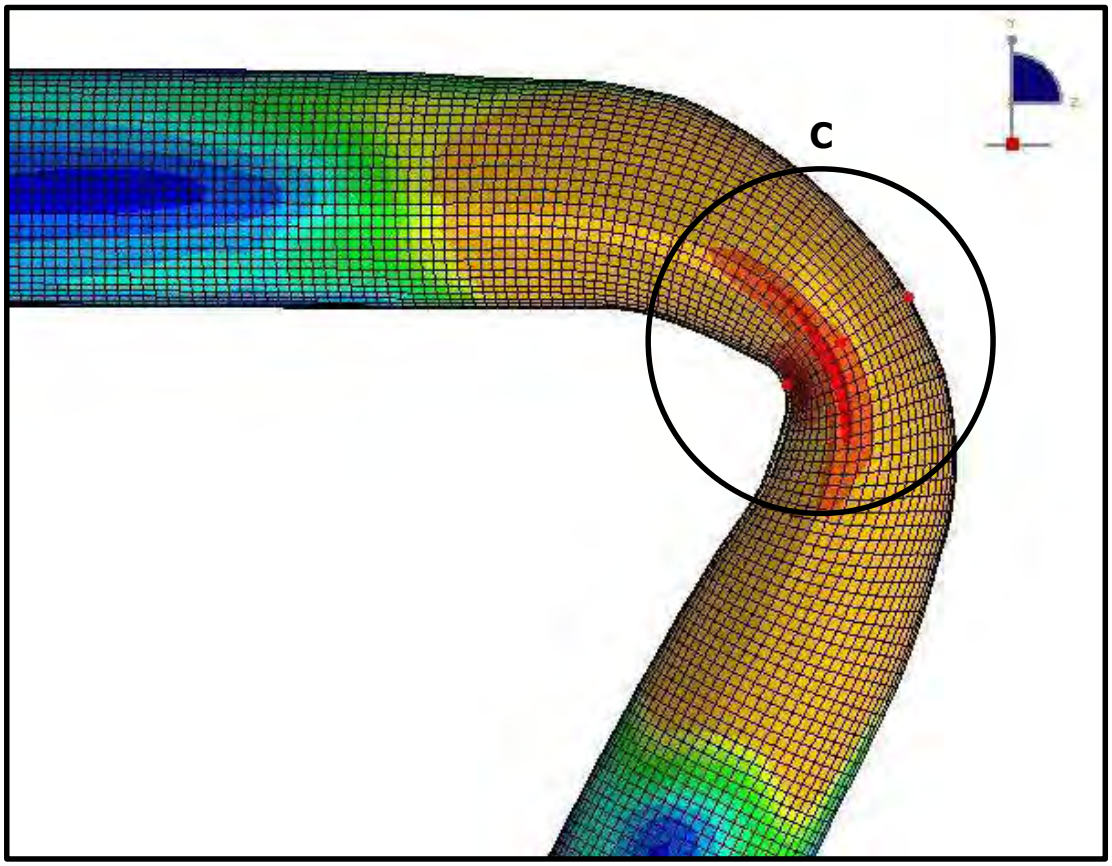

Figure 110: Cross-section C ovalization of 90-degree elbow under in-plane closing bending moment

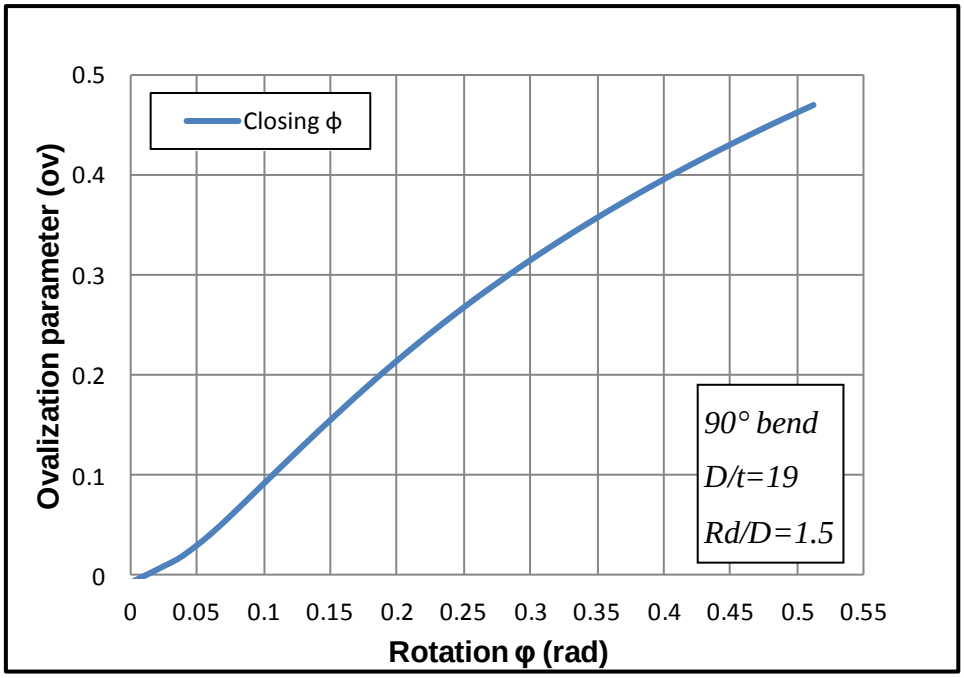

Figure 111: Ovalization of cross-section C of 90-degree elbow

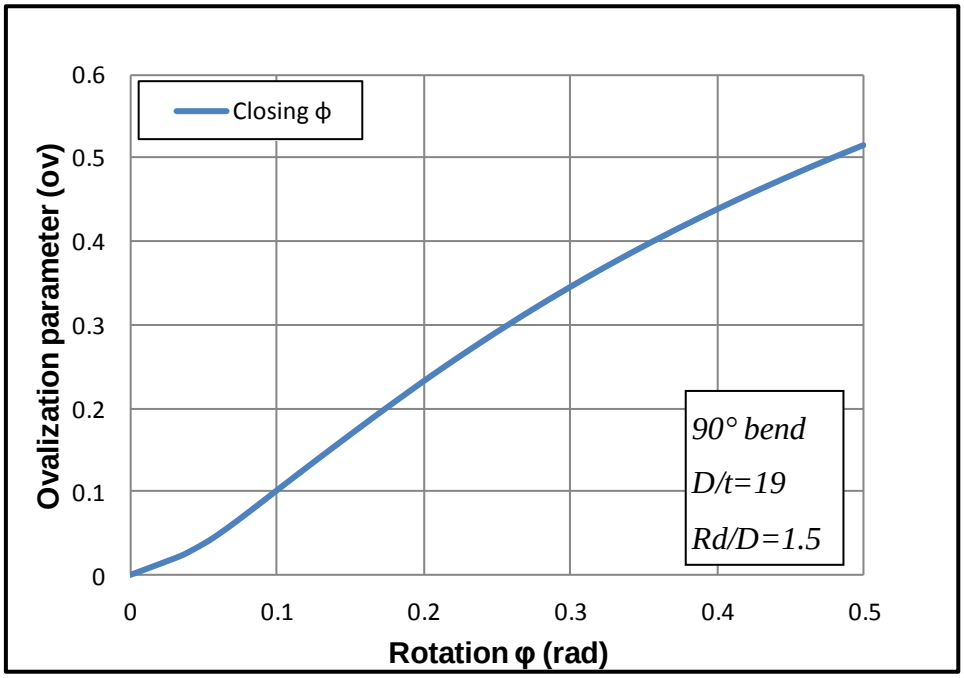

Figure 112: Ovalization of cross-section of 90-degree perfect elbow

Chapter 5

Conclusions

An improved three-dimensional-finite element (3D-FE) model was developed within the explicit code ABAQUS/Explicit for the purposes of this research. The present work was motivated by the need of industry to simulate tube bending process at different angles via the Rotary Draw Bending method (RDB). One of the basic issues examined was the effect of bending angle 30, 60 and 90 degrees on the elbow out-of straightness and out-of roundness compared with a perfect elbow. The 30-degree and 60-degree elbow out-of straightness showed a quite similar behavior for all three generators. More precisely, the upper generators showed, at the early bending stage, a deviation from the perfect curve, but as the angle along the bend increased the deformed shape obtained was very similar to the perfect. The middle generators showed a steady deviation from the perfect curve while the lower generators showed at first a good comparison with the perfect curve but as the angle along the bend increased the deviation increased. For the 90-degree elbow the three generators behaved in the same way, that is, the curve deviation increased as the bending angle increased. In addition, pipe wall thickness variation and stress distribution on the upper, middle and lower elbow generators were investigated. For all bending degrees, cross-section thinning was depicted in the upper generators while cross-section thickening was depicted in the lower generators. The stress distribution on the three generators was rather inhomogeneous with maximum values of Von Mises stress depicted in the middle generator.

In the final part of this study, the non-linear elastic-plastic response of the bent tubes under in-plane bending loading was examined to determine their structural capacity and performance. Opening and closing bending moments were applied to the elbows and the effect on their cross-section ovalization was evaluated. From the results, it was shown that the deformed elbow had almost the same behavior as the perfect elbow under structural loading.

The present study was aimed at providing a rigorous toll for predicting the behavior of a round, steel tube not only during the manufacturing bending

process but also when subjected to structural loading. Based on the present work, further numerical results, possibly supported by experimental testing, are necessary to validate the applicability of the present technique to predict the mechanical properties of an elbow created via the Rotary Draw Bending method.

References

[1] Department of Engineering and Material Science, NSFC. Development strategy report of mechanical engineering discipline (2011-2020). Beijing: Science Press, 2010. [in Chinese]

[2] Yang H, Sun Z C, Lin Y. Advanced plastic processing technology and research progress on tube forming, Journal of Plasticity Engineering 2001; 8(2): 83-85. [in Chinese]

[3] The Aerial Tube forming writing group. The aerial tube forming. Beijing: National Defence Industry Press, 1979. [in Chinese]

[4] Wang T H. Tube plastic processing technology. Beijing: China Machine Press, 1998. [in Chinese]

[5] YANG He, LI Heng, ZHANG Zhiyong, ZHAN Mei, LIU Jing, LI Guangjun, 2011, "Advances and Trends on Tube Bending Forming Technologies", Chinese Journal of Aeronautics 25 (2012) 1-12.

[6] K. Hasanpour, B. Amini, M. Poursina, M. Barati, 2011, "The Effect of Anisotropy on Thin-Walled Tube Bending", The 8th International Conference and Workshop on Numerical Simulation of 3D Sheet Metal Forming Processes, AIP Conf. Proc.

[7] Gangyao Zhao & Yuli Liu & He Yang, 2010, "Effect of clearance on wrinkling of thin-walled rectangular tube in rotary draw bending process", Springer-Verlag London Limited 2010

[8] H. Li, H. Yang and M. Zhan, 2009, "A study on plastic wrinkling in thin-walled tube bending via an energy-based wrinkling prediction model", IOP Publishing Ltd. Modelling Simul. Mater. Sci. Eng.17, 035007 (33pp)

[9] G.Y. Zhao, Y.L. Liu∗, C.S. Dong, H. Yang, X.G. Fan, 2010,"Analysis of wrinkling limit of rotary-draw bending process for thin-walled rectangular tube", Elsevier Journal of materials processing technology

[10] LI Heng*, YANG He, 2010, "A Study on Multi-defect Constrained Bendability of Thin-walled Tube NC Bending Under Different Clearance", Elsevier Chinese Journal of Aeronautics

[11] LI Heng, YANG He, ZHAN Mei, GU Rui-Jie, 2006, "Forming characteristics of thin-walled tube bending process with small bending

radius", Science Direct, Trans. Nonferrous Met. SOC. China 16, s613-s623.

[12] H. Li∗, H. Yang, M. Zhan, Y.L. Kou, 2009, "Deformation behaviors of thin-walled tube in rotary draw bending under push assistant loading conditions", Elsevier Journal of materials processing technology.

[13] YAN Jing, YANG He*, ZHAN Mei & LI Heng, 2009, "Forming limits under multi-index constraints in NC bending of aluminum alloy thin-walled tubes with large diameters", Science China Press and Springer-Verlag Berlin Heidelberg, Vol.53 No.2: 326–342.

[14] H. Li, H. Yang, * , J. Yan, M. Zhan, 2008, "Numerical study on deformation behaviors of thin-walled tube NC bending with large diameter and small bending radius, Elsevier, Computational Materials Science.

[15] H. Li, H. Yang, M. Zhan, Y.L. Kou, 2009, "Deformation behaviors of thin-walled tube in rotary draw bending under push assistant loading conditions", Elsevier, Journal of materials processing technology.

[16] Brazier, L. G., 1927, "On the flexure of thin cylindrical shells and other "thin" sections", Proceedings of the Royal Society, series A, Vol. 116, pp. 104-114.

[17] Sobel, L. H. and Newman, S. Z., 1980, "Comparison of Experimental and Simplified Analytical Results for the In-Plane Plastic Bending and Buckling of an Elbow", ASME *Journal of Pressure Vessel Technology*, **102**, pp. 400-409.

[18] Sobel, L. H. and Newman, S. Z., 1986, "Simplified, Detailed and Isochronous Analysis and Test Results for the In-Plane Elastic-Plastic and Creep Behavior of an Elbow", ASME *Journal of Pressure Vessel Technology*, 108, pp. 297-304.

[19] Dhalla, A. K., 1987, "Collapse Characteristics of a Thin-Walled Elbow", ASME *Journal of Pressure Vessel Technology*, **109**, pp. 394-401.

[20] Gresnigt, A. M. et al., 1986, *Test Results of Tests on Smooth Bends and Comparison with Proposed Analytical Models*, Report [in Dutch], Institute for Construction Materials and Structures, TNO-IBBC, Report BI-86-122, Delft, The Netherlands.

[21] Gresnigt, A. M., 1986, "Plastic Design of Buried Steel Pipelines in Settlement Areas", *Heron*, **31** (4), Delft, The Netherlands.

[22] Gresnigt, A. M. and van Foeken, 1995, "Strength and Deformation Capacity of Bends in Pipelines", *International Journal of Offshore and Polar Engineering*, **5** (4), pp. 294-307.

[23] Greenstreet, W. L., 1978, *Experimental Study of Plastic Responses of Pipe Elbows*, ORNL/NUREG-24 Report, Contract No. W-7405-eng-26.

[24] Hilsenkopf, P., Boneh, B. and Sollogoub, P., 1988, "Experimental Study of Behavior and Functional Capability of Ferritic Steel Elbows and Austenitic Stainless Steel Thin-Walled Elbows". *International Journal of Pressure Vessels and Piping*, **33**, pp. 111-128.

[25] Suzuki, N. and Nasu, M., 1989, "Non-Linear Analysis of Welded Elbows Subjected to In-Plane bending", *Computers and Structures*, **32** (3/4), pp. 871-881.

[26] Tan, Y., Matzen, V. C. and Yu, L. X., 2002, "Correlation of Test and FEA Results for the Nonlinear Behavior of Straight Pipes and Elbows", ASME *Journal of Pressure Vessel Technology*, **124**, pp. 465-475.

[27] Shalaby, M. A. and Younan, M. Y. A., 1998, "Limit Loads for Pipe Elbows with Internal Pressure Under In-plane Closing Bending Moments", ASME *Journal of Pressure Vessel Technology*, **120**, pp. 35-42.

[28] Shalaby, M. A. and Younan, M. Y. A., 1999, "Effect of Internal Pressure on Elastic-Plastic Behavior of Pipe Elbows Under In-plane Opening Bending Moments", ASME *Journal of Pressure Vessel Technology*, **121**, pp. 400-405.

[29] Mourad, H. M. and Younan, M. Y. A., 2001, "Nonlinear Analysis of Pipe Bends Subjected to Out-of-Plane Moment Loading and Internal Pressure", ASME *Journal of Pressure Vessel Technology*, **123** (2), pp. 253-258.

[30] Mourad, H. M. and Younan, M. Y. A., 2002, "Limit-Load Analysis of Pipe Bends Under Out-of-Plane Moment Loading and Internal Pressure", ASME *Journal of Pressure Vessel Technology*, **124** (1), pp. 32-37.

[31] Chattopadhyay J., Nathani, D. K., Dutta, B. K. and Kushwaha, H. S., 2000, "Closed-Form Collapse Moment Equations of Elbows Under Combined Internal Pressure and In-plane Bending Moment", ASME *Journal of Pressure Vessel Technology*, **122**, pp. 431-436.

[32] Karamanos, S. A., Giakoumatos, E. and Gresnigt, A. M., 2003, "Nonlinear Response and Failure of Steel Elbows Under In-Plane Bending and Pressure", ASME *Journal of Pressure Vessel Technology*, **125** (4), pp. 393-402.